



This is to certify that the  
thesis entitled

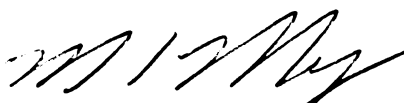
EFFECTS OF NANOSCALE INCLUSIONS ON THE  
DYNAMICS AND PROPERTIES OF POLYMER MELTS.

presented by

ANISH TUTEJA

has been accepted towards fulfillment  
of the requirements for the

Ph.D. degree in CHEMICAL ENGINEERING



Major Professor's Signature

7/26/06

Date

*MSU is an Affirmative Action/Equal Opportunity Institution*

LIBRARY  
Michigan State  
University

**PLACE IN RETURN BOX** to remove this checkout from your record.  
**TO AVOID FINES** return on or before date due.  
**MAY BE RECALLED** with earlier due date if requested.

DATE DUE	DATE DUE	DATE DUE

**EFFECTS OF NANOSCALE INCLUSIONS ON THE DYNAMICS  
AND PROPERTIES OF POLYMER MELTS**

By

Anish Tuteja

A DISSERTATION

Submitted to  
Michigan State University  
In partial fulfillment of the requirements  
for the degree of

DOCTOR OF PHILOSOPHY

Department of Chemical Engineering and Materials Science

2006



## **ABSTRACT**

### **EFFECTS OF NANOSCALE INCLUSIONS ON THE DYNAMICS AND PROPERTIES OF POLYMER MELTS**

By

Anish Tuteja

In recent times, nanofillers have attracted the interest of a variety of research groups as these materials can cause unusual mechanical, electrical, optical and thermal enhancements. These enhancements are induced by the presence of the nanoparticles, their interaction with the host matrix, and also quite critically, by their state of dispersion. In this work we find that nanoparticles can be dispersed in linear polymers, despite chemical dissimilarity, when the nanoparticle is smaller than the linear polymer, as demonstrated by the miscibility of polyethylene (PE) nanoparticles in linear polystyrene (PS) or PS nanoparticles in poly (methyl methacrylate) (PMMA) (PS-PE and PS-PMMA are classical phase separating systems). If the particles become larger than the polymer, phase separation occurs with even polystyrene nanoparticles phase separating from linear polystyrene. In addition, small angle neutron scattering shows the linear polymer becomes distorted on the addition of nanoparticles in the stable systems and is far from its equilibrium conformation. This aspect demonstrates the uniqueness of nanoscale thermodynamics as phase separation is expected (i.e. depletion flocculation) and we believe that the nanoparticles are stabilized by enthalpic gain. When properly dispersed, the addition of nanoparticles causes a large reduction (up to 90%) in the melt viscosity of the system, a result at odds with Einstein's century old prediction and experimental observations of the viscosity increase particles provide to liquids (i.e. slurries and

suspensions) and melts. Also, the addition of specific nanoparticles, apart from improving the polymer processing by reducing the viscosity, can simultaneously lead to enhanced electrical conductivity (greater than Maxwell's prediction), enhanced mechanical damping (up to 5 fold increase), enhanced thermal stability / fire retardancy, and can even make the polymers magnetic. The above and other unusual nanoscale phenomena are discussed in this work.

## TABLE OF CONTENTS

LIST OF TABLES .....	vi
LIST OF FIGURES .....	vii
CHAPTER 1: INTRODUCTION .....	1
Research Objectives.....	7
CHAPTER 2: THE MOLECULAR ARCHITECTURE AND RHEOLOGICAL CHARACTERIZATION OF NOVEL INTRAMOLECULARLY CROSSLINKED POLYSTYRENE NANOPARTICLES .....	9
Introduction.....	9
Experimental .....	13
Results and Discussion .....	20
Conclusion .....	38
Appendix Chapter 2. ....	40
CHAPTER 3 : GENERAL STRATEGIES FOR NANOPARTICLE DISPERSION .....	45
Introduction.....	45
Experimental .....	46
Results and Discussion .....	47
Conclusion .....	59
CHAPTER 4: NANOSCALE EFFECTS LEADING TO NON-EINSTEIN-LIKE REDUCTION IN VISCOSITY .....	60
Introduction.....	60
Experimental .....	61
Results and Discussion .....	62
Conclusion .....	76
CHAPTER 5 : EFFECT OF IDEAL, ORGANIC NANOPARTICLES ON THE FLOW PROPERTIES OF LINEAR POLYMERS: NON-EINSTEIN-LIKE BEHAVIOR .....	77
Introduction.....	77
Experimental .....	84
Results and Discussion .....	89
Conclusion .....	106

Appendix for Chapter 5 .....	107
CHAPTER 6: BREAKDOWN OF THE CONTINUUM STOKES-EINSTEIN RELATION FOR NANOSCALE INCLUSIONS IN POLYMER MELTS .....	109
Introduction.....	109
Results and Discussion .....	110
Conclusion .....	122
CHAPTER 7 : DESIGNING MULTIFUNCTIONAL NANOCOMPOSITES.....	123
Introduction.....	123
Experimental .....	124
Results and Discussion .....	125
Conclusion .....	143
CHAPTER 8: CONCLUSION .....	144
LIST OF PUBLICATIONS .....	148
REFERENCES .....	149

## LIST OF TABLES

<b>Table 2.1.</b> Number average molecular masses ( $M_n$ ) and polydispersity index (PDI) of the linear precursors for the lightly (2.5 mol% crosslinker) and tightly (20 mol% crosslinker) crosslinked nanoparticles together with their abbreviations.....	14
<b>Table 2.2.</b> Radius of gyration determined from a Guinier regression, Debye flexible polymer fit and hard sphere fit as well as the hydrodynamic radius for the various nanoparticles and their linear precursors in d-THF (SANS data) and THF (DLS data); concentration is 5 mg/ml and temperature is 35°C. Corresponding values with d-cyclohexane and cyclohexane as the solvents are provided in the Appendix (Table 2.4).	25
<b>Table 2.3:</b> The variation of Huggins and Kraemer coefficients with molecular weight for the 2.5% and 20% crosslinked nanoparticles in THF and cyclohexane, at 35°C. ....	40
<b>Table 2.4.</b> Radius of gyration determined from a Guinier regression, Debye flexible polymer fit, as well as the hydrodynamic radius for the various nanoparticles and their linear precursors in d-cyclohexane (SANS data) and cyclohexane (DLS data); concentration is 5 mg/ml and temperature is 35°C .....	42
<b>Table 2.5.</b> The shift factors as a function of temperature for linear polystyrene, lightly and tightly crosslinked nanoparticles.....	44
<b>Table 5.1.</b> Polystyrene materials used in this study. ....	85
<b>Table 5.2.</b> The plateau modulus for pure PS 393 kDa and its blends with various nanoparticles at 170°C .....	97
<b>Table 5.3.</b> The viscosity ratio, under terminal conditions, glass transition temperature and degree of confinement for the pure nanoparticles, linear polystyrenes and their blends.	104
<b>Table 7.1.</b> Design parameters for nanoparticle dispersion and producing multifunctional nanocomposites.....	141

## LIST OF FIGURES

<b>Figure 2.1.</b> Schematic representation of the intramolecular crosslinking process.....	15
<b>Figure 2.2.</b> Intrinsic viscosity normalized with the maximum value plotted against solubility parameter at 35°C. The data for the linear precursor (52.0kDa-20%-L, triangles) and the lightly crosslinked nanoparticles (60.1kDa-2.5%-X, squares) have been shifted by 2 and 1, respectively, from the tightly crosslinked nanoparticles' (52.0kDa-20%-X, circles) data.....	22
<b>Figure 2.3.</b> Scaling of the viscosimetric radius ( $R_h$ ) and the extrapolated hydrodynamic radius ( $R_{h0}$ ) with molecular mass. The data for the linear precursor (downward triangles) agrees well with that for polystyrene standards (upward triangles) while the lightly crosslinked (2.5% crosslinker, squares) and tightly crosslinked (20% crosslinker, circles) nanoparticles deviate significantly from the linear polymer scaling. However, neither approaches the scaling predicted for a sphere of density equal to that for bulk polystyrene. Example error bars are shown for the tightly crosslinked system.....	24
<b>Figure 2.4.</b> Burchard's $\rho$ -ratio (ratio of radius of gyration to hydrodynamic radius) variation for the lightly (2.5% crosslinked, circles) and tightly crosslinked (20% crosslinked, squares) nanoparticles with molecular mass in THF at 35°C. A non-draining hard sphere should have a value of 0.775 while a Gaussian coil has a range of values depending upon solvent conditions. The lightly crosslinked nanoparticles behave similar to coil while the tightly crosslinked nanoparticles approach the hard sphere limit, particularly at higher molecular weight. ....	28
<b>Figure 2.5.</b> Kratky plots for the lightly crosslinked (a) and the tightly crosslinked nanoparticles (b). A peak in the Kratky plot is indicative of particle-like behavior, while a plateau is expected for a Gaussian coil. ....	29
<b>Figure 2.6.</b> The glass transition temperatures for the lightly (a) and the tightly (b) crosslinked nanoparticles. The error bars represent the spread of the transition, indicating its beginning and end. ....	32
<b>Figure 2.7.</b> The complex viscosity as a function of frequency at 170°C, for the 3 arm polystyrene star and linear polystyrene (a), lightly crosslinked (b) and tightly crosslinked (c) nanoparticles. Increasing molecular mass and crosslink density causes an increase in the zero shear viscosity. A gel like behavior is evident for the high molecular mass, tightly crosslinked nanoparticles. (d) The zero shear viscosity as a function of molecular mass ( $M$ ) for polystyrene melts at 170°C. Data from Fox and Flory, <sup>64, 65</sup> Mackay and Henson <sup>99</sup> and Tuteja et al. <sup>96</sup> are used. The zero shear viscosities for the pure lightly and tightly crosslinked nanoparticles are also shown (a zero shear viscosity is not observed for the 52 kDa-20%-X and 135 kDa-20%-X NP's).....	34
<b>Figure 2.8.</b> The storage ( $G'$ ) and loss ( $G''$ ) modulus as a function of frequency for the 3 arm polystyrene star and linear polystyrene (a), lightly crosslinked (b) and tightly crosslinked (c) nanoparticles, at 170°C. A terminal zone behavior similar to linear	

polymers is evident for all of the lightly crosslinked nanoparticles, while a transition zone behavior similar to linear polymers is evident for both the lightly and tightly crosslinked nanoparticles. .... 36

**Figure 2.9.** Typical  $I$  ( $\text{cm}^{-1}$ ) versus  $q$  ( $\text{\AA}^{-1}$ ) graphs obtained after normalization of the SANS data in d-cyclohexane and d-THF. The data was obtained at  $35^\circ\text{C}$ , and the concentration was 5 mg/ml. The fits to the Debye function for the obtained data are also shown. .... 43

**Figure 3.1.** (a) Rapid precipitation of fullerene/polystyrene blends, followed by drying and melt processing allows manufacture of fibers. The fibers contains 1 wt%  $\text{C}_{60}$  fullerenes that were melt spun into long fibers with a diameter of *ca.* 1 mm. (b) Fullerene (1 wt%)/polystyrene blends developed through regular solvent evaporation produce large, phase separated domains which are not apparent in the fiber..... 49

**Figure 3.2.** (a) Cartoon showing branched, dendritic polyethylene. (b) TEM of a 4 wt% blend of dendritic polyethylene with 393 kDa linear polystyrene shows the individual polyethylene macromolecules with a size of order 20-30 nm. The  $R_g$  for the linear polystyrene is 17.4 nm and so is larger than the dendritic polyethylene. The inset shows a higher magnification. (c) Mixing with a smaller molecular mass polystyrene (75 kDa,  $R_g = 7.5$  nm) produces phase separation. Power law scattering of intensity ( $I$ ) versus wave vector ( $q$ ) is present at small wave vector for the lower mass polystyrene, whereas the higher mass system demonstrates miscibility without a power law region. The intensity profile can be fitted with a polydisperse sphere model yielding a mean radius (11.0 nm) for the dendritic polyethylene that agrees well with the TEM images. .... 51

**Figure 3.3.** (a) The polymer radius of gyration ( $R_g$ ), relative to that without nanoparticles ( $R_{g0}$ ), for three different molecular mass linear polystyrenes: 21, 63, 155 kDa, as a function of volume fraction ( $\phi$ ) of 52.0 kDa tightly crosslinked polystyrene nanoparticles. The nanoparticles clearly stretch the polymer chains. The solid line represents the radius of gyration variation if the polymer density does not change upon mixing, and the behavior  $[1+\phi]^{1/3}$  is expected. Instead, the data obeys  $1+c\phi$ , with  $c$  about one. (b) A polymer radius of gyration – nanoparticle radius phase diagram, with the filled circles representing data where phase separation was detected and the open circles where miscibility occurs. Open circles with an  $\times$  represent conditions where some agglomeration was detected by SANS, yet large scale phase separation was not observed. Squares are the  $\text{C}_{60}$ /polystyrene system; circles, the polystyrene nanoparticle/polystyrene system; and triangles, the dendritic polyethylene/polystyrene system. The dashed line represents the reptation tube radius suggesting phase stability does not depend on the entanglement structure. The nanoparticle fraction used to generate each data point was 2 wt%. (c) Cartoon illustrating that the attraction between pure nanoparticles is effective only over a fraction ( $A_C$ ) of the available surface area ( $A$ ) due to the limited range ( $\delta$ ) over which dispersion forces operate..... 55

**Figure 4.1.** Cartoon of the intramolecularly crosslinked nanoparticles produced from linear chain precursors having pendent crosslinking groups. Varying the amount of crosslinker allows fabrication of lightly (2.5 mol% crosslinker) or tightly

crosslinked (20 mol% crosslinker) nanoparticles. Nanoparticles were produced by dripping a solution into hot solvent to activate the crosslinking process. Typical conditions of volume ( $V$ ), concentration ( $c$ ), flow rate and temperature are given. .... 63

**Figure 4.2. SANS spectrum for lightly and tightly crosslinked nanoparticles demonstrating the particle-like nature of the nanoparticles when sufficient crosslinking is present. a,** Kratky plot of SANS intensity ( $I$ ) multiplied by wave vector ( $q$ ) squared as a function of  $q$  for solutions of linear precursor polymer or lightly crosslinked nanoparticle containing 2.5 mol% crosslinker. The lower concentration data of 2.5 wt% are for the 158 kDa linear chain precursor polymer and nanoparticle while the higher concentration curves, 5wt%, are for the precursor polymer and nanoparticle with 24.5kDa and 158 kDa nominal molecular masses. These data demonstrate the scattering from the lightly crosslinked nanoparticles is equivalent to a linear polymer. All data are in d-THF solvent and at 35°C. The plateau near  $0.2 \text{ \AA}^{-1}$  does not scale linearly with concentration due to concentration effects. **b,** Kratky plot for the tightly crosslinked nanoparticles containing 20 mol% crosslinker of various molecular masses (25.3kDa, 52kDa, 135kDa) compared to the linear chain precursors (curves labeled Linear). These nanoparticles demonstrate considerably different scattering behavior to the linear precursors with the curve maxima revealing particle-like behavior. Same solvent and temperature as in **a** were used, concentration is 5 wt%. The maximum does not significantly depend on the nanoparticle concentration..... 64

**Figure 4.3. SANS spectrum for 52.0 kDa tightly crosslinked nanoparticles blended with 63 kDa linear d-polystyrene at 50 wt% with the incoherent background subtracted from the intensity.** The solid line represents a hard sphere fit, including polydispersity, and a Lorentzian ( $I(0)/[1+\xi^2q^2]$ ,  $\xi = 29.5 \pm 0.2 \text{ nm}$  and  $I(0) = 623 \pm 7 \text{ cm}^{-1}$ ) to account for the deuterated polystyrene chains' conformation. The mean nanoparticle phase's radius from the hard sphere fit is  $2.66 \text{ nm} \pm 0.01 \text{ nm}$ , polydispersity (standard deviation divided by mean) is  $0.942 \pm 0.001$  and the volume fraction is 0.45. Power laws of 3 and 4 are shown, neither is satisfactory, suggesting that a fractal network is not present. The inset is a Kratky plot of the same data (solid line) compared to data for the same nanoparticles in dilute solution (0.05 wt% in THF at 35°C) demonstrating increased scatterer size. The intensity is in arbitrary units and the curves were shifted to overlap at high  $q$ . .... 67

**Figure 4.4. Viscosity and glass transition temperature for 52 kDa tightly crosslinked nanoparticles, 75 kDa linear polystyrene and their blends. a,** Viscosity versus frequency (measured with a Rheometrics ARES rheometer) for the neat nanoparticles (NP 52k), neat linear polystyrene (PS 75k) and selected blends containing 10 wt%, 50 wt% and 80 wt% nanoparticles. Note the pure nanoparticle system shows no terminal viscosity. Various temperatures were used and time-temperature superposition was followed, the reference temperature was 170°C. **b,** Terminal viscosity of the blends divided by neat 75 kDa linear polystyrene viscosity versus 52 kDa tightly crosslinked nanoparticle mass fraction. **c,** Glass transition temperature ( $T_g$ ) measured with differential scanning calorimetry (TA Instruments Q1000) for the blends showing a general decrease with nanoparticle addition up to moderate volume fractions. Note the  $T_g$  for the two pure components are equal. .... 70



**Figure 4.5** Graphs showing how the viscosity changes with temperature and nanoparticle concentration. **a**, Viscosity of 75 kDa neat polystyrene and nanoparticle blends as a function of  $T-T_g$ . Open circles are the viscosity for the neat polystyrene while the other symbols represent data for tightly crosslinked 52 kDa nanoparticles dispersed in the same polystyrene at various mass concentrations (5 – 80%). The measurement temperature range for all systems was 140 – 190°C with some extending down to 130°C. There is no clear trend with concentration and it is hypothesized that the viscosity is a unique function of distance from the glass transition temperature. **b**, Comparison of the lower concentration blends containing the tightly crosslinked 52 kDa nanoparticles in 75 kDa linear polystyrene (blue squares) and 393 kDa linear polystyrene (blue circles) at 170°C to the Einstein prediction. It is clear that a hydrodynamic contribution to the viscosity, in the contemporary sense, is not provided by the nanoparticles. To the contrary, addition of 1.6  $\mu\text{m}$  diameter crosslinked polystyrene microspheres shows the conventional viscosity increase with particle addition to 75 kDa linear polystyrene (white squares). ..... 74

**Figure 5.1.** Viscosity as a function of molecular mass ( $M$ ) for polystyrene melts at 170°C. Data from Fox and Flory<sup>2,3</sup>, Mackay and Henson<sup>5</sup> and this work are used to show how, below the critical molecular mass for entanglement coupling ( $M_c$ ) the Rouse model is followed, except from deviations caused by a free volume change. Above  $M_c$  the entangled regime results with a much larger power law exponent of viscosity with  $M$ . Changes in the entanglement structure or dynamics could reduce the viscosity to the Rouse limit. .... 79

**Figure 5.2.** (a) Neutron scattering intensity ( $I$ ) multiplied by the wave vector ( $q$ ) squared as a function of wave vector (Kratky plot) for 2 wt% 52 kDa NP blended with d-PS 155 kDa. The peak is associated with globular objects and the associated Schulz polydisperse hard sphere fit reasonably represents the data (mean radius of  $2.3 \pm 0.0_2$  nm with a radius spread of  $0.8 \pm 0.0_3$  nm). The other curve is the result of a simulation assuming a monodisperse system of spheres with a radius given by the Guinier result ( $4.0 \text{ nm} = \sqrt{(5/3) \times 3.1 \text{ nm}}$ ). (b) Log-log graph of intensity versus wave vector for the same system and the associated polydisperse hard sphere fit. .... 90

**Figure 5.3.** Viscosity ratio of the nanoparticle blends with respect to pure polystyrene, with polystyrene below (19.3 kDa) (a) and near (31.6 kDa) (b) the critical entanglement molecular mass at 170°C. The curves labeled theory are the values predicted by Batchelor's relation for this system, ending at the limit of the relation's applicability ( $\phi \sim 0.1$ ). It can be seen that the blend viscosity is much greater than the predicted value for the blend below  $M_c$ , however, when the polymer is near  $M_c$ , the viscosity hardly varies with addition of nanoparticles, again contradicting the Einstein and Batchelor predictions. .... 92

**Figure 5.4.** Viscosity ratio of the nanoparticle blends with respect to pure polystyrene for two different entangled systems, PS 75 kDa (a) and PS 393 kDa (b) at 170°C. The curves labeled theory are the values predicted by Batchelor's relation and these end at the limit of the relation's applicability ( $\phi \sim 0.1$ ). The viscosity falls precipitously when the radius of gyration is greater than the inter-particle half-gap for the entangled systems..... 94

**Figure 5.5.** (a) Complex viscosity as a function of frequency for PS 393 kDa, 52 kDa NP and their blends at 170°C. It can be seen that the pure nanoparticles display a gel like behavior with an infinite terminal viscosity. All the blends however have a distinct terminal viscosity which is lower than the pure component. (b) Storage modulus variation with frequency for the same systems at 170°C. Blends with a nanoparticle concentration below 10% have a plateau modulus equivalent to the virgin polymer while the 10% blend has a reduced modulus and complex viscosity at all frequencies..... 95

**Figure 5.6.** (a). Complex viscosity as a function of frequency for pure PS 393 kDa and its blends with 25 kDa NP at 170°C. In this case, the viscosity is decreased at all frequencies. A large viscosity reduction is apparent with just 1% addition of the nanoparticles. (b) Complex viscosity as a function of frequency for the blends of 135 kDa NP with PS 393 kDa also at 170°C. Here, only the terminal viscosity is reduced with nanoparticle addition until the concentration reaches 20%. .... 98

**Figure 5.7.** Complex viscosity (a) and storage modulus (b) data for pure PS 19.3 kDa and its blends with 52 kDa NP at 170°C. Both these properties increase at all frequencies upon nanoparticle addition. Same symbols used in each graph..... 99

**Figure 5.8.** Bulk density variation as a function of nanoparticle concentration for PS 19.3 kDa blends (a) and PS 393 kDa blends (b) at 25°C. For polymer molecular below  $M_c$ , the density increases, and when it is above  $M_c$ , the density decreases or remains constant, on nanoparticle addition..... 101

**Figure 5.9.** Relaxation spectra for pure PS 393 kDa and its blends with 52 kDa NP up to concentrations of up to 8% (a) and for a concentration of 10% (b). The Rouse, Plateau and Terminal regimes are also shown. It can be seen that the nanoparticles only affect the terminal regime, by reducing the longest relaxation time, at lower concentrations while at higher concentrations, a reduction occurs at all relaxation times. .... 102

**Figure 5.10.** Viscosity ratio of the nanoparticle blends with respect to pure polystyrene as a function of nanoparticle volume fraction, with different molecular weight linear polystyrenes' at 170°C: (a) 19.3 kDa, (b) 31.6 kDa, (c) 75 kDa, (d) 393 kDa. The curves labeled theory are the values predicted by Batchelor's relation for this system, ending at the limit of the relation's applicability ( $\phi \sim 0.1$ )..... 108

**Figure 6.1. Inorganic nanoparticles can be dispersed in polymer matrices by the process of rapid precipitation and cause a large reduction in the polymer melt viscosity.** a. TEM micrograph of a 38wt.% blend of oleic acid capped quantum dots dispersed in polystyrene (molecular mass 393kDa). The dispersion of inorganic nanoparticles is possible in polymers as long as the  $R_g$  of polymer > radius of nanoparticles. b. An optical picture of the QD-PS blend, showing the pink color of the blend. c. The complex viscosity as a function of frequency for pure PS and the PS-QD blend. The melt viscosity reduces by  $\sim 60\%$  on the addition of quantum dots even at this high weight loading, contradicting Einstein's prediction for a viscosity increase. d. A TEM micrograph of the 5 wt% blend of the magnetite nanoparticles in PS (molecular mass 393kDa). e. The complex viscosity as a function of frequency for pure PS and the

PS-magnetite nanoparticle blend. The addition of just 5 wt% of the magnetite nanoparticles causes ~ 90% reduction in the melt viscosity of pure polystyrene..... 112

**Figure 6.2. The diffusion coefficients of quantum dots and magnetite nanoparticles in PS (molecular mass 393 kDa).** **a.** A single frame (CCD image) obtained from the X-ray diffraction of the 5 wt% magnetite nanoparticles in PS. For each sample, 400-500 such frames were taken at each temperature, at intervals of 0.1 secs. **b.** Each frame was divided into equally spaced  $q$  regimes, based on their angular distance from the upper right hand corner of the frame (the centre of the X-ray beam). The scattering from these regimes was used to calculate the intensity-intensity autocorrelation function ( $g_2(q,t)$ ) using the mean  $q$  value from each regime. The data from 6 of those  $q$  values can be seen here ( $a$  is the radius of the nanoparticle = 5 nm; the sample is at 160°C). Each data set has been offset with respect to the previous data set by 0.2, starting from  $q \times a = 0.370$ , to allow for easier visibility (so the data set for  $q \times a = 0.370$  has been offset by 0.2, while the data set for  $q \times a = 0.998$  has been offset by 1). The data is then fitted to a single exponential (the solid blue line), to obtain  $\tau_r$  as a function of  $q$ . **c.** The ratio of the measured diffusion coefficient to the diffusion coefficient calculated from the SE relation for the quantum dots in PS. **d.** The same ratio for the magnetite nanoparticles in PS.... 117

**Figure 6.3. Addition of magnetite nanoparticles to 3-arm PS stars.** **a.** A TEM micrograph showing the dispersion of magnetite nanoparticles (2 wt%) in a 3 arm PS star (molecular mass of each arm ~ 108 kDa). **b.** The complex viscosity as a function of frequency for the pure 3 arm star as well as its blend with the magnetite nanoparticles. It can be seen that the addition of the nanoparticles causes a large increase in the viscosity of the star, in contrast to the viscosity decrease seen on the addition of the same nanoparticles to linear PS. **c.** The ratio of the measured diffusion coefficient (from XPCS data) to the diffusion coefficient from the SE relation. Even though the addition of the magnetite nanoparticles causes an increase in the melt viscosity, their diffusion coefficient is almost an order of magnitude higher than the prediction from the SE relation. .... 121

**Figure 7.1. It is possible to disperse fullerenes in polystyrene by rapid precipitation.** Fullerene-polystyrene nanocomposites developed through solvent evaporation produce large phase separated domains **a**, while rapid precipitation yields homogeneous blends that allow melt spinning of fibers **b**. The nanocomposites can also be compression molded to prepare free standing thin films as shown in the optical micrographs **c**, and **d**. Markings on the films are from the platens. .... 127

**Figure 7.2. Dispersion of 1 wt% fullerenes is possible, however, higher concentration mixtures tend to have slight phase separation with small crystallite formation.** **a.** Dispersion of 10 wt% fullerenes in 393 kDa polystyrene via rapid precipitation leads to a single (glass) transition of the nanocomposite (PS – 10 wt% C<sub>60</sub> RP) with a glass transition that is slightly greater than that for pure polystyrene (Pure 393 kDa PS). Pure fullerenes have a crystal structure transition around -15°C (Pure C<sub>60</sub>) which is absent in the nanocomposite produced by rapid precipitation, but is present in the phase separated film produced by solvent evaporation (PS – 10 wt% C<sub>60</sub> SE), as can be seen more clearly in the inset. **b.** The change in the polystyrene WAXS intensity

profile (Pure 393 kDa PS) with the addition of fullerenes for mixtures produced with rapid precipitation can be significant. At 5 and 10 wt% fullerenes (5 wt% RP and 10 wt% RP) evidence of a crystalline structure becomes clear while the amorphous halo for polystyrene is only slightly changed through addition of 1 wt% fullerenes (1 wt% RP). The lines at an intensity of 2000 are positions of the structure peaks seen for a fullerene single crystal plotted as a function of  $d$ -spacing. **c**, The WAXS intensity profiles, as a function of  $q$ -vector, for 10 wt% fullerene – polystyrene mixtures produced via rapid precipitation (PS – 10 wt% C<sub>60</sub> RP) and solvent evaporation (PS – 10 wt% C<sub>60</sub> SE) are vastly different with the latter showing low  $q$  scattering indicative of large scale phase separation. The data for the sample prepared by rapid precipitation agrees well with that for pure polystyrene (Pure 393 kDa PS) at low  $q$ -vector. **d**, A TEM micrograph for the 10 wt% fullerene mixture produced by rapid precipitation shows some phase separated crystallites. **e**, An electron diffraction pattern from a crystallite (present in a blend prepared by solvent evaporation) at room temperature demonstrating six-fold symmetry. **f**, Electron diffraction pattern from another crystallite, from the same sample, at -50°C.

..... 132

**Figure 7.3. Addition of fullerenes to linear polystyrene has multifunctional effects on the properties including a viscosity reduction, increase in dissipation, increase in degradation time and increase in conductivity.** **a**, The addition of fullerenes to polystyrene leads to a sharp decrease in the melt viscosity as long as the samples are prepared by rapid precipitation. This behavior directly contradicts Einstein's prediction (theory) of a viscosity increase in such a system. The inset shows the effect of fullerene addition on the viscosity of unentangled polystyrene ( $M_w = 19.3$  kDa). The blend was prepared by rapid precipitation. **b**, Minimal changes are seen in the storage ( $E'$ ) modulus on the addition of fullerenes while a five fold increase is observed in the loss ( $E''$ ) modulus, indicating a significant improvement in the damping properties of the composite. The samples are pure 393 kDa polystyrene (Pure 393 kDa PS) and the same polystyrene containing 50 wt% fullerenes produced by rapid precipitation (PS- 50 wt% C<sub>60</sub> RP). **c**, The addition of fullerenes, when well dispersed, greatly reduce the rate of thermal decomposition of the nanocomposite as shown by weight loss curves obtained by heating the samples to 330°C, under a nitrogen atmosphere. The samples containing 1 and 10 wt% C<sub>60</sub> samples were produced by rapid precipitation (labeled RP) and when compared to pure 393 kDa polystyrene (Pure 393 kDa PS) have a much greater time to degrade. For comparison, phase separated fullerenes perform much worse and a 10 wt% blend prepared by solvent evaporation (PS – 10 wt% C<sub>60</sub> SE) only slightly increases the degradation time. **d**, Conductivity of C<sub>60</sub> - 393 kDa polystyrene nanocomposites, relative to pure polystyrene. When fullerenes are well dispersed in polystyrene, prepared by rapid precipitation the conductivity rises above the Maxwell model prediction for an infinitely conducting particle. In comparison a sample containing phase separated structures produced by solvent evaporation has a relative conductivity that is ~ 90% lower than pure polystyrene. Conductivity was measured at a variety of frequencies and only the  $10^{-1}$ ,  $10^2$  and  $10^5$  Hz data are shown..... 139

**Figure 7.4. It is possible to disperse ferromagnetic nanoparticles in linear polystyrene (393 kDa) to make a ferromagnetic polymeric material.** **a**, Polystyrene is slightly colored by the dispersed magnetite nanoparticles which cause the sample to be

attracted to a permanent magnet. **b**, A TEM micrograph showing the nanoparticle dispersion with gross phase separation. **c**, Nanoparticle - polystyrene blends developed through solvent evaporation produce large phase separated domains. Also, as shown for the fullerene nanoparticles, the magnetite nanoparticles at 5 wt% reduce the amount of degradation (**d**) and the melt viscosity at all frequencies (**e**). The degradation experiment was performed at 330 °C under a nitrogen atmosphere and the viscosity was measured at multiple temperatures and shifted to a reference temperature of 170 °C. .... 142

# **CHAPTER 1**

## **INTRODUCTION**

---

Polymer composites are an important class of functional materials formed by the incorporation of useful organic/inorganic materials (filler) into the matrix of the host polymer. The composite produced aims to successfully combine the attractive electronic, optical or magnetic properties of the filler with the elasticity, film formation ability and processability of conventional polymers.

Recently, polymer–nanoparticle composite materials have attracted the interest from a variety of research groups. These materials offer the unique opportunity to synergistically combine the properties of the various components on a nanoscale, and have been used to provide enhanced mechanical,<sup>1</sup> electrical,<sup>1</sup> optical<sup>2, 3</sup> and thermal properties<sup>1,4</sup> both in solution and in bulk. These enhancements are induced by the physical presence of the nanoparticle, its degree of dispersion and by the interaction of the polymer with the particle.<sup>1,5, 6</sup> The biggest advantage of nanoparticles, as polymer additives, is their extremely large surface area per unit mass, as compared to traditional additives, which usually leads to low loading requirements. Efficient nanoparticle dispersion combined with good polymer–particle interfacial adhesion presents the exciting possibility of developing multifunctional<sup>7</sup> coatings and membranes.

In this project we attempt to provide a deeper understanding of first the various methods of creating nanocomposites and then detail the advantages of using nanoparticle filled polymeric systems over traditional composites. It was recently seen that the

addition of nanoscale fillers to materials can change various properties which cannot be accounted for using traditional models.<sup>8-10</sup> With the increased trend towards miniaturization in recent years, the need to understand the differences in the properties between micron sized or colloid filled bulk polymer systems and nanoparticle filled polymeric systems has greatly enhanced. To provide a better understanding of nanoparticle – polymer systems, we start out by studying the ideal system of polystyrene nanoparticles<sup>11</sup> blended with linear polystyrene.

In Chapter 2 of this thesis, we present the complete solution and rheological characterization of the above mentioned polystyrene nanoparticles. They were synthesized by the controlled intramolecular crosslinking of linear polymer chains to produce well defined single-molecule nanoparticles of varying molecular mass, corresponding directly to the original linear precursor chain.<sup>11</sup> These nanoparticles were also ideal to study the relaxation dynamics/processes of high molecular mass polymer melts,<sup>12</sup> as the high degree of intramolecular crosslinking potentially inhibits entanglements.<sup>13-16</sup> Both the nanoparticles and their linear analogs were first characterized by measuring their intrinsic viscosity, hydrodynamic radius ( $R_h$ ) and radius of gyration ( $R_g$ ).<sup>17, 18</sup> The ratio  $R_g/R_h$ <sup>19</sup> was computed to characterize the molecular architecture of the nanoparticles in solution, revealing a shift towards the constant density sphere limit with increasing crosslink density and molecular mass.<sup>20</sup> Further, confirming particulate behavior, Kratky plots obtained from neutron scattering data show a shift towards particle-like nature.<sup>18</sup> The rheological behavior of the particles was found to be strongly dependent on both the extent of intramolecular crosslinking and molecular mass, with a minimal viscosity change at low crosslinking levels and a gel-like behavior

evident for a large degree of crosslinking. These and other results suggest the presence of a secondary mode of polymer relaxation/movement besides reptation in these molecules, which in this case is influenced by the total number of crosslinked loops present in the nanoparticle.<sup>21, 22</sup>

In Chapter 3 of this thesis, we address the issue of miscibility between nanoparticles and polymers, with the objective of understanding the key parameters that enable nanoparticle dispersion.<sup>23</sup> Traditionally, the dispersion of particles in polymeric materials has proven difficult and frequently results in phase separation and agglomeration.<sup>24</sup> Contrary to the observation in colloid – polymer blends, recent simulations have shown that nanoparticles can slow down the phase separation of two incompatible polymers, suggesting the use of nanoparticles as compatibilizers in polymer blends.<sup>25</sup> There have also been some experimental studies on the dispersion / distribution of nanoparticles in polymer blends, suggesting enhanced miscibility of nanoparticles in polymers. For example, in our previous work we showed that 2.7 nm radius polystyrene nanoparticles<sup>8</sup> could be blended with linear polystyrene to large volume fraction ( $\phi \approx 0.5$ ) without the expected phase separation.

We show in this chapter that thermodynamically stable dispersion of nanoparticles into a polymeric liquid is enhanced for systems where the radius of gyration of the linear polymer is greater than the radius of the nanoparticle. Dispersed nanoparticles swell the linear polymer chains, resulting in a polymer radius of gyration which grows with the nanoparticle volume fraction. It is proposed that this entropically unfavorable process is offset by an enthalpy gain due to an increase in molecular contacts at dispersed nanoparticle surfaces, as compared to the surfaces of phase-separated



nanoparticles. It was also found that even when the dispersed state is thermodynamically stable,<sup>26</sup> it may be inaccessible unless the correct processing strategy<sup>8, 27</sup> is adopted, which is particularly important for the case of fullerene dispersion into linear polymers.<sup>28,</sup>

29

With this understanding of nanoparticle dispersion in polymers, we move towards the potential applications of the produced nanocomposites and extend our work by first looking at their rheological properties. To minimize extraneous enthalpic or other effects,<sup>8</sup> the polystyrene nanoparticles<sup>11</sup> (characterized in Chapter 2), were blended with linear polystyrene macromolecules. Nanoparticles have been demonstrated to influence mechanical properties of polymers;<sup>30-32</sup> however, transport properties such as viscosity have not been adequately studied. This may be due to the common observation that particle addition to liquids produces a viscosity increase, even in polymeric liquids, as predicted by Einstein nearly a century ago.<sup>33</sup> Yet, confinement and surface effects provided by nanoparticles have been shown to produce conformational changes to polymer molecules and so it is expected that nanoparticles will affect the macroscopic viscosity. Remarkably, the addition of polystyrene nanoparticles to linear polystyrene was found to decrease the blend viscosity and scale with the free volume change introduced by the nanoparticles and not with entanglement reduction. Indeed, the entanglements did not appear to be affected at all, suggesting unusual polymer dynamics. These and other rheological results have been discussed in detail in Chapter 4.

In Chapter 5, we extend our work on the study of the rheological properties of polystyrene nanoparticles - linear polystyrene blends. First, homogeneous blends are developed based on our understanding of the key parameters for nanoparticle dispersion<sup>34</sup>

(Chapter 3) and next the dispersion in the blends is confirmed through small angle neutron scattering (SANS) experiments.<sup>18</sup> In Chapter 4 we discussed that nanoparticles can reduce the viscosity of high molecular mass linear PS. On extending our work to lower nanoparticle concentrations, we find that the confinement of entangled polymers is necessary for the viscosity reduction since lower concentrations provide a viscosity increase. Further, the viscosity behavior is found to be dependent on the presence or absence of entanglements, and confinement is seemingly not important for unentangled polymers. It is proposed that constraint release<sup>15, 35</sup> caused by the addition of nanoparticles is responsible for some of the observed changes in viscosity although it is suspected that the introduction of free volume by the nanoparticles is certain to play a key role.

The possibility that constraint release might be an important factor causing the reduction in viscosity is discussed further in Chapter 6. The knowledge of the translational diffusion coefficient of nanoparticles is extremely useful for a variety of fields. First, various research groups have investigated the kinetics for the directed and self assembly of nanoparticles<sup>23, 36-38</sup> and bionanoparticles<sup>39, 40</sup> in polymer matrices of natural and synthetic origin. Any study targeting the assembly of nanostructures requires an understanding of the nanoparticle dynamics, spatial arrangement and ordering kinetics in the polymer matrix, thus requiring the knowledge of the translational diffusion coefficient of the nanoparticles. Further, with the development of new techniques like microrheology,<sup>41, 42</sup> the direct measurement of the diffusion coefficient of nanoparticles has become critical for experimental planning and data interpretation. Also, as stated above, the surprising viscosity decrease in entangled polymers on the addition of

nanoparticles is expected to be related the diffusion of nanoparticles in the polymer matrices. In this chapter we report the first successful, direct measurements of the translational diffusion coefficients of different inorganic nanoparticles dispersed in entangled polymer matrices, using X-ray photon correlation spectroscopy (XPCS).<sup>43, 44</sup> The diffusion coefficients of the nanoparticles were found to be as much as 100 times faster than predictions from the continuum Stokes - Einstein relation based on the measured viscosity of the polymer. We hypothesize that the extremely fast diffusion coefficients contribute to the observed reduction in viscosity of nanoparticle-linear polymer blends that we have found, by providing a faster mode for polymer relaxation. The nanoparticle dynamics is sure to influence the usual kinetics of self assembly as well as the transport properties, which we exemplify through the viscosity.

Finally, in Chapter 7, again with our understanding the important parameters for the dispersion of nanoparticles (Chapter 3), we study different nanoparticle – polymer systems with the final aim of producing multifunctional nanocomposites. As we stated before, nanomaterials hold the promise of providing new properties that exceed traditional material performance. However, in many instances, significant improvements in material properties of nanocomposites have not been achieved as yet,<sup>7, 45, 46</sup> mainly because the factors affecting nanoparticle dispersion are poorly understood.<sup>47</sup> We study first the dispersion of fullerenes ( $C_{60}$ , diameter  $\sim 0.7$  nm) into polystyrene and show that their incorporation into the polymer matrix is possible by employing the rapid precipitation technique.<sup>34, 48</sup> The addition of fullerenes in this manner simultaneously leads to better processability (reduction in viscosity of up to 80%, contrary to Einstein's prediction),<sup>48, 49</sup> higher electrical conductivity (greater than Maxwell's prediction),<sup>50</sup>

improved mechanical damping and enhanced thermal stability, leading to a first truly ‘multifunctional’ nanocomposite.<sup>7</sup> Our study is then extended by utilizing rapid precipitation as a tool for dispersing an inorganic filler (magnetite nanoparticles) into the polystyrene matrix. The addition of these nanoparticles, apart from making the nanocomposite ferromagnetic, also reduces the viscosity by ~ 90% while simultaneously enhancing the nanocomposite thermal stability. These observations suggest the exciting possibility of manufacturing materials with desired electrical or magnetic properties, coupled with enhanced thermal stability and a reduced viscosity enabling easier and faster processing using existing industrial technologies.

### **Research Objectives**

The two major objectives of this research are to understand the fundamental factors affecting the miscibility / dispersion and flow properties of nanoparticle – polymer systems. We start out by studying the ideal<sup>51</sup> system of polystyrene nanoparticles being added to polystyrene. After understanding the basic factors affecting the miscibility in this system, we extend our work to study a wide variety of organic and inorganic nanoparticles blended with various polymers. The final goal of the work is to apply this acquired knowledge to create multifunctional nanocomposites, having enhanced thermal, mechanical and rheological properties.

A summary of the specific objectives in this work is as follows:

1. Characterize the intramolecularly crosslinked polystyrene nanoparticles in solution to determine the effect of crosslinking on their molecular architecture and rigidity.
2. Examine in detail the various factors affecting the miscibility and phase stability in nanoparticle-polymer systems.
3. Determine the effects of nanoparticle addition on the rheological properties of various nanoparticle - polymer blends.
4. Test the hypothesis that the unusual viscosity decrease seen for various nanoparticle – polymer blends is related to the diffusion of the nanoparticles within the polymer matrix by measuring the diffusion coefficients of various nanoparticles in an entangled polymer matrix and comparing them with the predictions from the Stokes – Einstein relation.
5. Create multifunctional nanocomposites with the understanding of the various factors affecting nanoparticle dispersion and flow properties. These composites have the specific optical, electric or magnetic properties required for an application, and are coupled with enhanced mechanical, thermal and flow properties.

## CHAPTER 2

# THE MOLECULAR ARCHITECTURE AND RHEOLOGICAL CHARACTERIZATION OF NOVEL INTRAMOLECULARLY CROSSLINKED POLYSTYRENE NANOPARTICLES

---

### Introduction

There has been a phenomenal growth of interest in the development and study of nanomaterials due to the many unusual and unique effects that can only be seen in this size range. Nanoparticles serve the role of being an important building block for the production of nanomaterials with a broad range of future and present applications in electronic, mechanical, and biomedical processes.<sup>52</sup>

Various polymer particles with size ranging from 50 nm to several microns are now commercially available; however, the synthesis and study of smaller polymeric nanoparticles still remains a challenge. In this work, we characterize unimolecular, organic (polystyrene) nanoparticles produced by the intramolecular crosslinking of functional polymers, having sizes ranging from 3-15 nm. These molecules are then used to discern the various modes of relaxation in both low and high molecular mass polymers as a function of crosslink density.

The synthesis<sup>11</sup> of the nanoparticles was accomplished by first incorporating the crosslinking agent 4-vinylbenzocyclobutene (denoted as BCB in Fig. 2.1) into the linear polystyrene chain as a comonomer, and subsequently collapsing the chain under ultra-dilute conditions by intramolecular crosslinking. The extent of crosslinking within the nanoparticles produced by this method can therefore be controlled by the amount of crosslinker that is copolymerized within the linear polymer.

Considerable work has been done previously to initiate intramolecular crosslinking within polymers and then to measure the effects of this crosslinking on the polymer properties in solution. Kuhn and Balmer<sup>53</sup> carried out crosslinking in an aqueous solution of poly(vinyl alcohol) by the addition of terephthalaldehyde, and then studied the intrinsic viscosity behavior of the crosslinked polymer as a function of increasing solution concentration of the starting monomer. They found that when the monomer concentration was low, the intrinsic viscosity of the solution decreased indicating a decrease in polymer size because of intramolecular crosslinking; however, at higher monomer concentrations the intrinsic viscosity increased, indicating intermolecular crosslinking. Also, Longi et al.<sup>54</sup> synthesized intramolecularly crosslinked styrene - methyl acrylate copolymers and found that the intrinsic viscosity decreased in proportion to the number of crosslinks per polymer.

Research in this area was furthered by Martin and Eichinger<sup>55, 56</sup> who conducted the first complete theoretical and experimental analysis to determine the change in the unperturbed radius of gyration ( $R_{g0}(\theta)$ ) of a linear coil caused by intramolecular crosslinking. First, they developed a method to determine  $R_{g0}(\theta)$  by assuming that the crosslinked polymer consists of a number of sub-polymer Gaussian chains. Eichinger<sup>57</sup> had found earlier that  $R_{g0}(\theta)$  for any Gaussian chain can be computed by finding its Kirchhoff matrix and its generalized inverse. Thus, the unperturbed dimensions of the whole molecule could be computed, as the sum of its parts. Using this analysis, for an intramolecularly crosslinked polymer chain, the Zimm-Stockmayer contraction factor ( $g$ ) is given as

$$g = 1 - 0.7\rho_x^{0.5} \quad (2.1)$$

where  $g$  is the ratio of  $R_{g0}(\theta)^2$  for the crosslinked molecule to that of the equivalent linear chain and  $\rho_x$  is the crosslink density defined as the moles of crosslinks per mole of Gaussian statistical segments.

To confirm their theoretical analysis, they produced intramolecularly crosslinked polystyrene using a Friedel-Crafts crosslinking reaction, with (dichloromethyl)benzene as the crosslinking agent. The change in the molecules' hydrodynamic radii ( $R_h$ ), caused by the crosslinking, was then experimentally measured by means of photon correlation spectroscopy (dynamic light scattering). The results were related to the Zimm-Stockmayer contraction factor by the relation

$$h = \sqrt{g} \quad (2.2)$$

where  $h$  is the ratio of  $R_{ho}(\theta)$  for the crosslinked particle to that for the linear chain and  $R_{ho}(\theta)$  is the unperturbed hydrodynamic radius. Indeed they found close agreement between the observed unperturbed dimensions of the crosslinked molecules and their theoretical predictions.

Our systems differ from theirs primarily due to the extent of intramolecular crosslinking induced in polystyrene. The most heavily crosslinked polystyrene used by Martin and Eichinger had 100 crosslinks per molecule which amounts to 1 in every 48 monomer units on average being crosslinked (mention of a more tightly crosslinked sample is given in a table, yet, no data are presented on this system). In contrast, even the lightly crosslinked polystyrene synthesized in this study has 1 in 40 monomer units on average crosslinked, whereas the more tightly crosslinked molecule has 1 in every 5 monomer units crosslinked.



At this point it is important to mention the significant work done by Antonietti et al. in the development and rheological characterization of intramolecularly crosslinked polystyrene microgels. Apart from detailing the clever techniques employed by the authors to synthesize and characterize the microgels,<sup>58-61</sup> their work also provides a descriptive introduction to the rheological behavior of intramolecularly crosslinked particles.<sup>12, 62</sup> Comparison between these studies and the present work is however reserved for the results and discussion section and next we provide a brief introduction to the mechanism of chain motion in polymer melts.

The terminal viscosity of polymer melts is a strong function of the polymer molecular mass ( $M$ ). Below the so called critical mass for *entanglement coupling*<sup>13</sup> ( $M_c$ ) the viscosity scales as  $M^1$  while above  $M_c$  a much larger power law, approximately 3.4-3.8 power,<sup>63-65</sup> is present. This steep increase of viscosity above  $M_c$  is attributed to the presence of entanglements, which are basically constraints on the motion of polymer chains caused by the fact that the chains cannot pass through each other. Such a geometrically constrained environment thus limits molecular motion/diffusion of the chain to a snake like motion along its own contour,<sup>66</sup> denoted as reptation.<sup>67</sup>

The reptation model has been very useful in providing a mechanistic understanding of bulk polymer dynamics, as well as in providing a quantitative explanation of the plateau modulus, diffusion coefficient and scaling of viscosity with molecular mass (in its native form the theory predicts a power law as 3 instead of 3.4). However, results from many computer simulations and experiments<sup>68</sup> on widely differing systems (for example ring polymers,<sup>69</sup> star polymers,<sup>70, 71</sup> crosslinked microgels,<sup>12</sup> block copolymers<sup>72</sup> and polymer blends<sup>73-75</sup>) do not match reptation predictions, clearly

demonstrating that the model doesn't provide a complete understanding of all the diffusion or molecular motions in high molecular mass polymer melts, at least in its present form. The nanoparticles considered in this work are ideal for discerning the presence of other mobility mechanism besides reptation as the high degree of intramolecular crosslinking minimizes chain entanglements (the network chains/loops are too short), even for the high molecular mass nanoparticles.

The nanoparticles<sup>11</sup> considered here were found to produce anomalous flow behavior when blended with linear polymer.<sup>76</sup> Yet, this behavior depended strongly on the degree of crosslinking with light crosslinking producing no unusual effect while tight crosslinking yielded unusual rheological behavior. The purpose of the present work is thus two fold; to characterize these unique nanoparticles in dilute solution to determine their molecular architecture and to study the dynamics of polymer relaxation in this novel and ideal system as a function of that architecture.

## **Experimental**

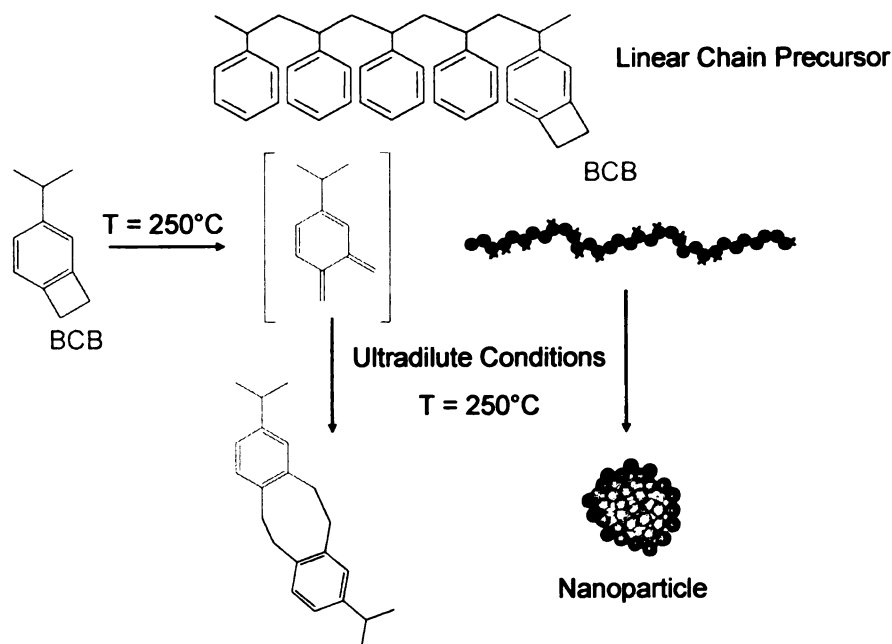
**Materials.** The synthesis of the nanoparticles and their linear analogs has been discussed previously.<sup>11</sup> Table 2.1 shows the molecular masses and polydispersity indexes (PDI = weight to number average molecular mass ratio) of the linear precursors for the **lightly** (2.5 mol% crosslinker) and **tightly** (20 mol% crosslinker) crosslinked nanoparticles used in this study together with abbreviations. The molecular weights were determined using Gel permeation chromatography relative to linear polystyrene standards. All polymers were dissolved in tetrahydrofuran (THF) and passed through a

Waters chromatograph equipped with four 5- $\mu$ m Waters columns (300 mm  $\times$  7.7 mm) connected in series with increasing pore size (100, 1000, 100,000, 1,000,000 Å).

**Table 2.1.** Number average molecular masses ( $M_n$ ) and polydispersity index (PDI) of the linear precursors for the lightly (2.5 mol% crosslinker) and tightly (20 mol% crosslinker) crosslinked nanoparticles together with their abbreviations.

$M_n$ (kDa)	% crosslinker (mol%)	PDI	Abbreviation if linear (crosslinked)
24.5	2.5	1.14	24.5kDa-2.5%-L (-X)
60.1	2.5	1.16	60.1kDa-2.5%-L (-X)
158	2.5	1.40	158kDa-2.5%-L (-X)
25.3	20	1.08	25.3kDa-20%-L (-X)
52.0	20	1.18	52.0kDa-20%-L (-X)
135	20	1.20	135kDa-20%-L (-X)

Figure 2.1 illustrates the crosslinking process. The linear precursors are first dissolved in an excess of benzyl ether (BCB concentration  $\sim$  0.2 M) and then this solution is added drop wise to a reservoir of hot benzyl ether. The high temperature ( $T = 250^\circ\text{C}$ ) initiates the crosslinking process and the ultra-dilute conditions (final BCB concentration  $\sim$  0.05 M) ensure that intermolecular crosslinking is minimized. Thus, the crosslinked nanoparticles potentially have the same molecular mass as the linear precursors. All the solvents were purchased from Sigma-Aldrich and used as received.



**Images in this dissertation are presented in color.**

**Figure 2.1.** Schematic representation of the intramolecular crosslinking process.

**Intrinsic viscosity.** The solutions for the measurement of intrinsic viscosity were prepared at least 1 day before the measurement by dissolving the polymer in pure solvent. Before usage, the solution was filtered with a  $1\mu\text{m}$  filter to remove any undissolved impurities. The intrinsic viscosity was calculated by measuring the density of the solution, the flow time in a Cannon–Manning Semi-Micro viscometer (size 75) of the pure solvent and the solution, and the concentration of the solution. The measurements were made at low shear rates (typical flow times were close to 200 seconds), with four different concentrations, at a constant temperature of  $35^{\circ}\text{C}$ . The data obtained was then analyzed using the two leading terms in the Huggins<sup>77</sup> and Kraemer<sup>78</sup> relations

$$\eta_{sp}/c = [\eta] + k_h [\eta]^2 c + \dots \quad (2.3.a)$$

and

$$\ln(\eta_{\text{rel}})/c = [\eta] - k_k [\eta]^2 c + \dots \quad (2.3.b)$$

where  $\eta_{\text{sp}}$  is the specific viscosity ( $[\eta_{\text{solution}} - \eta_{\text{solvent}}] / \eta_{\text{solvent}}$ ),  $\eta_{\text{rel}}$ , the relative viscosity ( $\eta_{\text{solution}} / \eta_{\text{solvent}}$ ),  $[\eta]$ , the intrinsic viscosity,  $c$ , the polymer concentration (g-polymer / mL-solution) and  $k_h$  and  $k_k$ , the Huggins and Kraemer coefficients (the values for these constants in THF and cyclohexane are given in appendix, Table 2.3), respectively. The  $[\eta]$  values obtained from both these relations agreed within  $\pm 2\%$ , therefore, only the  $[\eta]$  values obtained from the Huggins relation are reported in this paper.

For each of the different polymer nanoparticles and their linear analogs, the intrinsic viscosity was measured in 5 different solvents. Each solvent had a different solubility parameter ( $\delta$  in  $(\text{cal}/\text{cm}^3)^{1/2}$  at  $25^\circ\text{C}$ ) shown in parentheses: cyclohexane (8.2), toluene (8.9), tetrahydrofuran (THF, 9.1), benzene (9.2) and chloroform (9.3).<sup>79</sup>

**Light scattering.** The hydrodynamic radius ( $R_h$ ) was measured using a Protein-Solutions Dynapro dynamic light scattering (DLS) instrument. In the instrument, fluctuations in the intensity of the scattered light are related to the diffusion coefficient of the molecules ( $D_\theta$ ). Then,  $R_h$  is calculated from the diffusion coefficient using the Stokes-Einstein relation<sup>33</sup>

$$D_\theta = \frac{k_B T}{6\pi\eta_{\text{solvent}} R_h} \quad (2.4)$$

where  $k_B$  is the Boltzman constant and  $T$ , temperature. Thus, the  $R_h$  obtained from DLS data is the size of a spherical particle that would have a diffusion coefficient equivalent to that of the molecule tested.<sup>80</sup>

Again, all the solutions used for dynamic light scattering were prepared at least one day before the measurement and filtered with a  $0.1\mu\text{m}$  filter to remove any

undissolved impurities. To compare with the intrinsic viscosity measurements, all experiments were performed at 35°C. Further, as  $R_h$  is a function of concentration<sup>81-83</sup> the extrapolated value to zero concentration ( $R_{h0}$ ) was used and determined as described in the Appendix.

**Neutron scattering.** The small angle neutron scattering (SANS) measurements were carried out using the 30m NG3 and NG7 SANS instruments at the National Institute of Standards and Technology (NIST), Centre for Neutron Research (NCNR) in Gaithersburg, MD. Two instrument configurations were used. The first had five guides, a sample to detector distance of 600 cm with a 25cm detector offset, giving a scattering vector ( $q$ ) range of 0.0084-0.1136 Å<sup>-1</sup>. The second configuration also had five guides, a sample to detector distance of 135 cm with a 25 cm detector offset, giving a  $q$  range of 0.018-0.47 Å<sup>-1</sup>. Both configurations had a neutron wavelength of 6 Å with a 15% spread. All the measurements were performed at 35°C, in deuterated solvents. The use of deuterated solvents greatly reduces the scattering time required for each solution by significantly enhancing the scattering contrast, even though this might slightly affect the polymer-solvent interactions. Several concentrations were used to examine the effect of concentration on  $R_g$  to determine the extrapolated value ( $R_{g0}$ ). The modified Zimm analysis we used to account for this effect is provided in the Appendix for this chapter.

**Kratky and Guinier plots.** Further quantification of the molecular characteristics can be gleaned through careful consideration of neutron scattering data. The Debye function<sup>17</sup> is used to characterize polymer chains in the theta condition (second virial coefficient,  $A_2 = 0$ ) and can describe scattering from polymer molecules in a good solvent. The scattering intensity (or differential cross-section)  $I(q)$  is given as<sup>18,12</sup>

$$I(q) = \phi \times V(\Delta\rho)^2 \left\{ 2(\exp(-(qR_g)^2) + (qR_g)^2 - 1)/(qR_g)^4 \right\} \quad (2.5)$$

Here,  $\phi$  is the volume fraction of scattering centers,  $V$ , the volume of a single scattering center,  $(\Delta\rho)^2$ , the difference in the scattering length densities between solvent and scatterer (or the contrast) and  $q$ , the scattering vector ( $4\pi/\lambda \times \sin(\theta/2)$ ;  $\theta$  is the scattering angle and  $\lambda$ , the neutron wavelength.). The term in the curly brackets is the form factor ( $P(q)$ ) that describes how  $I(q)$  is modulated by neutron interference effects from the different parts of the same scattering center. In the high  $q$  limit, eq 2.5 reduces to

$$I(q) \times q^2 = 2\phi \times V(\Delta\rho)^2 / (R_g^2) \quad (2.6)$$

For a given sample,  $\phi$ ,  $V$ ,  $\Delta\rho$ ,  $R_g$  are constant, thus, from eqs 2.5 and 2.6, a plot of  $I(q) \times q^2$  versus  $q$  should asymptotically approach a plateau value at high  $q$  values for a Gaussian coil and is known as a Kratky plot. Deviations from the asymptotic behavior in the Kratky plot can be used as an indicator of the segment distribution within the system. Both ring and star polymers have a peak (maximum) prior to the asymptote revealing different distributions than linear polymers.<sup>84</sup> Indeed a gel-like crosslinked polymer nanoparticle has a large peak.<sup>85</sup> However, the high  $q$  limit is still a constant asymptote as Gaussian chains are present between the robust crosslinks. Finally a constant density sphere has no plateau and a series of ever decreasing peaks is seen. Thus, the Kratky plot shape is a good indicator of the molecular architecture and is used by us to infer particle-like nature.

In the low  $q$  scattering range, one can use the Guinier approximation, when  $q \times R_g$  is small ( $\ll 1$ ), and the scattering function can be written as

$$\log I(q) = \log I(0) - \frac{(qR_g)^2}{3} \quad (2.7)$$

where  $I(0)$  is given by  $\phi V(\Delta\rho)^2$ . The Guinier plot,<sup>86</sup>  $\log(I(q))$  versus  $q^2$ , allows determination of  $R_g$  and, further, can be used as a concentration check through the neutron intensity at zero wave vector.

**Burchard's  $\rho$ -ratio.** An extremely useful, quantitative indicator of the molecular conformation and the segment density within a polymer molecule is Burchard's  $\rho$ -ratio<sup>19</sup> which requires SANS (or other scattering) as well as hydrodynamic data. This ratio can be computed from the molecular architecture of the molecule without the knowledge of chemical details and is given by

$$\rho = R_{g0} / R_{h0} \quad (2.8)$$

The radius of gyration of a molecule is intimately related to the segment density variation  $\rho(r)$  within the molecule (where  $r$  is the radial distance from the centre of mass). For a spherical architecture one finds,

$$R_g^2 = \left( \int_0^R r^4 \rho(r) dr \right) / \left( \int_0^R r^2 \rho(r) dr \right) \quad (2.9)$$

where  $R$  is the radius of the sphere. Since a hard sphere is non-draining, one has  $R = R_{h0}$  and finds  $\rho = \sqrt{3/5} \approx 0.775$  while Gaussian coils have  $\rho = 1.2 - 1.6$  depending on solvent conditions.<sup>20</sup>

**Differential scanning calorimetry (DSC) measurements.** A TA instruments Q-1000 DSC was used to perform all glass transition ( $T_g$ ) measurements. All of the samples were subjected to at least three heating - cooling cycles, where each cycle consisted of heating the sample from 0°C – 200°C, at a rate of 5°C / min, followed by cooling back to 0°C, also at 5°C / min. The inflection point for the heat flow as a function of temperature



was taken as the glass transition temperature for a particular cycle. The glass transition temperatures reported in this work are the mean of the glass transition temperatures obtained from the second and the third run cycle.

**Rheology measurements.** The nanoparticles were molded by compression, under vacuum, in a pellet press (8 mm diameter) to ensure that no trapped air remained in the sample. The samples were then aged at 130–170°C, under vacuum, for several hours. The 8-mm diameter discs obtained from the pellet press were placed on the 8-mm parallel plates fixture of a Rheometrics ARES rheometer set at a gap of approximately 0.4 mm. Measurements were done in the dynamic (oscillatory) mode. Frequency sweeps in the range 0.1-100 rad/sec were performed at various temperatures (130°C-230°C). These were then combined using time-temperature superposition<sup>87</sup> to yield a master curve at 170°C (all quoted temperatures refer to the surface temperature of the lower plate).

## **Results and Discussion**

**Hydrodynamic Properties.** The utility of dilute solution viscosity measurements is well known,<sup>88</sup> more recently, Burchard<sup>19</sup> illustrates the importance of studying dilute solutions with a variety of techniques to fully understand a given system. Further, the polymer volume change with solvent under dilute conditions is a good indicator of the polymer – solvent thermodynamic interaction<sup>26</sup> which may be dependent on molecular architecture. The solvent in which the polymer has the greatest intrinsic viscosity (highest volume) is assumed to have the same solubility parameter as the polymer.<sup>89</sup> This method

allows determination of the best solvent for the polymer as well as the change in the molecular volume with solvent type.

Fig. 2.2 shows the intrinsic viscosity variation as a function of the solvent solubility parameter for the 52.0 kDa tightly crosslinked nanoparticle and linear analog as well as the 60.1 kDa lightly crosslinked nanoparticle. The intrinsic viscosity is made into a dimensionless ratio by the maximum intrinsic viscosity to compare the relative change in volume for each polymer.

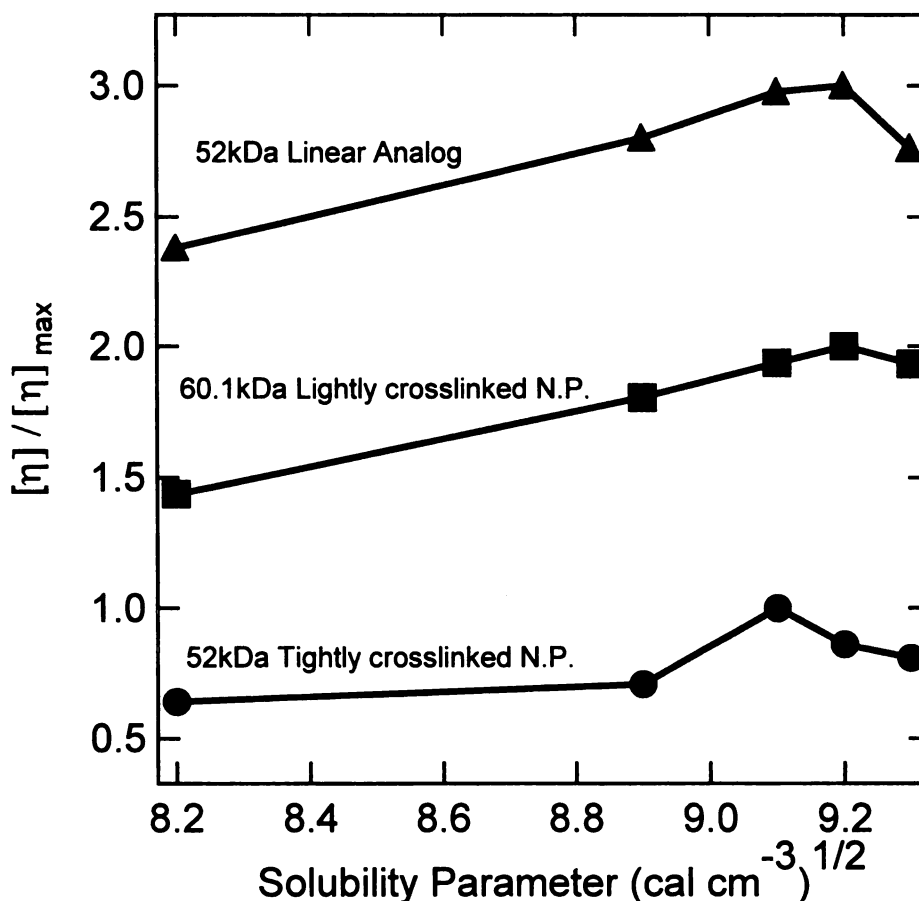


**Figure 2.2.** Intrinsic viscosity normalized with the maximum value plotted against solubility parameter at 35°C. The data for the linear precursor (52.0kDa-20%-L, triangles) and the lightly crosslinked nanoparticles (60.1kDa-2.5%-X, squares) have been

shifted by 2 and 1, respectively, from the tightly crosslinked nanoparticles' (52.0kDa-20%-X, circles) data.

It can be seen that the relative intrinsic viscosity for the tightly crosslinked nanoparticles varies between 0.64 (cyclohexane) and 1 (THF) while for the lightly crosslinked nanoparticles, it varies between 0.44 (cyclohexane) and 1 (benzene). On the other hand, for the linear precursors of the tightly crosslinked nanoparticles, it varies between 0.38 (cyclohexane) and 1 (benzene) revealing that the tightly crosslinked nanoparticles do not expand or contract as much as the lightly crosslinked particles or its linear analog.

Also, the linear analog and the lightly crosslinked 60.1 kDa nanoparticle have a maximum at a solubility parameter of  $9.2 \text{ (cal/cc)}^{1/2}$  (benzene), while the tightly crosslinked particle has a maximum at  $9.1 \text{ (cal/cc)}^{1/2}$  (THF). So the degree of crosslinking has a slight effect on the polymer solubility parameter and hence the thermodynamic interactions between the nanoparticles and the solvents. However, these results clearly indicate that the solubility parameter for all the systems is quite close to that frequently quoted for linear polystyrene ( $9.1 - 9.2 \text{ (cal/cm}^3)^{1/2}$ ).<sup>79</sup>

When the viscosimetric radius was determined from the intrinsic viscosity ( $R_\eta$ )<sup>26</sup> and compared to the hydrodynamic radius, we found little difference. In Fig. 2.3, the variation of the hydrodynamic radius with molecular mass in THF is shown for the lightly crosslinked nanoparticles, tightly crosslinked nanoparticles and their linear analogs. The viscosimetric radius for polystyrene standards (Scientific Polymer Products) in THF is also shown. It can be seen that the linear analog has radius values within experimental error to pure polystyrene indicating that the linear analog does indeed

behave similarly to linear polystyrene. It can also be seen that the nanoparticles radius decreases with increasing crosslink density, with the linear analog being the largest and the tightly crosslinked nanoparticles the smallest in size. This suggests that, as may be expected, intramolecular crosslinking causes a collapse of the linear polymer chain. Also shown is the scaling for a constant density sphere, of equal density to bulk polystyrene, showing that the tightly crosslinked nanoparticles are not exactly equivalent to hard spheres when in solution.

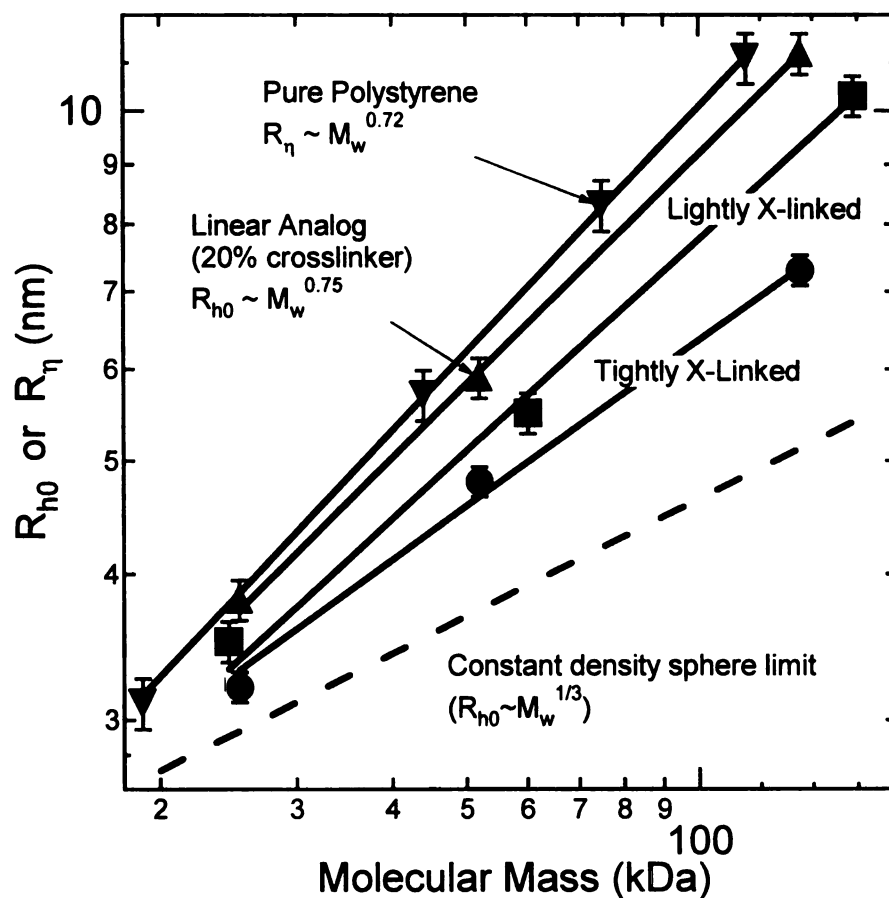


**Figure 2.3.** Scaling of the viscosimetric radius ( $R_h$ ) and the extrapolated hydrodynamic radius ( $R_{h0}$ ) with molecular mass. The data for the linear precursor (downward triangles) agrees well with that for polystyrene standards (upward triangles) while the lightly crosslinked (2.5% crosslinker, squares) and tightly crosslinked (20% crosslinker, circles) nanoparticles deviate significantly from the linear polymer scaling. However, neither

approaches the scaling predicted for a sphere of density equal to that for bulk polystyrene. Example error bars are shown for the tightly crosslinked system.

**Neutron scattering.** Small angle neutron scattering (SANS) was used to measure the radius of gyration of the particles in solution (due to a paucity of scattering time, measurements were carried out in d-THF (deuterated THF) and d-cyclohexane only). The raw SANS data was reduced to an absolute scale ( $I$  ( $\text{cm}^{-1}$ ) versus  $q$  ( $\text{\AA}^{-1}$ )) using the standard NIST procedure (Typical  $I$  ( $\text{cm}^{-1}$ ) versus  $q$  ( $\text{\AA}^{-1}$ ) graphs obtained after normalization have been shown in the appendix, Fig. 2.9). To determine the molecular size (radius of gyration), each absolute data set was then analyzed by fitting to both the Debye equation (Gaussian coil fit) as well as the hard sphere form factor. The fits obtained from both these equations were compared with the  $R_g$  values obtained from the Guinier plots. The fitting results for the Gaussian coil model (typical fits of the data with the Debye model have been shown in the appendix, Fig. 2.9), hard sphere model as well as the Guinier radii for the samples in d-THF, are given in Table 2.2.

It can be seen that the Guinier fits for the lightly crosslinked nanoparticles and the linear analogs compare well with the fits obtained from the Debye equation for flexible polymers, showing that the lightly crosslinked particles as well as the linear precursors indeed behave similar to a Gaussian coil in solution. However, the data for the tightly crosslinked particles could not be accurately fitted with the Debye equation. Instead, their Guinier radii were found to be close to the radii obtained by fitting the data to a hard sphere model.

Defining the contraction as the ratio of hydrodynamic radii of the NPs', with respect to the linear precursor, at zero concentration ( $h$ , Table 2.2), one can see that the

size of the nanoparticles is greatly reduced on crosslinking. For Antonietti et al.'s microgels,<sup>58</sup> which had 1 in every 10 monomer units (on average) crosslinked, the  $h$  value varied between 0.96-0.98. In comparison, the lightly X-linked NP's have  $h$  values similar to those reported in their work, whereas the tightly X-linked NP have an  $h$  value between 0.65-0.86. Thus, the use of a larger amount of BCB as the crosslinking agent<sup>11</sup> does provide greater reduction in nanoparticle volume as compared to p-bis(chloromethyl) benzene.<sup>58</sup>

**Table 2.2.** Radius of gyration determined from a Guinier regression, Debye flexible polymer fit and hard sphere fit as well as the hydrodynamic radius for the various nanoparticles and their linear precursors in d-THF (SANS data) and THF (DLS data); concentration is 5 mg/ml and temperature is 35°C. Corresponding values with d-cyclohexane and cyclohexane as the solvents are provided in the Appendix (Table 2.4).

$M_n$ (kDa)	% crosslinker	Nature	Guinier regression (nm)	Flexible polymer fit (nm) <sup>a</sup>	Hard-sphere fit (nm) <sup>b</sup>	$R_h$ (nm) <sup>c</sup>	$h^d$
25.3	20	linear	2.5±0.03	2.6±0.04	NA	3.5 (3.7)	1
52	20	linear	3.0±0.02	2.8±0.03	NA	5.4 (5.8)	1
135	20	linear	3.0±0.02	3.1±0.03	NA	8.7(11.2)	1
25.3	20	crosslinked	2.0±0.01	2.9±0.06	1.9±0.02	3.1(3.2)	0.86
52	20	crosslinked	2.3±0.01	3.8±0.05	2.4±0.01	4.7(4.8)	0.82
135	20	crosslinked	3.4±0.01	8.5±0.05	3.9±0.03	6.9(7.3)	0.65
24.5	2.5	linear	2.4±0.02	2.6±0.03	NA	3.5(3.6)	1
60.1	2.5	linear	2.8±0.03	2.8±0.04	NA	5.4(5.7)	1
158	2.5	linear	3.2±0.02	3.1±0.04	NA	9.2(10.8)	1
24.5	2.5	crosslinked	2.4±0.01	2.5±0.03	NA	3.3(3.5)	0.97
60.1	2.5	crosslinked	2.8±0.01	3.0±0.02	NA	5.0(5.5)	0.96
158	2.5	crosslinked	3.5±0.02	3.4±0.03	NA	8.7(10.3)	0.95

<sup>a</sup>Debye flexible polymer fit :  $I(q) = \phi V(\Delta\rho)^2 \{ 2(\exp(-(qR_g)^2) + (qR_g)^2 - 1)/(qR_g)^4 \}$

<sup>b</sup>Hard-Sphere fit:  $I(q) = \phi V(\Delta\rho)^2 \{ 3(\sin(qR) - qR\cos(qR))/(qR)^3 \}^2$ ;  $R_g = \sqrt{(3/5)} \times R$ ,  $R$  is the sphere radius.

<sup>c</sup> $R_{h0}$  values are shown in parentheses.

<sup>d</sup> $h = R_{h0}$  (crosslinked nanoparticle) /  $R_{h0}$  (linear polymer)

Burchard's  $\rho$ -ratio ( $R_{g0}/R_{h0}$ ) is shown in Fig. 2.4 as a function of the molecular mass for both the tightly and lightly crosslinked nanoparticles. The Gaussian coil and the hard sphere (constant density) limits are also shown. It is seen that the lightly crosslinked nanoparticles always have a value close to or within the range determined for a Gaussian coil. The tightly crosslinked nanoparticles, however, always have a value between the hard sphere and the Gaussian coil limits. Also, the ratio decreases with increasing molecular mass showing a shift towards the hard sphere limit. Thus, particle-like behavior for the tightly crosslinked nanoparticles is suggested, which becomes more apparent as the molecular mass is increased.

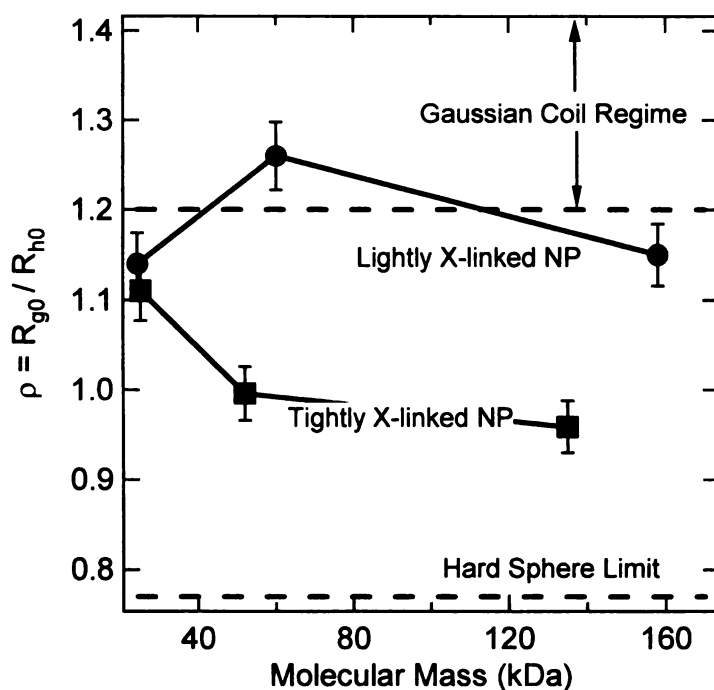


**Figure 2.4.** Burchard's  $\rho$ -ratio (ratio of radius of gyration to hydrodynamic radius) variation for the lightly (2.5% crosslinked, circles) and tightly crosslinked (20% crosslinked, squares) nanoparticles with molecular mass in THF at 35°C. A non-draining hard sphere should have a value of 0.775 while a Gaussian coil has a range of values depending upon solvent conditions. The lightly crosslinked nanoparticles behave similar



to coil while the tightly crosslinked nanoparticles approach the hard sphere limit, particularly at higher molecular weight.

The neutron scattering data were also used to construct Kratky plots for both the lightly and tightly crosslinked nanoparticles. The Kratky plot for the lightly crosslinked nanoparticles (Fig. 2.5.a) demonstrates the behavior expected for a Gaussian coil. The data for the tightly crosslinked nanoparticles (Fig. 2.5.b), on the other hand, shows a peak in the Kratky plots, indicative of particle-like behavior. It is also seen that the peak becomes more pronounced with increasing molecular mass of the tightly crosslinked nanoparticles. This trend further supports the shift towards particle-like behavior with increasing molecular mass as seen with the  $\rho$ -ratio values (Fig. 2.4).

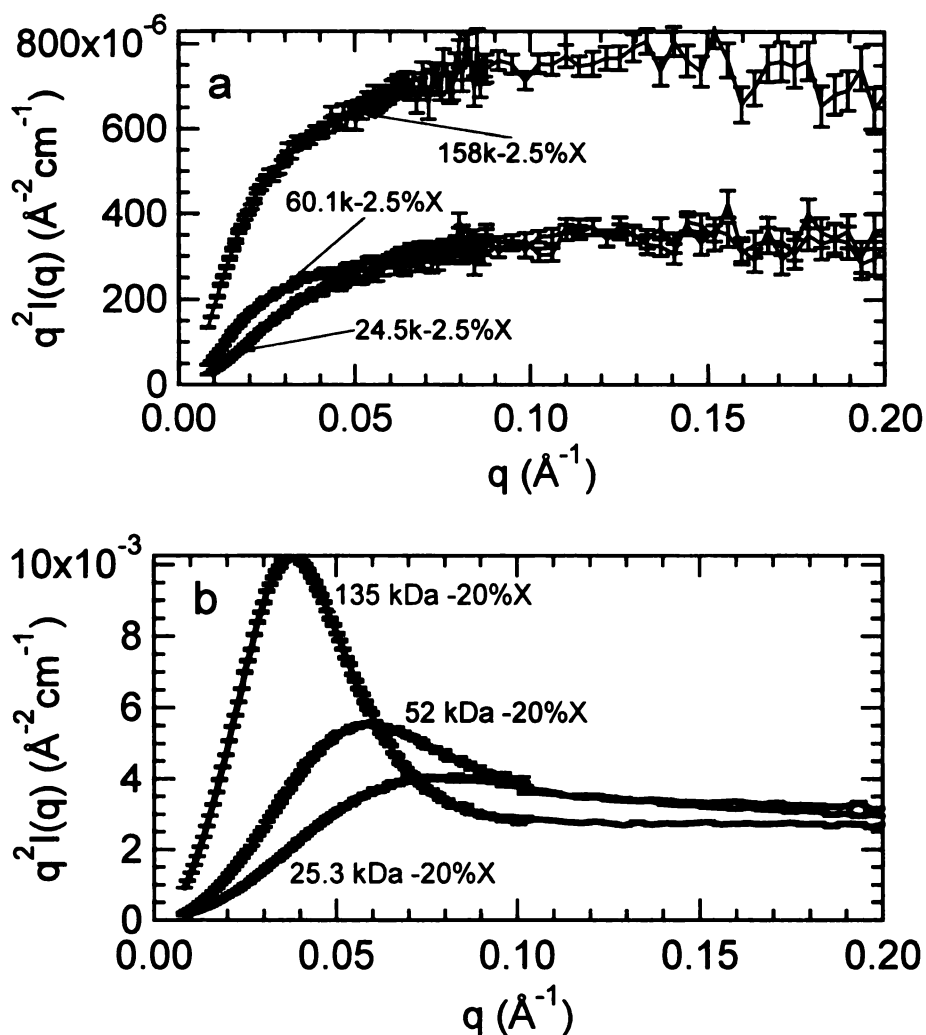


**Figure 2.5.** Kratky plots for the lightly crosslinked (a) and the tightly crosslinked nanoparticles (b). A peak in the Kratky plot is indicative of particle-like behavior, while a plateau is expected for a Gaussian coil.

Note though that there is a plateau at large wave vector,  $q$ , seen in Fig. 2.5.b. Hence, the overall segment distribution is apparently Gaussian, however, organized in such a manner as to give a maximum due to constraints contributed by the crosslinked monomer units. Modeling of the segment distribution more than this is beyond the scope of this work. Clearly, assumptions would have to be made regarding the segment distribution and possibly larger wave vector data would be needed to determine the pair

distribution function and to perform detailed analysis. However, the peak in the Kratky plot together with the suppressed  $\rho$ -ratio and smaller variation of intrinsic viscosity with solvent change clearly indicate particle-like behavior.

Certainly the degree of crosslinking has an effect on the ultimate molecular morphology developed, as expounded above. However, the results in Figs. 2.4 and 2.5.b suggest molecular mass affects the segment density distribution and hence morphology. Recalling the work of Kuhn and Balmer<sup>53</sup> and Kuhn and Majer,<sup>90</sup> we note that the average number of statistical segments in a cycle,  $\langle k \rangle$ , at small degree of intramolecular crosslinking, is related to the number of statistical segments in a molecule,  $N$ , by

$$\langle k \rangle = 2\sqrt{2/3} \times \sqrt{N} \approx \sqrt{N}$$

One may expect that the initial cycles formed in the intramolecularly crosslinked nanoparticles will have 35 monomer units for the 25.3 kDa tightly crosslinked nanoparticle and increase to  $\sim 80$  for the highest molecular mass, 135 kDa (there are 5 monomer units in a statistical segment<sup>79</sup>). This phenomenon could affect the ultimate molecular morphology after crosslinking is completed and could account for the decrease in the  $\rho$ -ratio with molecular mass shown in Fig. 2.4. We also note the ring polydispersity,<sup>90</sup>  $\langle k^2 \rangle^{1/2} / \langle k \rangle$ , is  $\sim 0.46N^{1/4}$  and so higher mass molecules could potentially have a greater difference in initial ring size. These effects are noted here as they could affect the ultimate molecular morphology and final molecular properties surely deserving more attention in future studies since our system is simpler to study in terms of molecular “folding” than polypeptides.<sup>91</sup>

**Bulk properties.** The thermal analysis performed on both the lightly and tightly crosslinked nanoparticle systems also reinforces the observations above. It can be seen

from Fig. 2.6 that the glass transition for both the lightly and tightly crosslinked particles increases with increasing molecular mass (the error bars represent the beginning and the end of the glass transition). Also, the  $T_g$  for the tightly crosslinked nanoparticles is always greater than the  $T_g$  of the lightly crosslinked nanoparticles of similar molecular mass. It should be noted that the increase in  $T_g$ , caused by the intramolecular crosslinking of polystyrene, although significant, is still less than the elevation caused in polystyrene networks formed by the copolymerization of polystyrene and divinylbenzene,<sup>92, 93</sup> as has been seen before.<sup>58</sup> For example, Nielsen<sup>94</sup> developed a simple relation to find the glass transition temperature rise due to crosslinking:  $39 \text{ kDa} \cdot ^\circ\text{C}/M_x$ , where  $M_x$  is the molecular mass between crosslinks. One would expect a  $9^\circ\text{C}$  (lightly crosslinked) and  $75^\circ\text{C}$  (tightly crosslinked) increase above  $T_g$  for the equivalent linear polymer, which is clearly not the case. In fact, a slight  $T_g$  decrease may be apparent for the lightly and tightly crosslinked nanoparticles at low molecular weight. Thus, the discrete crosslinked nature of the bulk nanoparticles clearly affects the glass transition temperature in unusual ways.

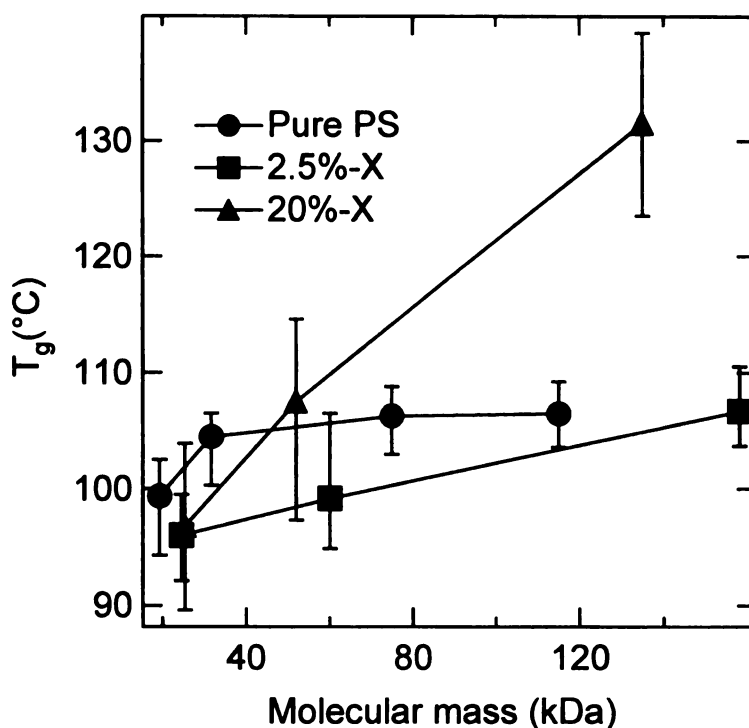


**Figure 2.6.** The glass transition temperatures for both the lightly and the tightly crosslinked nanoparticles compared to pure linear polystyrene. The error bars represent the spread of the transition, indicating its beginning and end.

Furthermore, it was seen before that addition of the tightly crosslinked nanoparticles caused a decrease in the glass transition temperature of linear polystyrene.<sup>76</sup> This observation is quite interesting and contrary to the general mixing rule considering that high molecular mass linear PS has a  $T_g$  of  $\sim 106^\circ\text{C}$ , while the 135 kDa-20%-X NP's have a  $T_g$  of  $\sim 132^\circ\text{C}$  and a 1% blend of the nanoparticles in linear polymer was found to have a  $T_g$  of  $103.5^\circ\text{C}$ .<sup>95</sup>

The complex viscosity as a function of frequency is shown for a 3 arm polystyrene star (molecular mass for each branch  $\sim 108$  kDa) and linear polystyrene (molecular mass 19.3 kDa, 75 kDa, 115 kDa), (Fig. 2.7.a), and the lightly (Fig. 2.7.b) and tightly (Fig. 2.7.c) crosslinked nanoparticles (the data has been shifted to  $170^\circ\text{C}$  using

time-temperature superposition;<sup>13</sup> the shift factors have been tabulated in the appendix, Table 2.5). Clearly, the rheological behavior of the crosslinked nanoparticles does not match the behavior observed for the linear or star shaped polystyrene. Also, from Fig. 2.7.c it is apparent that only the lowest molecular mass (25.3 kDa) tightly crosslinked nanoparticle shows a terminal viscosity. All of the higher molecular mass tightly crosslinked nanoparticles in fact show a gel-like behavior, which is to be expected for a crosslinked network.<sup>60</sup> Note that we tried to measure the melt surface tension<sup>96, 97</sup> of the 25.3k-20%-X-NP sample. At 220°C we found the surface tension was extremely large and of order 150 mN/m, while linear polystyrene should have a surface tension of order 20 mN/m at this temperature. We conclude that this sample must have a terminal modulus or yield stress that is small and probably less than 10 Pa. So this sample may be similar to the higher mass 20%-X-NP samples, with a gel-like behavior, that is disrupted in the rheological testing.

The observation of gel-like behavior for relatively low molecular mass tightly crosslinked nanoparticles is in contrast to the behavior seen by Antonietti et al.<sup>12</sup> In their work, a zero shear viscosity was observed even for very high molecular mass ( $M_w=1.03 \times 10^6$ ,  $R = 7.3$  nm) microgels.<sup>12</sup> However, the microgels only had 1 in every 10 monomer units crosslinked and the higher degree of crosslinking present in this work can cause a significant impediment to the motion of the small chains between the crosslinks. Antonietti et al. postulated that the viscosity behavior was linked to the cooperative nature of the crosslinked loops' motion. Thus, the gel-like behavior we observe may be expected, and it is certainly affected by the intramolecular crosslink density and nanoparticle size (or molecular mass).

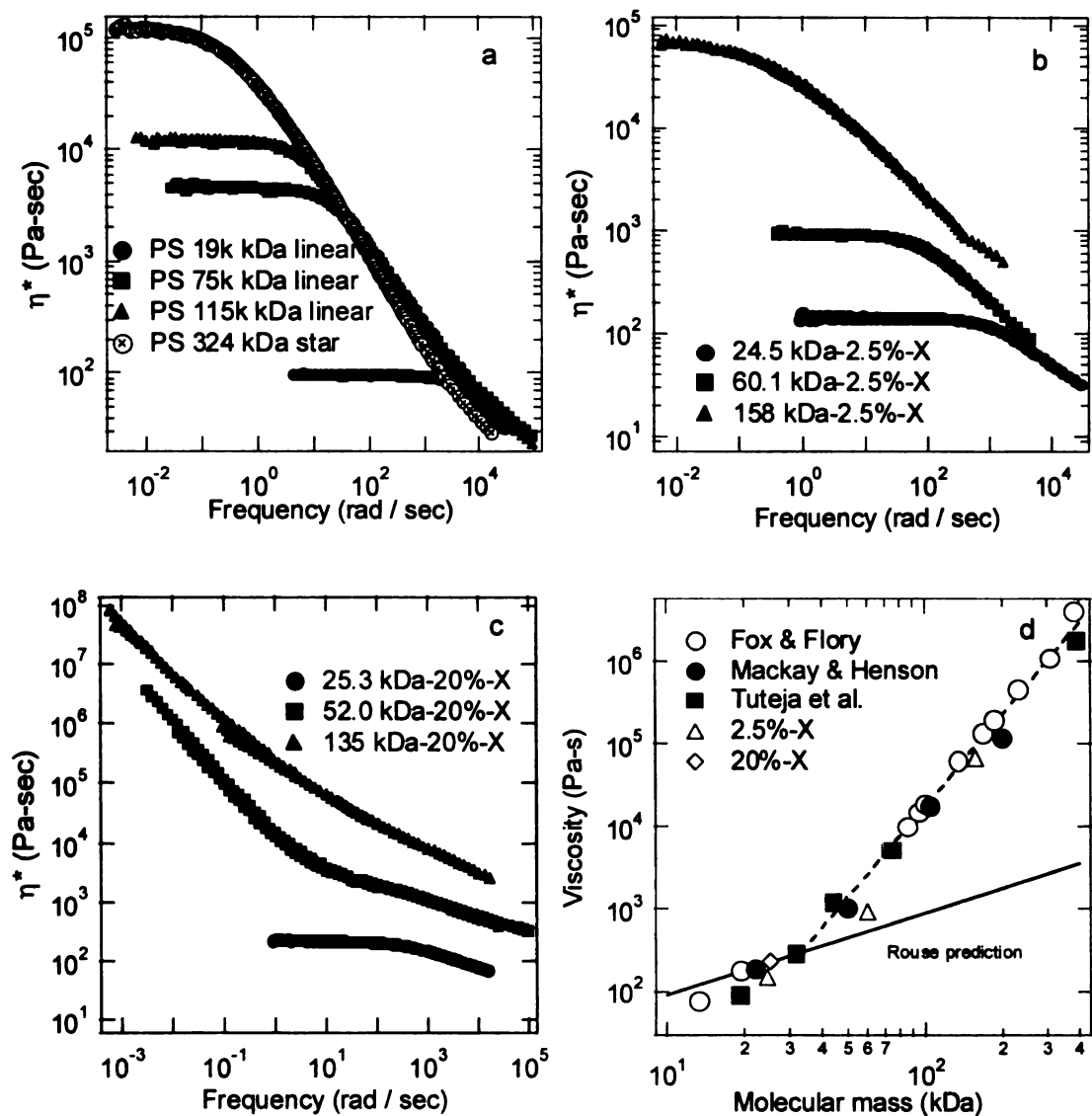


**Figure 2.7.** The complex viscosity as a function of frequency at 170°C, for the 3 arm polystyrene star and linear polystyrene (a), lightly crosslinked (b) and tightly crosslinked (c) nanoparticles. Increasing molecular mass and crosslink density causes an increase in the zero shear viscosity. A gel like behavior is evident for the high molecular mass, tightly crosslinked nanoparticles. (d) The zero shear viscosity as a function of molecular mass ( $M$ ) for polystyrene melts at 170°C. Data from Fox and Flory,<sup>63, 64</sup> Mackay and Henson<sup>98</sup> and Tuteja et al.<sup>95</sup> are used. The zero shear viscosities for the pure lightly and tightly crosslinked nanoparticles are also shown (a zero shear viscosity is not observed for the 52 kDa-20%-X and 135 kDa-20%-X NP's).

The zero shear viscosity as a function of molecular mass for linear polystyrene at 170°C is shown in Fig. 2.7.d together with the values for the lightly and tightly crosslinked nanoparticles. The lightly crosslinked nanoparticles may have a lower zero shear viscosity as compared to linear polystyrene of similar molecular weight,<sup>12</sup> suggesting easier mobility of the crosslinked molecule as compared to the linear chains, however, this is a tentative conclusion.

The modes for polymer relaxation and the effects of the relative motion of crosslinked loops become clearer by viewing the storage modulus data. The storage and loss modulus as a function of frequency for the 3 arm polystyrene star and linear polystyrene of comparable molecular mass to the lightly and tightly crosslinked nanoparticles is shown in Fig. 2.8, together with the nanoparticles' data. All of the lightly crosslinked nanoparticles as well as the 25 kDa-20%-X-NP show typical terminal zone behavior with  $G' \sim \omega^2$  and  $G'' \sim \omega'$  at low frequencies ( $\omega$ ), with the caveat that the 20% crosslinked system may have a delicate gel-like behavior.



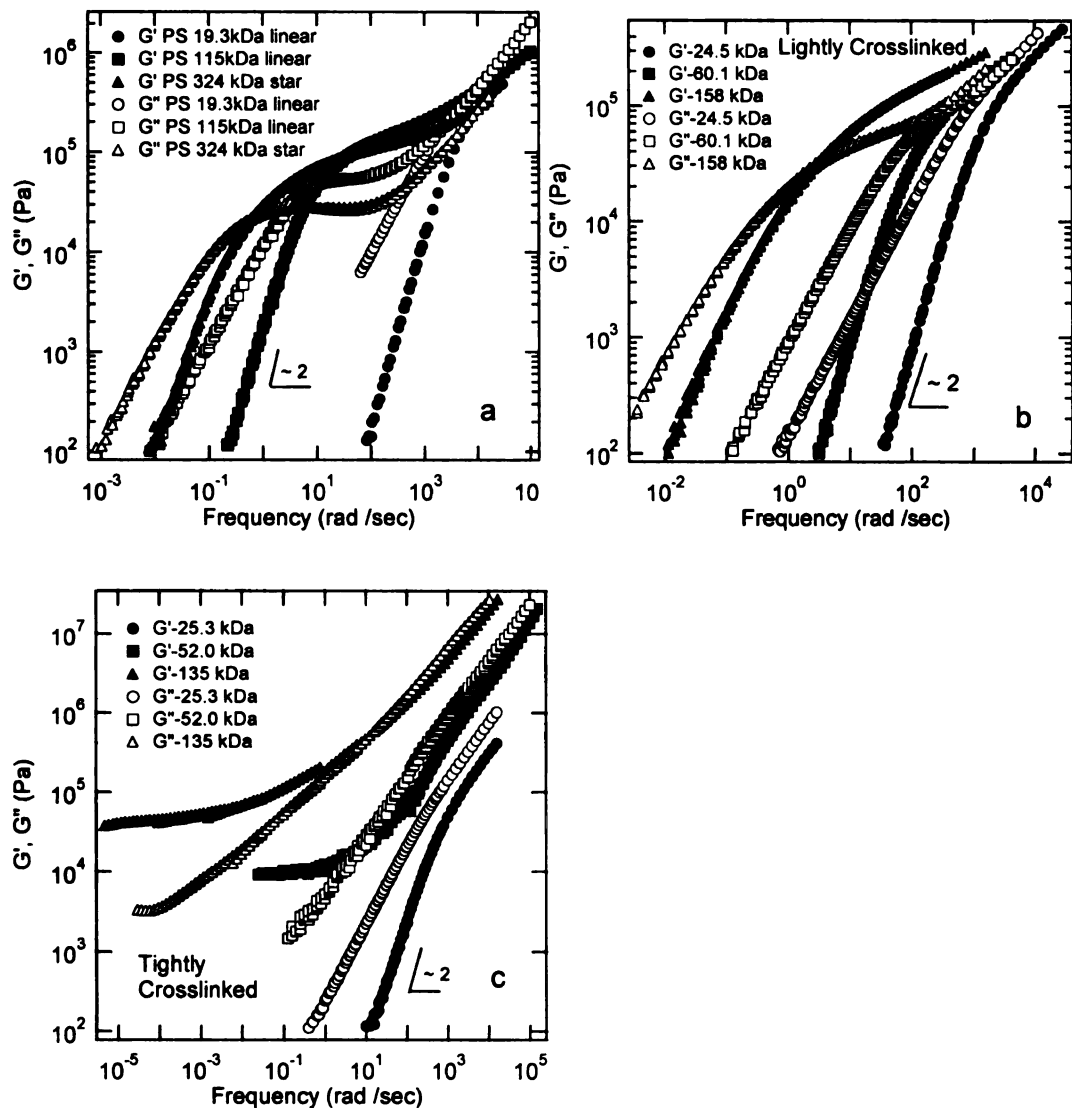


**Figure 2.8.** The storage ( $G'$ ) and loss ( $G''$ ) modulus as a function of frequency for the 3 arm polystyrene star and linear polystyrene (a), lightly crosslinked (b) and tightly crosslinked (c) nanoparticles, at 170°C. A terminal zone behavior similar to linear polymers is evident for all of the lightly crosslinked nanoparticles, while a transition zone behavior similar to linear polymers is evident for both the lightly and tightly crosslinked nanoparticles.

On increasing the molecular mass for the lightly crosslinked nanoparticles, the development of a plateau zone (corresponding traditionally to the presence of entanglements) can be seen and a  $\sim 10\%$  increase in the plateau modulus is observed

(determined through the minima in  $\tan \delta = G''/G'$ <sup>99</sup>). Traditionally the plateau modulus corresponds to the entanglement density present in polymer melts. Clearly, reptation motion, at least the way it is thought of traditionally, cannot account for the rheological behavior observed in these crosslinked particles, even though the rheological spectra of higher molecular mass lightly crosslinked nanoparticles is similar to the spectra obtained for higher molecular mass entangled linear polymers.

This trend is reinforced as we look at the rheological behavior of the tightly crosslinked nanoparticles. As the number of crosslinked loops present in the molecule increase from  $\sim 25$ / molecule (25.3 kDa-20%-X-NP) to  $\sim 50$ /molecule (52 kDa-20%-X-NP), a distinct change in the terminal behavior of the molecules is observed. With the increasing number of crosslinked loops, the storage modulus becomes essentially constant with respect to frequency (for low frequencies), a behavior typical of gels.<sup>12</sup> At this point it can be imagined that the large number of intramolecularly crosslinked loops present in the molecule, cannot move cooperatively, to allow for the molecules' relaxation; and essentially a high stress (yield stress) is required to allow for the loops to move together and hence for the molecule to relax. Further, the molecules become more particle-like with increasing molecular mass, as discussed above, probably contributing to the gel-like flow properties.

The observation of a constant storage modulus at low frequency as shown in Fig. 2.8.c, also provides some interesting insights about the nature of the crosslinked particles. As can be seen, the modulus at low frequency increases with increasing nanoparticle molecular weight (radius), with the caveat that the lowest molecular weight sample, 25.3 kDa-20%-X, has a very small terminal modulus as determined through our surface

tension measurements.<sup>96</sup> However, predictions of flocculated suspensions show that modulus should scale inversely to the particle radius raised to a power;<sup>100, 101</sup> indeed, even jammed particle systems, at zero temperature, show a scaling inversely proportional to the radius raised to the power of the system dimensionality.<sup>102</sup> The modulus increase seen in our system may then be related to two factors. Firstly, our results above point to the fact that the larger molecular weight system is more “particle-like” in nature which can be expected to influence the flow properties (as demonstrated by the other rheological properties). Secondly, the glass temperature for the 135 kDa-20%-X system is approximately 25°C higher than that for the 52.0 kDa-20%-X. For a given testing temperature, 170°C in our case, this would tend to increase the flow properties by a factor of approximately 30 – 40, accounting for the observed trend.

## **Conclusion**

An innovative synthesis process was used to induce intramolecular crosslinks within linear polystyrene. It was seen from intrinsic viscosity and dynamic light scattering measurements that crosslinking causes a decrease in the size of the chain and also that the tightly crosslinked nanoparticles have much limited changes in dimensions between different solvents as compared to the lightly crosslinked and linear precursor chains. This demonstrates that intramolecular crosslinking limits the expansion and contraction of the molecule.

Small angle neutron scattering was used to show that the lightly crosslinked nanoparticles and the linear precursors behave like Gaussian coils in solution. On the other hand, the tightly crosslinked nanoparticles showed a peak in the Kratky plot

indicative of particle-like behavior. It was also seen that the peak in the Kratky plot becomes more pronounced with increasing molecular mass of the nanoparticles. This trend was reinforced by determining Burchard's  $\rho$ -ratio for the various nanoparticles. It was seen that the  $\rho$ -ratio values for lightly crosslinked particles are indeed close to the Gaussian range while the values for tightly crosslinked nanoparticles were seen to move towards the hard sphere limit with increasing molecular mass.

These molecules were ideal to study the rheological/relaxation behavior of high molecular mass polymers in the absence of entanglements; as the high crosslink density present in these molecules should influence entanglement coupling. It was seen that these molecules show most of the rheological characteristics of both unentangled and entangled polymeric systems. The terminal viscosity increased with increasing molecular mass and increasing crosslink density (contrary to earlier observations for particles with lower intramolecular crosslinking densities),<sup>12</sup> with the limiting case of high molecular mass samples with high degree of intramolecular crosslinking showing gel like behavior, with an infinite terminal viscosity. It was postulated that the mobility of these molecules is not governed by the motion of individual chains, but rather by the cooperative and relative motion of the crosslinked loops present in the system in accord with Antonietti et al.'s<sup>12</sup> hypothesis. This type of motion is indeed intuitive as the crosslinking present between the molecules must cause many of the loops to move together.

It can then be said that the reptation model (or the presence of a tube for relaxation) does not explain many of the important rheological features seen for our systems. Clearly coupling or cooperative motion has to play a significant nature in the relaxation processes of these molecules. Indeed, Schweizer<sup>21, 22</sup> postulated a coupling

theory for polymers which predicts many of the polymer relaxation modes observed experimentally.

## Appendix Chapter 2.

### Huggins and Kraemer Coefficients.

Equation 2.3 can be used to calculate the Huggins and Kraemer coefficients through intrinsic viscosity measurements. Table 2.3 shows the variation of Huggins and Kraemer coefficients with molecular weight for the 2.5% and 20% crosslinked nanoparticles in THF and cyclohexane, at 35°C.

**Table 2.3:** The variation of Huggins and Kraemer coefficients with molecular weight for the 2.5% and 20% crosslinked nanoparticles in THF and cyclohexane, at 35°C.

<b>Tightly Crosslinked</b>	<b>THF</b>		<b>Cyclohexane</b>	
<b>Molecular Weight (Da)</b>	<b>k<sub>h</sub></b>	<b>k<sub>k</sub></b>	<b>k<sub>h</sub></b>	<b>k<sub>k</sub></b>
25300	1.24	-0.55	2.57	-1.8
52000	0.64	-0.13	2.97	-0.23
135000	0.23	0.26	NA <sup>a</sup>	NA <sup>a</sup>
<b>Lightly Crosslinked</b>	<b>THF</b>		<b>Cyclohexane</b>	
<b>Molecular Weight (Da)</b>	<b>k<sub>h</sub></b>	<b>k<sub>k</sub></b>	<b>k<sub>h</sub></b>	<b>k<sub>k</sub></b>
24500	0.62	0.003	NA	NA
60100	0.58	0.002	0.82	-0.55
158000	0.49	0.005	0.57	-0.33

<sup>a</sup> The 135 kDa tightly crosslinked nanoparticles had a very low solubility (< 1mg/ml) in cyclohexane.

### Modified Zimm and Yamakawa approaches to size variation of macromolecules.

The Zimm equation is written<sup>18, 103</sup>

$$k_I/I(q) = \{1 + \frac{1}{3} \times q^2 R_g^2\} / cM + 2 \times A_2$$

where  $k_I$  is  $[\Delta\rho]^2 / N_A \rho_m^2$ , with  $\rho_m$  being the mass density of the scatterer. This

equation can be arranged to

$$\begin{aligned}\log(I) &= \ln(C_0) - \log(1 + \frac{1}{3} \times q^2 R_{g0}^2 / \{1 + 2 \times A_2 c M\}) \\ &\approx \ln(C_0) - \frac{1}{3} \times q^2 R_{g0}^2 / \{1 + 2 \times A_2 c M\}\end{aligned}$$

where  $C_0$  is a grouping of variables that is constant for a given system and concentration. Performing a Guinier analysis on the scattering data at low  $q$  will yield an apparent radius of gyration,  $R_g$ , which is given by

$$R_g^{-2} = R_{g0}^{-2} \times \{1 + 2 \times A_2 c M\} \quad (2.A1)$$

Thus, a plot of the inverse square of the apparent radius of gyration versus concentration will yield the true radius of gyration,  $R_{g0}$ , at zero concentration. This equation is useful when only a few concentrations are available for analysis thereby not warranting a full Zimm analysis and explains the (apparent) radius of gyration variation with concentration. This extrapolation procedure was used by us to determine  $R_{g0}$  and yielded good linear regression.

Yamakawa<sup>81</sup> applied non-equilibrium thermodynamics to determine the translational diffusivity, and hence  $R_h$ , as a function of concentration via

$$R_h^{-1} = R_{h0}^{-1} \times \{1 + k_D c\} \quad (2.A2)$$

where the subscript “0” is again the zero concentration value and  $k_D$  is a constant. This relation was used by us to determine the true hydrodynamic radius.

### **Radius of Gyration variation in cyclohexane.**

The Radius of gyration determined from a Guinier regression, Debye flexible polymer fit, as well as the hydrodynamic radius for the various nanoparticles and their linear precursors in d-cyclohexane is provided in Table 2.4.

**Table 2.4.** Radius of gyration determined from a Guinier regression, Debye flexible polymer fit, as well as the hydrodynamic radius for the various nanoparticles and their linear precursors in d-cyclohexane (SANS data) and cyclohexane (DLS data); concentration is 5 mg/ml and temperature is 35°C

Molecular Weight(kDa)	% crosslinker	Nature	Guiner Radius(nm)	Flexible Polymer fit(nm) <sup>a</sup>	R <sub>h</sub> <sup>c</sup> (nm)
25.3	20	linear	4.6±0.02	5.0±0.02	3.0(4.2)
52	20	linear	7.0±0.05	7.8±0.02	4.7(6.7)
135	20	linear	8.6±0.11	8.8±0.05	8.0(9.1)
25.3	20	X-linked	NA <sup>a</sup>	NA <sup>a</sup>	NA <sup>a</sup> (2.8)
52	20	X-linked	NA <sup>a</sup>	NA <sup>a</sup>	NA <sup>a</sup> (3.7)
135	20	X-linked	NA <sup>a</sup>	NA <sup>a</sup>	NA <sup>a</sup> (5.9)
24.5	2.5	linear	4.8±0.02	5.0±0.01	2.6(4.2)
60.1	2.5	linear	7.8±0.01	8.5±0.01	5.3(7.1)
158	2.5	linear	7.8±0.04	8.7±0.02	7.8(8.3)
24.5	2.5	X-linked	5.3±0.01	5.0±0.02	2.5(4.1)
60.1	2.5	X-linked	6.1±0.03	6.6±0.02	5.2(6.4)
158	2.5	X-linked	7.7±0.02	8.0±0.03	8.0(9.1)

<sup>a</sup> The tightly crosslinked nanoparticles were insoluble in cyclohexane at this high concentration.

#### **SANS intensity data after normalization.**

The scattering intensity as a function of the wave vector  $q$  for the 25.3 kDa and 52.0 kDa-20%X-linear precursors in d-cyclohexane and d-THF at 35°C, as reference to typical data obtained after normalization, yet without background subtraction, is shown in Fig. 2.9. As can be seen in the figure, the data is fitted well by Debye function. All of the scattering data except for the data obtained for the tightly crosslinked nanoparticles could be fitted quite well with the Debye function.

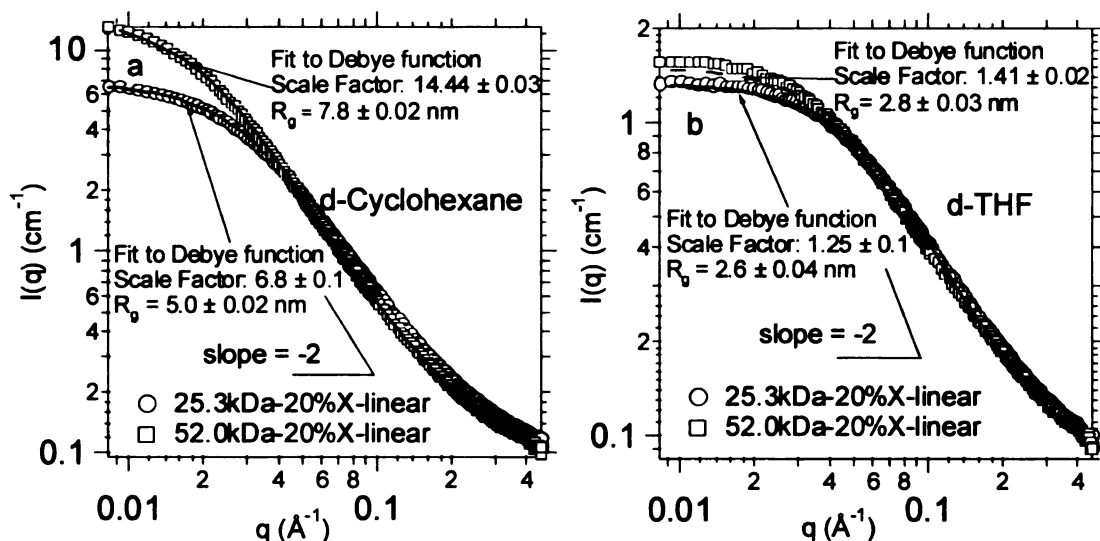


**Figure 2.9.** Typical  $I$  ( $\text{cm}^{-1}$ ) versus  $q$  ( $\text{\AA}^{-1}$ ) graphs obtained after normalization of the SANS data in d-cyclohexane and d-THF. The data was obtained at  $35^\circ\text{C}$ , and the concentration was 5 mg/ml. The fits to the Debye function for the obtained data are also shown.

#### Shift Factors for rheological data.

The shift factors<sup>13</sup> ( $a_T$ ) at various temperatures used for the time-temperature superposition of data shown in Fig. 2.7 and Fig. 2.8 are listed in Table 2.5. It can be seen that the shift factors for both the lightly and tightly crosslinked nanoparticles are similar to the shift factors for linear polystyrene. Note the glass transition temperature for the crosslinked nanoparticles is different to that of linear polymer (Fig. 2.6), accounting for some differences in the shift factors for a given temperature.



**Table 2.5.** The shift factors<sup>13</sup> as a function of temperature for linear polystyrene, lightly and tightly crosslinked nanoparticles.

<b>Linear polystyrene</b>					
Linear PS 19k		Linear PS 75k		Linear PS 115k	
Temp(°C)	a <sub>T</sub>	Temp(°C)	a <sub>T</sub>	Temp(°C)	a <sub>T</sub>
130	284	130	881	130	966
140	45.8	140	85.2	140	92.0
150	10.3	150	14.8	150	15.1
160	4.12	160	3.44	160	3.48
170	1.00	170	1.00	170	1.00
180	0.26	180	0.35	180	0.35
		190	0.14	190	0.14
		200	0.07	200	0.06
<b>Lightly crosslinked</b>					
24.5 kDa-2.5%-X		60.1 kDa-2.5%-X		158 kDa-2.5%-X	
Temp(°C)	a <sub>T</sub>	Temp(°C)	a <sub>T</sub>	Temp(°C)	a <sub>T</sub>
130	310	140	44.7	150	15.4
140	51.1	150	10.1	160	3.45
150	11.1	160	2.89	170	1.00
160	3.04	170	1.00	180	0.35
170	1.00	180	0.41	190	0.15
180	0.24	190	0.20	200	0.08
190	0.09	200	0.10	210	0.05
		210	0.05	220	0.03
<b>Tightly crosslinked</b>					
25.3 kDa-20%-X		52 kDa-20%-X		135 kDa-20%-X	
Temp(°C)	a <sub>T</sub>	Temp(°C)	a <sub>T</sub>	Temp(°C)	a <sub>T</sub>
130	155	130	982	150	75.4
140	35.8	140	131	160	12.5
150	6.93	150	39.15	170	1.00
160	2.23	160	10.1	180	0.35
170	1.00	170	1.00	190	0.08
		180	0.21	200	0.05
		190	0.02	210	0.02

## CHAPTER 3

### GENERAL STRATEGIES FOR NANOPARTICLE DISPERSION

---

#### Introduction

Polymer phase stability in solution<sup>26</sup> or with another polymer<sup>104</sup> has been studied for over 50 years and found to be a delicate balance of entropic and enthalpic contributions to the total free energy. For example, it is possible to fractionate a polymer by size with a small change in solvent quality,<sup>105</sup> and to control miscibility of chemically identical polymers whose only difference is architecture (branching).<sup>106</sup> More recently the phase stability of nanoparticle/polymer blends has attracted intense scrutiny<sup>107</sup> and is challenging to predict due to computational difficulty in accessing the relevant length and time scales. Flory theories, density functional theories and molecular dynamics methods provide essential guidance, though accurate calculations are restricted to two or at most a few nanoparticles in the relevant size regime.<sup>108, 109</sup> Despite these difficulties a vast array of applications are emerging that require nanoparticle dispersion such as the use of fullerenes to enhance the efficiency of polymer-based photovoltaic devices<sup>110, 111</sup> and in the control of polymer viscosity using nanoparticles.<sup>8</sup>

We demonstrate here strategies for control of nanoparticle dispersion in linear polymer melts. We start with discussion of processing procedures which enable stable dispersion of fullerenes and then present an experimental characterization of the

parameters which control the phase boundary between the dispersed and phase segregated states of carefully considered nanoparticle/polymer mixtures. Moreover it has been proven possible to disperse polyethylene nanoparticles in polystyrene despite the fact that linear polyethylene/linear polystyrene is a classic phase separating blend, which implies that nanoparticle morphology may actually enhance dispersion. This hypothesis is tested by using a system consisting of polystyrene nanoparticles dispersed in linear polystyrene as the monomer-monomer contacts in this system are the same for all of its constituents. An enthalpic mechanism that arises from nanoparticle packing effects operates at the nanoscale and is necessary in order to understand dispersion in this size regime. A Flory theory which includes this enthalpic contribution as well as chain stretching caused by nanoparticle dispersion and the standard mixing entropy is used to reconcile the experimental observations and emphasize the importance of the nanoparticle to polymer size ratio in controlling nanoparticle dispersion.

## **Experimental**

Polyethylene nanoparticles consisting of dendritic polyethylene, with a number-averaged molecular weight of 225 kDa (polydispersity index of 1.6) as measured by a Wyatt Technologies multi-angle light scattering detector, were synthesized at 0.1 atm ethylene pressure using a chain walking palladium catalyst.<sup>112</sup> They were then blended with 393 kDa linear polystyrene in a common solvent, rapidly precipitated in methanol and dried to ensure complete solvent removal. A maximum polyethylene concentration of 5-10 wt%, relative to polystyrene, was used and the mixture heated to *ca.* 230°C for up to

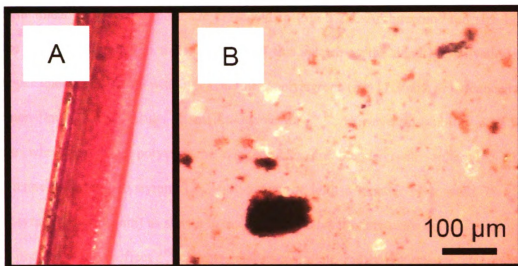
24 hrs. to observe phase stability. Differential scanning calorimetry (TA Instruments) reveals a broad transition at  $\sim -40^{\circ}\text{C}$  for pure polyethylene which disappears in the blend. The blend glass transition temperature ( $T_g$ ) is slightly affected although not as much as that seen for a phase separating blend containing 7 wt% tetracontane ( $\text{n-C}_{40}\text{H}_{82}$ ) prepared in the same manner. Here the pure tetracontane melting point is observed at  $81^{\circ}\text{C}$  in the blend with a *ca.*  $10^{\circ}\text{C}$  reduction in  $T_g$  for polystyrene ( $94^{\circ}\text{C}$ ) after the third heat cycle. Conversely, the nanoparticle – polymer blend has a  $T_g$  reduction of  $1 - 2^{\circ}\text{C}$ .<sup>8, 113</sup> The fact that dendritic polyethylene is soluble in linear polystyrene while tetracontane is not is further confirmation of molecular architecture affecting phase stability.

## Results and Discussion

First the dispersion of fullerenes into polystyrene is discussed motivated by earlier work which suggested that fullerene dispersion in polymers<sup>114</sup> is poor, limiting their utility, for example, in solar cells.<sup>110, 111</sup> For a polymer blend, the insertion energy of a linear polymer chain with another controls dispersion and grows with the number of monomers in the chain. So, the insertion enthalpy of a chain of  $N$  monomers is proportional to  $N\chi$ , where  $\chi$  is the Flory mixing parameter and is the primary cause of phase separation in incompatible blends. Nanoparticles have an insertion enthalpy which grows in proportion to the surface area of the nanoparticle yielding an insertion enthalpy of  $s \sim A\chi$ , where  $A=4\pi a^2$  for a nanoparticle of radius  $a$ . Though this enhancement is not as strong as for polymer blends, dispersion of nanoparticles still depends critically on  $\chi$ . Our experimental observation is that it is possible to disperse up to a concentration of 2

vol% of  $C_{60}$  in linear, monodisperse polystyrene. At small nanoparticle concentration, Flory theory<sup>115</sup> gives a binodal or phase stability volume fraction ( $\phi_B$ ) of:  $\phi_B \approx \text{Exp}(-[1+s])$ , assuming the phase separated fullerenes form a pure nanoparticle phase. Using the experimental value of  $\phi_B = 0.02$  yields an insertion enthalpy per fullerene which is of order  $s \approx 3$ . The molecular insertion energy per monomer ( $\epsilon$ ) is given by  $s = z\epsilon/k_B T$ , where  $z$  is the coordination number,  $k_B$ , the Boltzmann constant and  $T$ , the temperature, yielding an insertion energy of  $\epsilon \approx 0.02$  eV for fullerenes in polystyrene. This relatively small energy may be rationalized by the fact that favorable molecular contacts between the aromatic rings on polystyrene and the hexagons on the surface of  $C_{60}$  may occur.

Fullerene dispersion is enabled by use of our technique of rapidly precipitating the components in a mutual non-solvent<sup>51, 116</sup> to arrive at a dried powder that is then thermally aged, allowing melt processing and fiber spinning (Fig. 3.1.a). It is known that fullerenes have limited solubility in organic solvents,<sup>117</sup> of order 5 – 10 mg/mL. Solvent evaporation from a fullerene/polymer solution will lead to a fullerene supersaturated state at low overall concentration and likely phase separation (Fig. 3.1.b). Thus, to reach the thermodynamically favored state the processing procedure for nanoparticle dispersion has to be carefully controlled to avoid a kinetically trapped condition.

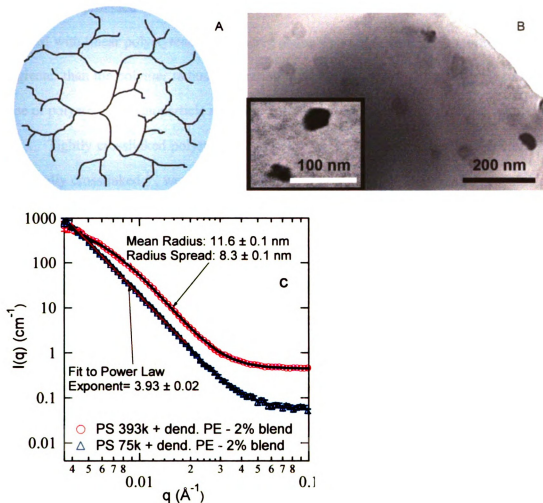


**Images in this dissertation are presented in color.**

**Figure 3.1.** (a) Rapid precipitation of fullerene/polystyrene blends, followed by drying and melt processing allows manufacture of fibers. The fibers contains 1 wt%  $C_{60}$  fullerenes that were melt spun into long fibers with a diameter of *ca.* 1 mm. (b) Fullerene (1 wt%)/polystyrene blends developed through regular solvent evaporation produce large, phase separated domains which are not apparent in the fiber.

A more surprising result is the fact that we observe dispersion of large branched polyethylene nanoparticles<sup>112</sup> in polystyrene (see Fig. 3.2). This is surprising since linear polystyrene/linear polyethylene blends<sup>118</sup> have an unfavorable mixing enthalpy and are a classic phase separating system, with complete phase separation occurring at molecular weights typical of those used here. We have taken TEM images and collected SANS data for a wide variety of mixtures. The TEM image in Fig. 3.2.b illustrates the dispersion of dendritic polyethylene nanoparticles in 393 kDa linear polystyrene from which a nanoparticle radius of 10 – 15nm can be extracted. Moreover, a Guinier analysis of SANS data<sup>18, 84</sup> from polyethylene nanoparticles in dilute solution yields a polyethylene nanoparticle radius of  $12.8 \pm 0.1$  nm which is consistent with the TEM measurement. Neutron scattering data for the same nanoparticles blended with different molecular

weight linear polystyrene melts are presented in Fig. 3.2.c. Architecture and size both make a clear difference in the miscibility of this system as the dendritic polyethylene nanoparticles are miscible with 393 kDa linear polystyrene ( $R_g=17.3$  nm) as evidenced by the non-fractal SANS results at small wave vector<sup>18, 84</sup>. However, miscibility does not occur when the same polyethylene nanoparticles are blended with either 155 kDa (deuterated) linear polystyrene ( $R_g = 10.5$  nm) or with a smaller protonated 75 kDa polystyrene ( $R_g = 7.5$  nm) as shown in the figure. The latter experiment demonstrates that it is not the isotope effect<sup>119</sup> causing phase separation, rather the relative size of the nanoparticle and polymer is key.<sup>120-122</sup>



**Images in this dissertation are presented in color.**

**Figure 3.2.** (a) Cartoon showing branched, dendritic polyethylene. (b) TEM of a 4 wt% blend of dendritic polyethylene with 393 kDa linear polystyrene shows the individual polyethylene macromolecules with a size of order 20-30 nm. The  $R_g$  for the linear polystyrene is 17.4 nm and so is larger than the dendritic polyethylene. The inset shows a higher magnification. (c) Mixing with a smaller molecular mass polystyrene (75 kDa,  $R_g = 7.5$  nm) produces phase separation. Power law scattering of intensity ( $I$ ) versus wave vector ( $q$ ) is present at small wave vector for the lower mass polystyrene, whereas the higher mass system demonstrates miscibility without a power law region. The intensity profile can be fitted with a polydisperse sphere model yielding a mean radius (11.0 nm) for the dendritic polyethylene that agrees well with the TEM images.

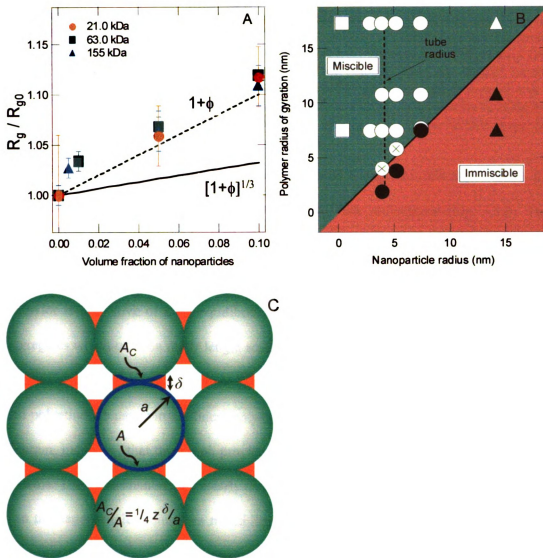


A particularly clear illustration of the importance of the ratio  $a/R_g$  on nanoparticle dispersion is provided by a mixture consisting of crosslinked polystyrene nanoparticles<sup>11</sup> blended with linear polystyrene. We observe phase separation when the nanoparticle size is greater than the polymer radius of gyration in a manner similar to that observed in the case of polyethylene nanoparticle mixtures discussed above.

Tightly crosslinked polystyrene nanoparticles, where every fifth monomer unit is potentially crosslinked<sup>11</sup>, were blended with linear polystyrene.<sup>8</sup> This system produces a stable blend even when the interparticle gap reaches surprisingly small distances suggesting the linear polystyrene molecule is highly distorted.<sup>8</sup> The distortion was directly measured through a SANS Guinier analysis from a sample in which 2 wt% deuterated linear polystyrene was blended with protonated linear polystyrene of similar molecular weight and various concentrations of protonated polystyrene nanoparticles (Fig. 3.3.a). The radius of gyration for the linear polystyrene increases with nanoparticle concentration and the linear chains remain globular in nature, as determined through careful analysis using models which distinguish between sphere-like, rod-like and disk-like shapes.<sup>123</sup>

Chain stretching has been observed in some Monte Carlo simulations<sup>124</sup> though in many others chain contraction has been noted.<sup>125</sup> Both chain expansion and chain contraction has been observed in neutron scattering from isotopically labeled polydimethylsiloxane (PDMS) blends containing silica particles.<sup>126</sup> In this system, nanoparticles of radius  $\sim 1$  nm were blended with linear polymers with a similar radius of gyration,  $R_g \sim 3 - 10$  nm. It was observed that the polymer mixtures with smaller  $R_g$  experienced chain contraction upon nanoparticle addition, while the polymer mixtures

with a larger  $R_g$  experienced chain expansion with nanoparticle addition. In our system the linear polymer  $R_g$  was varied between 4 – 11 nm and the nanoparticle radius is approximately 3 nm, and we observe chain expansion in all cases (see Fig. 3.3.a). Moreover, excluded volume does not fully account for the radius increase, since if it is assumed that the individual polymer and nanoparticle densities do not change on mixing, then the radius of gyration relative to that without nanoparticle incorporation ( $R_g/R_{g0}$ ) is expected to vary as  $[1+\phi]^{1/3}$ . The chain stretching is larger than that suggested by this relation and is empirically close to  $1 + c\phi$ , with  $c$  approximately one.



Images in this dissertation are presented in color.

**Figure 3.3.** (a) The polymer radius of gyration ( $R_g$ ), relative to that without nanoparticles ( $R_{g0}$ ), for three different molecular mass linear polystyrenes: 21, 63, 155 kDa, as a function of volume fraction ( $\phi$ ) of 52.0 kDa tightly crosslinked polystyrene nanoparticles. The nanoparticles clearly stretch the polymer chains. The solid line represents the radius of gyration variation if the polymer density does not change upon mixing, and the behavior  $[1 + \phi]^{1/3}$  is expected. Instead, the data obeys  $1 + c\phi$ , with  $c$  about one. (b) A polymer radius of gyration – nanoparticle radius phase diagram, with the filled circles representing data where phase separation was detected and the open circles where miscibility occurs. Open circles with an  $\times$  represent conditions where some

agglomeration was detected by SANS, yet large scale phase separation was not observed. Squares are the C<sub>60</sub>/polystyrene system; circles, the polystyrene nanoparticle/polystyrene system; and triangles, the dendritic polyethylene/polystyrene system. The dashed line represents the reptation tube radius suggesting phase stability does not depend on the entanglement structure. The nanoparticle fraction used to generate each data point was 2 wt%. (c) Cartoon illustrating that the attraction between pure nanoparticles is effective only over a fraction ( $A_C$ ) of the available surface area ( $A$ ) due to the limited range ( $\delta$ ) over which dispersion forces operate.

Despite the linear polymer distortion, we found a large miscible region exists for crosslinked polystyrene nanoparticles blended with linear polystyrene (Fig. 3.3.b). The data were determined from SANS through the presence or absence of fractal-like scattering at small wave vector and at nanoparticle concentrations of 2 wt%. Fractal-like behavior is indicative of a nonequilibrium state consisting of irregular phase separated aggregates which exist on many length scales, despite the fact that the phase separation is driven by a gain in equilibrium free energy. Data from the fullerene/linear polystyrene and polyethylene nanoparticle/linear polystyrene systems are also included in this phase diagram, indicating that this graph provides a useful guide for a range of nanocomposite systems. The experimental data clearly demonstrate that if the linear polymer  $R_g$  is larger than the nanoparticle radius then miscibility is promoted. Note that both the polymer  $R_g$  and nanoparticle radius were experimentally determined via SANS.

To experimentally determine the Flory  $\chi$  parameter we found the second virial coefficient for 211 kDa tightly crosslinked polystyrene nanoparticles dissolved in 473 kDa deuterated linear polystyrene to be  $(5.3 \pm 3.4) \times 10^{-5}$  cc-mol/g<sup>2</sup> at 127°C and  $(2.4 \pm 0.6) \times 10^{-5}$  cc-mol/g<sup>2</sup> at 170°C, using SANS data and a Zimm analysis.<sup>18, 84</sup> A standard analysis, strictly valid for linear/linear architecture blends<sup>127, 128</sup>, yields Flory parameters of  $\chi = -2.7 \times 10^{-3}$  (127°C) and  $-1.2 \times 10^{-3}$  (170°C), demonstrating that mixing is favored at both temperatures. Note that Bates and Wignall<sup>119</sup> found  $\chi$  to be  $\sim 10^{-4}$  for

deuterated polystyrene blends indicating that the negative mixing enthalpy is not due to isotopic substitution. Furthermore, the  $\chi$  parameter is found to follow  $\sim +0.01 - 6/T(K)$  confirming that favorable enthalpic interactions, which are geometric in origin, are responsible for the phase stability.

This unusual behavior is explained by considering the number of molecular contacts between monomers in the isolated nanoparticle state compared to that of a nanoparticle in the dispersed state as illustrated in the idealized model given in Fig. 3.3.c. The energy gain of a monomer-monomer contact is taken to be  $\epsilon_{np}$ . However, the van der Waals force operates over an effective distance ( $\delta$ ) so that only a fraction of the nanoparticle area ( $A_C$ ) =  $[z\delta/4a] \times A$  has this favorable molecular contact. Here  $z$  is the average coordination number of the nanoparticle aggregate. The remaining uncovered surface area of the nanoparticle ( $A_U \equiv A - A_C$ ) does not profit from favorable contacts with other nanoparticles. Nanoparticles may thus *gain* enthalpically favorable monomer-monomer contacts by dispersion in the polymer melt, as has been noted in recent PRISM calculations.<sup>109</sup> Smaller nanoparticles do not experience this enthalpic driving force since  $A_C$  tends towards  $A$  in this limit confirming that C<sub>60</sub> fullerenes are miscible solely through a favorable mixing entropy.

The mixing enthalpy of a nanoparticle,  $s$ , can be related to the Flory parameter via  $s = A_C\chi + A_U(\chi - \epsilon_{np}/k_B T) \equiv s_0 - s_I$ . Here  $s_0 = A\chi$ , is the insertion enthalpy in the absence of geometric effects due to uncovered area and  $s_I = A_U \times \epsilon_{np}/k_B T$  is the reduction in enthalpy within the pure nanoparticle phase due to uncovered area. The areas are expressed in lattice site dimensions and so are dimensionless with  $s_0$  representing the insertion energy per nanoparticle and  $\chi$  that of a monomer unit. Even though the

uncovered area can be quite small on a given nanoparticle the enthalpy gain via dispersion can be substantial due to their large number given by  $\phi/v_{np}$  with  $v_{np}$  being the nanoparticle volume ( $^{4/3} \pi a^3$ ). So, the expected enthalpic stabilization is given by  $\phi/v_{np} \times s_l$  which exhibits a maximum at a nanoparticle radius of  $z\delta/2$ . This is truly a nanoscopic effect since  $\delta$  is of order 1 nm and  $z$ , 6 for random packing,<sup>102</sup> making the optimum radius for dispersion of order 3 nm, the size scale we have used in the present study. If the nanoparticles are too small then solubility suffers from too little or no uncovered area to achieve sufficient enthalpic gain, similar to that experienced by the fullerenes, while a system containing larger particles has a reduced mixing enthalpy by a reduction in nanoparticle number for a given volume fraction.

The above argument hinges on uncovered area developed by rigid particles (Fig. 3.3.c) and is related to an increase in the cohesive energy of a material from its pure state. The dendritic polyethylene nanoparticle system is a liquid at room temperature and so application of the cartoon to this system is suspect. However, using SANS of thermally annealed samples we measured the virial coefficient for this molecule dissolved in 393 kDa linear polystyrene to be  $(2.1 \pm 1.7) \times 10^{-5}$  cc-mol/g<sup>2</sup> at room temperature yielding  $\chi = - (1.7 \pm 1.3) \times 10^{-3}$ , again a negative mixing enthalpy is found. This result is rationalized first by noting the density of this material was determined to be quite small,  $0.81 \pm 0.02$  g/cc, compared to the linear polyethylene amorphous density extrapolated to room temperature<sup>129</sup>, 0.86-0.89 g/cc. Secondly, the melt surface tension<sup>130, 131</sup> at 160°C was measured and found to be  $\approx 30\%$  lower than polyethylene of similar molecular weight (236 kDa). Both these results point to a reduced internal energy in the isolated nanoparticle melt by using the semi-empirical relation between the surface tension (ST)

and the cohesive energy density (CED = internal energy per unit volume);  $ST \sim CED^{2/3}$ <sup>132</sup> and is consistent with the enthalpy gain on mixing discussed above (*i.e.* negative  $\chi$ ).

We generalized our observations by using a Flory lattice theory which has proven useful in interpreting the phase morphology of complex systems such as nanoparticle dispersion in polymer blends, where reasonable agreement with lattice density functional theory has been demonstrated (20). The first free energy term considered is the mixing entropy described by,  $F_m/Vk_B T = [\phi \log(\phi)]/v_{vp} + [(1-\phi)\log(1-\phi)]/N$ , where  $F_m$  is the entropic gain due to mixing,  $N$ , the number of monomers in the linear polymer and  $V$ , the sample volume. Polymer chain expansion (Fig. 3.3.a) yields a loss of entropy and so a “stretching” free energy cost ( $F_s$ ) for each molecule<sup>133, 134</sup> is included and approximated by  $F_s/Vk_B T = 3/2 [1-\phi][R_g^2/R_{g0}^2 - 1]/N$ . Previous work<sup>122, 135</sup> has used a chain stretching term which is based on the analysis of polymer brushes which does not show as large an  $R_g$  variation with  $\phi$  as we see experimentally. Combining the above terms, including the enthalpy of mixing discussed above, we find,

$$v_{vp}F/Vk_B T = s \phi [1-\phi] + \phi \log(\phi) + t [1-\phi] \log(1-\phi) + 3/2 t [1-\phi][R_g^2/R_{g0}^2 - 1] \quad (1)$$

where  $t = v_{vp}/N$ , which in terms of experimentally accessible parameters is  $t = [a/R_{g0}]^3 \rho/\rho_0$ , where  $\rho$  is the bulk density of the linear polystyrene melt and  $\rho_0$  is the density associated with one chain in the bulk polystyrene melt (*i.e.* the density of a single chain based on its  $R_g$  and molecular weight). The fact that  $t$  increases as the cube of the size ratio  $a/R_{g0}$  implies that the stretching term is very unfavorable for  $a > R_{g0}$ , which is the basic reason why large nanoparticles do not disperse.

For the case of polystyrene nanoparticles in a linear polystyrene melt, we estimate the effect of the linear polymer stretch, the third term in Eq. (1), using the data of Fig.

3.3.a approximated by  $R_g/R_{g0} \approx 1+c\phi$ . By setting the first and second derivatives of Eq. (1) with respect to  $\phi$  to zero one finds the binodal at  $\phi_B = \text{Exp}(-[1+s+(3c-1)t]) = \text{Exp}(-\{1+s+(3c-1)[\rho/\rho_l][a/R_{g0}]^3\})$  and the spinodal at  $\phi_s = 1/[2s+(6c-3c^2-1)t]$  for small  $\phi$ . In Ginzburg's work<sup>122</sup> an additional non-ideal term, the Carnahan-Starling term, is used to assess interaction effects between nanoparticles which does not alter the binodal at small concentration. Validity of the model is confirmed by calculating  $s$  from the predicted binodal concentration assuming  $c$  is one (Fig. 3.3.a). Further, letting  $a/R_{g0}$  be one, to delineate the phase boundary (Fig. 3.3.b), and calculating  $\rho/\rho_0 (= 1.7 \times \sqrt[3]{M(\text{kDa})})$  for polystyrene,  $M$  is molecular weight in kDa) then  $s$  values of -15 and -64 for molecular weights of 30 kDa ( $R_{g0} = 5$  nm) and 320 kDa ( $R_{g0} = 15$  nm), respectively, are determined. Dividing these values with the nanoparticle area results in  $\chi$  of order  $-3 \times 10^{-3}$ , in good agreement with the values determined above via neutron scattering.

## Conclusion

We have shown that nanoparticle dispersion in a polymer melt is promoted when the nanoparticle radius is less than the radius of gyration of the melt chains. In this size regime, we find that  $\chi$  or  $s$  is negative for polyethylene nanoparticles in polystyrene and also for polystyrene nanoparticles in polystyrene and we present a plausible enthalpic mechanism for this effect based on packing arguments. Furthermore, as illustrated in the case of fullerene dispersion into linear polystyrene, the processing procedure must be carefully controlled in order to access the dispersed state, even when it is thermodynamically favored.



## CHAPTER 4

### NANOSCALE EFFECTS LEADING TO NON-EINSTEIN-LIKE REDUCTION IN VISCOSITY

---

#### Introduction

Rheology of particulate suspensions has a long history beginning with Einstein<sup>33</sup> who demonstrated that the viscosity increase *Brownian* particles impart is solely a function of the particle volume fraction ( $\phi$ ) and suspending liquid viscosity. This prediction has been experimentally confirmed many times<sup>100, 136</sup> when a simple or monomeric suspending fluid is used. Suspension of particles in polymeric liquids produces a similar viscosity increase<sup>137</sup> even when clay-polymer nanocomposites are studied.<sup>138</sup> In the case of the clay system, the particles are nanoscopic in one direction and significantly larger than the polymeric liquids' structural length scale in the other two.

Siegel<sup>139</sup> described how mesoscopic physics or nanotechnology can change the macroscopic physical properties of materials. Indeed Mayo et al.<sup>31, 32</sup> demonstrated how ceramic materials can change from brittle to ductile through grain boundary sliding when cluster sizes below 15 nm are present. In a similar vein, Roberts et al.<sup>9</sup> blended small silicate clusters (radius,  $a \sim 0.35$  nm) with linear polymers and observed a viscosity decrease, again pointing to the unusual effect that nanoscale processes and materials may provide. However, these particles are almost molecular in size and approach the monomer length scale, so, interpretation may be clouded by delineating the difference between a plasticizer molecule and nanoparticle. Indeed Roberts et al. state these small clusters behave more like a solvent than a particle akin to the function of a plasticizer.

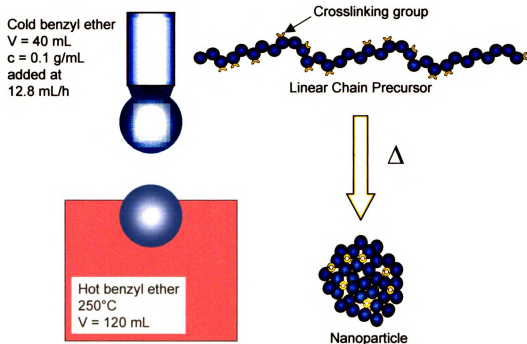
To unequivocally investigate this issue, polystyrene nanoparticles were suspended in linear polystyrene to eliminate enthalpic interactions. Further, since the particles and polymer are essentially the same material having the same refractive index, dispersion forces are minimized<sup>100, 140</sup> creating a hard sphere system where only excluded volume forces are apparent. Thus, this is an ideal system to study and delineate nanoscopic effects without the nuisance of enthalpic or other forces.

### **Experimental.**

Blends of the tightly crosslinked nanoparticles with linear PS were prepared through co-dissolution in THF and rapid precipitation with methanol followed by drying in vacuum at 40°C for at least a week to ensure complete solvent removal. The powder was then compression molded under vacuum in a pellet press to ensure no trapped air was in a sample. The samples were aged at 120-170°C under vacuum for several hours to ensure homogeneity. The 8 mm diameter disks were placed on the 8 mm parallel plates fixture of a Rheometrics ARES rheometer set at a gap of *ca.* 0.5 mm. Various temperatures were used and the strain during the dynamic shear test was kept small enough to ensure all response was in the linear viscoelastic region. Glass transition temperatures were determined with a TA Instruments modulated differential calorimeter model Q1000. Sample sizes on the order of 4 mg were used and the instrument was fully calibrated.

## Results and Discussion

Here, low polydispersity spherical nanoparticles ( $a \sim 3\text{-}5\text{ nm}$ ), synthesized via an intramolecular collapse methodology,<sup>11</sup> are blended with linear polystyrene macromolecules of approximately the same molecular dimensions. For example, at a molecular mass of 52 kDa, with every fifth monomer unit crosslinked on average, the nanoparticles are of order 5 nm in radius and comparable to the linear polymer radius of gyration ( $R_g$ ), 7.5-15 nm. Two types of nanoparticles were used, lightly crosslinked (2.5 mol% crosslinker) and tightly crosslinked (20 mol% crosslinker, see Fig. 4.1), that were synthesized with a variety of molecular weights and hence molecular sizes. The procedure is relatively simple and robust enough to produce gram quantities of nanoparticles with controlled size and crosslinking densities from linear precursor chains.



**Images in this dissertation are presented in color.**

**Figure 4.1. Cartoon of the intramolecularly crosslinked nanoparticles produced from linear chain precursors having pendent crosslinking groups.** Varying the amount of crosslinker allows fabrication of lightly (2.5 mol% crosslinker) or tightly crosslinked (20 mol% crosslinker) nanoparticles. Nanoparticles were produced by dripping a solution into hot solvent to activate the crosslinking process. Typical conditions of volume ( $V$ ), concentration ( $c$ ), flow rate and temperature are given.

Crosslinking imposes a particle-like nature to the linear precursor chains that small angle neutron scattering (SANS) can delineate as shown in Figs. 4.2.a, b. Lightly crosslinked nanoparticles exhibit very similar scattering behavior to the linear precursor chains while the tightly crosslinked nanoparticles demonstrate a peak in the Kratky plot, indicative of particle-like behavior. The similarity of the lightly crosslinked nanoparticles to the linear polymer, at least in their segment density profile, translates to a likeness in their rheological properties. This does not invalidate the hypothesis of Antonietti et al.<sup>141</sup>

that crosslinked microgels and linear polymers are rheologically alike and indeed may strengthen it since even light crosslinking will produce cycles within the molecule.

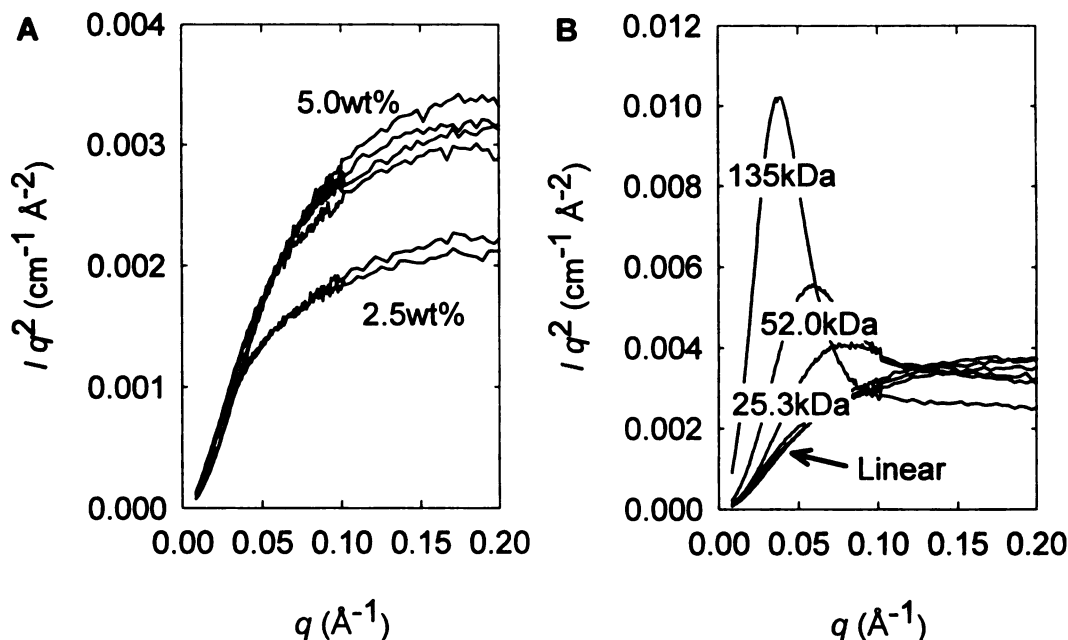


**Figure 4.2. SANS spectrum for lightly and tightly crosslinked nanoparticles demonstrating the particle-like nature of the nanoparticles when sufficient crosslinking is present. a,** Kratky plot of SANS intensity ( $I$ ) multiplied by wave vector ( $q$ ) squared as a function of  $q$  for solutions of linear precursor polymer or lightly crosslinked nanoparticle containing 2.5 mol% crosslinker. The lower concentration data of 2.5 wt% are for the 158 kDa linear chain precursor polymer and nanoparticle while the higher concentration curves, 5wt%, are for the precursor polymer and nanoparticle with 24.5kDa and 158 kDa nominal molecular masses. These data demonstrate the scattering from the lightly crosslinked nanoparticles is equivalent to a linear polymer. All data are in d-THF solvent and at 35°C. The plateau near 0.2 Å<sup>-1</sup> does not scale linearly with concentration due to concentration effects. **b,** Kratky plot for the tightly crosslinked nanoparticles containing 20 mol% crosslinker of various molecular masses (25.3kDa, 52kDa, 135kDa) compared to the linear chain precursors (curves labeled Linear). These nanoparticles demonstrate considerably different scattering behavior to the linear precursors with the curve maxima revealing particle-like behavior. Same solvent and temperature as in **a** were used, concentration is 5 wt%. The maximum does not significantly depend on the nanoparticle concentration.

A high wave vector plateau is present for the tightly crosslinked nanoparticles after a local maximum, unlike the observed behavior for a homogeneous density hard sphere.<sup>84</sup> This phenomenon was seen by Tande et al.<sup>142</sup> for poly(benzyl ether) dendrimers suggestive of both particle and Gaussian chain behavior. The ratio, radius of gyration to viscosimetric radius (determined from the intrinsic viscosity), call this  $P$ , is an important quantity to delineate segment density profiles and physics.<sup>19</sup> The dendrimer system displayed values that decreased from the Gaussian coil value (1.2-1.8, depending on solvent conditions) to the homogenous hard sphere value ( $0.775 = \sqrt{3/5}$ ) with increasing generation number (molecular mass). The tightly crosslinked nanoparticles show a similar phenomenon with  $P$ -values of: 1.24 (25.3 kDa), 1.15 (52.0 kDa) and 0.93 (135 kDa); in a good solvent (tetrahydrofuran, THF, at 35°C) that approach the hard sphere value with increasing molecular weight. However, the constant segment density profile is not achieved which contributes to the plateau in the Kratky plot. Thus, the tightly crosslinked nanoparticles are intermediate between a polymer chain and homogeneous density sphere and remarkably resemble the Gaussian soft sphere.<sup>143</sup> Indeed the Gaussian soft sphere scattering form factor looks very similar to that for the tightly crosslinked nanoparticles.

A critical feature of these systems is the poor dispersion resulting from nanoparticle agglomeration and/or interpenetration in the tightly crosslinked nanoparticle - linear PS blends. Indeed agglomeration may be expected due to depletion flocculation, however, the results of Cosgrove et al.<sup>144</sup> clearly show that 16 nm diameter silica nanoparticles are stable in poly(ethylene oxide)/water solution up to high polymer and particle concentrations. In this case, the particle half-separation distance is much lower

than the polymer  $R_g$  (equal to 10 - 35 nm) in many of their experiments and no evidence of agglomeration is seen even up to particle concentrations of 18 vol% which must be due to the nanoparticle size and scale.

The results in Fig. 4.3 for a 50 wt% blend show that the blends are well dispersed since the intensity profile shows no upturn at small wave vector and no fractal-like regime at high wave vector, therefore, compact objects are present. A Gaussian plateau occurs and a fit for a hard sphere model together with a Lorentzian, to account for the linear polymer conformation, yields an average particle size of 2.7 nm. From the nanoparticle molecular mass and this radius one can calculate the nanoparticles have collapsed to a density equivalent to bulk polystyrene. While the model results are not conclusive it is clear that the 52 kDa tightly crosslinked nanoparticles have collapsed to a smaller size than in dilute solution where the hydrodynamic radius is 4.8 nm in THF. Clearly, the SANS results and modeling are suggestive of nanoparticles collapsed to a density equivalent to bulk polystyrene, yet, a fractal-like nanoparticle network is not present. Further, a highly contorted linear chain is suggested by the Lorentzian mesh length of  $\sim 30$  nm. We recognize that a mesh length of 30 nm is extreme and is justified below.

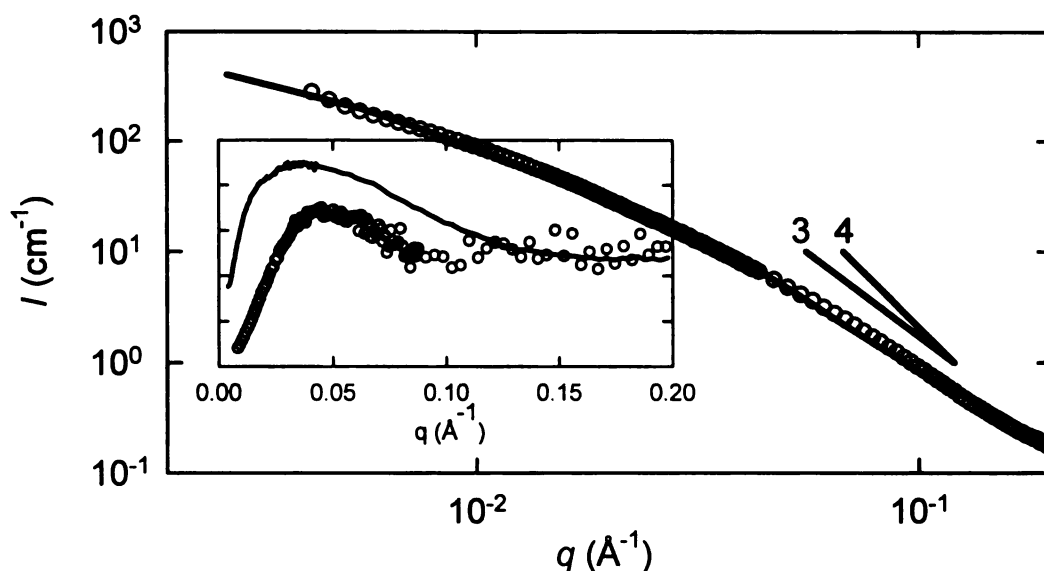


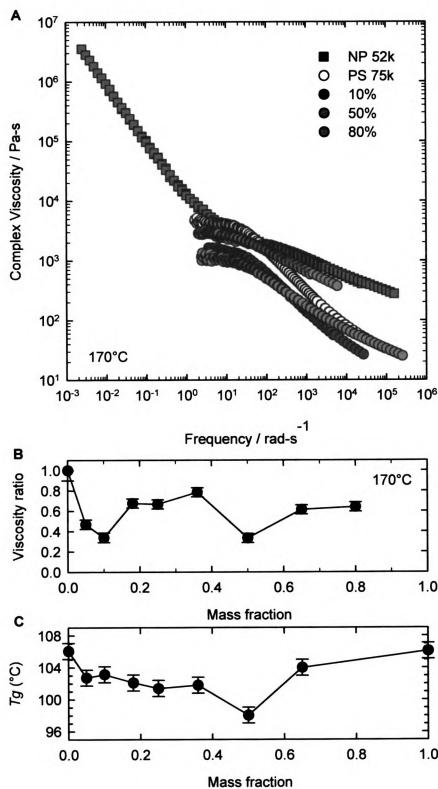
**Figure 4.3.** SANS spectrum for 52.0 kDa tightly crosslinked nanoparticles blended with 63 kDa linear d-polystyrene at 50 wt% with the incoherent background subtracted from the intensity. The solid line represents a hard sphere fit, including polydispersity, and a Lorentzian ( $I(0)/[1+\xi^2q^2]$ ,  $\xi = 29.5 \pm 0.2$  nm and  $I(0) = 623 \pm 7$  cm<sup>-1</sup>) to account for the deuterated polystyrene chains' conformation. The mean nanoparticle phase's radius from the hard sphere fit is  $2.66 \text{ nm} \pm 0.01 \text{ nm}$ , polydispersity (standard deviation divided by mean) is  $0.942 \pm 0.001$  and the volume fraction is 0.45. Power laws of 3 and 4 are shown, neither is satisfactory, suggesting that a fractal network is not present. The inset is a Kratky plot of the same data (solid line) compared to data for the same nanoparticles in dilute solution (0.05 wt% in THF at 35°C) demonstrating increased scatterer size. The intensity is in arbitrary units and the curves were shifted to overlap at high  $q$ .

The (complex) viscosity was measured as a function of frequency as shown in Fig. 4.4.a. Different temperatures were used and time-temperature superposition was followed to create a master curve at a reference temperature of 170°C. The neat tightly crosslinked nanoparticles do not exhibit a terminal viscosity even at very low frequencies. It is clear that all blends, even up to 80 wt%, show a terminal (zero frequency) viscosity.

The terminal viscosity was determined from the data and found to decrease upon nanoparticle addition (Fig. 4.4.b) despite the fact that the pure 52 kDa nanoparticles show



no terminal viscosity.<sup>141</sup> Concentrations of order 50 wt% demonstrate a viscosity decrease by a factor of 4 while predictions from either the Einstein or Kreiger-Dougherty<sup>145</sup> models suggest a large viscosity increase. For example, utilization of the Kreiger-Dougherty model estimates the suspension – pure polymer viscosity ratio should be ~ 10 rather than the measured 0.2-0.3. Further, the 80 wt% nanoparticle blend displays a terminal viscosity when a gel-like response is expected at such high concentration.<sup>100</sup> This result points to nanoparticle shape change and possible agglomeration and polymer interpenetration. However, if significant agglomeration were present a viscosity increase should occur.



**Images in this dissertation are presented in color.**

**Figure 4.4. Viscosity and glass transition temperature for 52 kDa tightly crosslinked nanoparticles, 75 kDa linear polystyrene and their blends. a,** Viscosity versus frequency (measured with a Rheometrics ARES rheometer) for the neat nanoparticles (NP 52k), neat linear polystyrene (PS 75k) and selected blends containing 10 wt%, 50 wt% and 80 wt% nanoparticles. Note the pure nanoparticle system shows no terminal viscosity. Various temperatures were used and time-temperature superposition was followed, the reference temperature was 170°C. **b,** Terminal viscosity of the blends divided by neat 75 kDa linear polystyrene viscosity versus 52 kDa tightly crosslinked nanoparticle mass fraction. **c,** Glass transition temperature ( $T_g$ ) measured with differential scanning calorimetry (TA Instruments Q1000) for the blends showing a general decrease with nanoparticle addition up to moderate volume fractions. Note the  $T_g$  for the two pure components are equal.

Slip or inhomogeneous flow could account for the viscosity decrease.<sup>98</sup> This was checked by using different gaps between the parallel plates used to characterize the viscosity, gaps from 100 – 500  $\mu\text{m}$  were utilized with the 10 wt% blend and no gap effect was seen, thus, slip and inhomogeneous flow is not a factor in the rheological measurements.

Supplementary testing with the blends shows a concomitant glass transition ( $T_g$ ) decrease with nanoparticle addition, despite each component having almost identical  $T_g$ 's, see Fig. 4.4.c. It should be noted that  $T_g$  does not change when the lightly crosslinked nanoparticles are added to the linear polystyrene, both have equivalent  $T_g$ 's, and the viscosity is intermediate between the two components following a normal mixing rule based on the weight average molecular mass. Starr et al.<sup>146</sup> show a polymer  $T_g$  reduction near nanoparticles when excluded volume interactions are present, however, if an attractive potential is present  $T_g$  is predicted to increase. As discussed above, we have an ideal system that can only interact via excluded volume. Yet, it is believed our system is different to the simulations performed by Starr et al. as they do not specifically simulate confinement effects. However, similar results of a  $T_g$  change are seen in

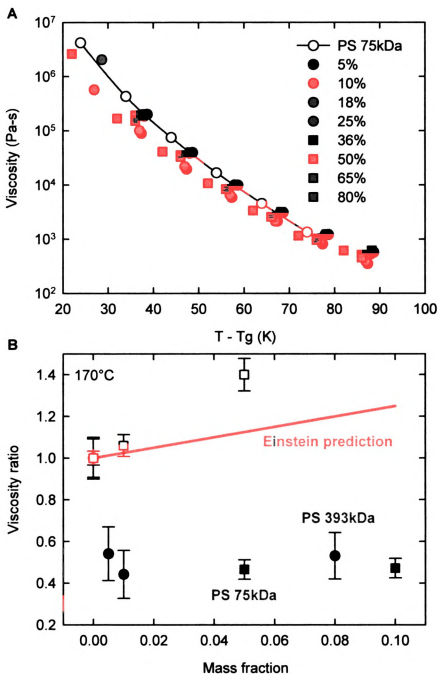
confined thin polymer films,<sup>147</sup> although it is admitted here that this is a complicated and rapidly advancing area. It is hypothesized that nanoparticle confinement effects produce the  $T_g$  decrease since the interparticle half-gap ( $h$ ) achieves quite small values. Further, all the data in this work are at concentrations where  $h$  is less than or equal to  $R_g$ .

Using a simple relation ( $h/a \approx [\phi_m/\phi]^{1/3} - 1$ ,  $\phi_m = 0.638$ ) or an empirical relation developed from Cosgrove et al.'s data<sup>144</sup> ( $h/a \approx [3.11/\phi]^{1/4.34} - 1$ ,  $0.18 > \phi > 0.03$ ) yields  $h$  equal to 0.2 – 1.4 nm for a volume fraction of 0.5. A half-gap of order 1 nm is much smaller than the linear polymer  $R_g$  and approaches the monomer length scale and so produces severe chain confinement and distortion. Note the above relations do not include the volume of the interstices between the particles which is substantial thereby allowing some volume for the polymer to occupy. However, the polymer molecule is distorted as confirmed through the SANS modeling in Fig. 4.3 where the Lorentzian mesh length is of order 30 nm. This is an exceptional value and can be rationalized by realizing the nanoparticle volume fraction is 0.5 making the volume ratio of nanoparticle ( $V_{NP}$ ) to linear polymer ( $V_{PS}$ ) equal to unity. The volume ratio is equal to the ratio of length scales to the third power ( $[d_{NP}/d_{PS}]^3$ ) and the mesh length,  $\xi$ , is  $d_{NP} + d_{PS}$ . Realizing the polymer length scale will be on the order of twice its radius of gyration ( $\sim 7\text{nm}$ ) one finds  $\xi$  equal to 28 nm in agreement with the model fitting parameter. This clearly indicates some degree of distortion.

Both the virgin linear polymer and its blend with tightly crosslinked nanoparticles follow time-temperature superposition<sup>13</sup> with similar shift factors. The terminal viscosity of the pure linear polymer is plotted as a function of temperature above  $T_g$  in Fig. 4.5.a and the usual viscosity decrease with increasing temperature is apparent. Graphing the

blends' viscosity in a similar manner, thereby accounting for the  $T_g$  decrease, shows the viscosity is a unique function of temperature above the glass transition temperature.

Nanoparticles do not, apparently, contribute to the hydrodynamics of highly entangled linear polystyrenes with molecular masses of 75 kDa and 393 kDa as shown in Fig. 4.5.b. If they did then the viscosity would follow Einstein's model<sup>33</sup> at low concentrations or Batchelor's correction for moderate concentration<sup>148</sup> and it is graphically shown that these relations are not followed. Larger particle systems in polymer melts clearly produce a viscosity increase<sup>137</sup> and so our results are a unique product of a nanosystem. To expand on this point we measured the viscosity of 1.6  $\mu\text{m}$  diameter latex microspheres (polystyrene crosslinked with divinylbenzene) blended with 75 kDa linear polystyrene. The results are shown in Fig. 4.5.b and a clear viscosity increase is seen in agreement with previous results.



Images in this dissertation are presented in color.

**Figure 4.5** Graphs showing how the viscosity changes with temperature and nanoparticle concentration. **a**, Viscosity of 75 kDa neat polystyrene and nanoparticle blends as a function of  $T - T_g$ . Open circles are the viscosity for the neat polystyrene while the other symbols represent data for tightly crosslinked 52 kDa nanoparticles dispersed in

the same polystyrene at various mass concentrations (5 – 80%). The measurement temperature range for all systems was 140 – 190°C with some extending down to 130°C. There is no clear trend with concentration and it is hypothesized that the viscosity is a unique function of distance from the glass transition temperature. **b**, Comparison of the lower concentration blends containing the tightly crosslinked 52 kDa nanoparticles in 75 kDa linear polystyrene (blue squares) and 393 kDa linear polystyrene (blue circles) at 170°C to the Einstein prediction. It is clear that a hydrodynamic contribution to the viscosity, in the contemporary sense, is not provided by the nanoparticles. To the contrary, addition of 1.6  $\mu\text{m}$  diameter crosslinked polystyrene microspheres shows the conventional viscosity increase with particle addition to 75 kDa linear polystyrene (white squares).

Thus, we expect that the nanoparticles affect a physical process within the polymer melt. Based on the increased free volume silica nanoparticles produce in poly(4-methyl-2-pentyne)<sup>10</sup> and that expanded polystyrene coils have a 45°C glass transition temperature decrease,<sup>149</sup> as well as our results in Fig. 4.5.a, we investigate whether nanoparticles can induce a free volume increase. It is simple to determine that if a spherical excluded volume of thickness  $\Delta$  exists around each nanoparticle then the fractional free volume is increased by approximately  $3\Delta/a \times \phi$  assuming the continuous phase's (i.e. linear polystyrene's) free volume does not change in the bulk. The fractional free volume increases by order 0.01, a significant change,<sup>13</sup> for a 0.1 nm shell thickness and the volume fractions used in this study. This free volume increase could explain the glass transition temperature decrease and apparently the viscosity decrease as well.

Based on the work of Merkel et al.<sup>10</sup> it may be expected that free volume is a critical factor in determining the rheological behavior, yet, the concepts of entanglements<sup>13</sup> or reptation<sup>67</sup> have not been addressed. The terminal (zero shear) viscosity for all nanoparticle concentrations is lower than that of neat polymer as shown in Figs. 4.4 and 4.5. However, concentrations above approximately 18 wt% have a viscosity at large frequencies higher than or approaching that of the virgin polymer, the 5 wt% and 10 wt% blends have a viscosity that is always lower than the pure polymer. The

80% blend exhibits minimal shear thinning and a large viscosity at high frequencies (see Fig. 4.4.a), yet, the loss modulus is always larger than the storage indicative of enhanced dissipation. This is in contrast to the neat nanoparticle system that has an equilibrium storage modulus at small frequencies. These are unusual effects and could indicate constrained polymer chains as well as entanglement or reptative changes.

Yet, drawing from the scaling theory presented by deGennes<sup>67</sup> and furthered by Doi and Edwards<sup>150</sup> one finds the terminal viscosity ( $\mu_0$ ) should scale as  $G_N^0 t_R \times [M/M_e]$ , where  $G_N^0$  is the plateau modulus,  $t_R$ , the Rouse time scale,  $M$ , the polymer molecular mass and  $M_e$ , the mass between entanglements. Further, simple rubber elasticity<sup>13</sup> shows that the plateau modulus is given by a simple combination of the density ( $\rho$ ), gas constant ( $R$ ) and temperature ( $T$ ) as well as the entanglement molecular mass,  $\rho RT/M_e$ . Should the viscosity reduction be caused by an increase in  $M_e$ , representing a decreasing number of entanglements, one would expect both the plateau modulus and the terminal viscosity to decrease. This does not seem to be the case. No clear trend of plateau modulus with nanoparticle concentration is seen and its average for all concentrations is approximately the same as that for the pure polymer. For example, the plateau modulus for 393 kDa linear polystyrene is  $(1.7 \pm 0.1) \times 10^5$  Pa, the average values for the polymer-nanoparticle composites are  $(1.5 \pm 0.3) \times 10^5$  Pa and  $(1.7 \pm 0.2) \times 10^5$  Pa for 52 kDa and 135 kDa tightly crosslinked nanoparticle blends, respectively. Further, at constant concentration (5-10 wt%) of the 52 kDa tightly crosslinked nanoparticles, the viscosity scales with the linear polymer molecular mass to the 3.5 power while neat linear polymer shows a scaling of 3.6 for the molecular masses studied. These are power laws close to that found in the



literature for entangled linear polymers,<sup>13</sup> if the polymer were completely disentangled a power law of one is expected.

Thus, entanglement modification does not explain the observed viscosity decrease and, as shown in Fig. 4.5.a, a free volume increase produces the effect. This manifests itself through the Rouse time scale and its subsequent relation to the monomeric friction factor in an unusual manner.

## **Conclusion**

We have discussed how free volume as well as certain configurational changes to the linear polymer must account for the viscosity decrease. The exact mechanism is unknown at this point and is a challenge for theoreticians. However, it is clear that nanoparticles do not contribute hydrodynamically to the viscosity in the traditional sense predicted by Einstein. Rather they produce a change in the polymer conformation and free volume to reduce the viscosity. In other words, the system's properties change with nanoparticle addition and different physics come into play to produce the viscosity decrease.

## CHAPTER 5

### EFFECT OF IDEAL, ORGANIC NANOPARTICLES ON THE FLOW PROPERTIES OF LINEAR POLYMERS: NON-EINSTEIN-LIKE BEHAVIOR

---

#### Introduction

The terminal viscosity of polymer melts is an increasing and unique function of molecular mass ( $M$ ). Below the critical mass for *entanglement coupling*<sup>13</sup> ( $M_c$ ) the viscosity scales as  $M^1$  while above  $M_c$  a much larger power law is evident, approximately 3.4-3.8 power<sup>63-65</sup> (see Fig. 5.1, data from Fox and Flory<sup>63, 64</sup>, Mackay and Henson<sup>98</sup> and this work are included in the figure). The lower, or *Rouse*,<sup>151</sup> regime actually occurs over a relatively small mass range unless correction to constant fractional free volume ( $f$ ) is made. The upper regime has an enhanced power law due to what has been denoted as entanglements whose physics can be described by *reptation*.<sup>67, 150</sup> Regardless of the physical process<sup>152</sup> unique flow behavior occurs at  $M_c$  evidenced by the power law change.

The exact mechanism that causes entanglement coupling is not truly known, however, it is clear that the free volume is essentially constant for masses greater than  $M_c$ . Below this critical mass the free volume changes essentially in concert with the specific volume. This observation does not give a fundamental picture of the complicated polymer dynamics and merely provides empirical foundation to likely explanations that incorporate a constant free volume within an entangled polymer melt.

An interesting study was performed to elucidate how entanglements, or lack thereof, affect the flow behavior of polymer melts.<sup>153</sup> Polymer molecules were freeze dried or crystallized from dilute solution then physically compressed and viscosity measured; no change in viscosity was found after the first 20 mins, the time for the first data point to be recorded. This is in contradiction to the results of Liu and Morawetz<sup>154</sup> who show that individual polymer molecules take an extraordinary length of time ( $> 16$  h) to reach equilibrium in a melt. However, Farrington<sup>155</sup> determined that the storage modulus ( $G'$ ) changed significantly within the first 20 mins for samples prepared similar to above or for microemulsion polymerized polystyrene nanoparticles that were allowed to interdiffuse upon heating (particle size  $\sim 40$  nm,  $M \sim 10^6$  Da). This process depended on temperature and when compared to the relaxation or reptation time ( $t_d$ ) approximately  $10 \times t_d$  was required for equilibrium. Although this study could follow the kinetics of entanglement formation, the true equilibrium, in accord with the work of Liu and Morawetz, was not achieved suggesting polymer melts are either never at true equilibrium and/or flow properties are not sensitive to non-equilibrium structure.

Despite the apparent difficulty in robustly degrading entanglements through physical means one can eliminate them through flow.<sup>156</sup> Shear can reduce entanglements or constraints,<sup>157</sup> and as shown in Fig. 5.1, the possible change in viscosity to the free Rouse chain limit exemplifies the overall effect of entanglements. If entanglements could be eliminated by solution precipitation techniques one would expect the Rouse limit to similarly apply.<sup>150</sup>

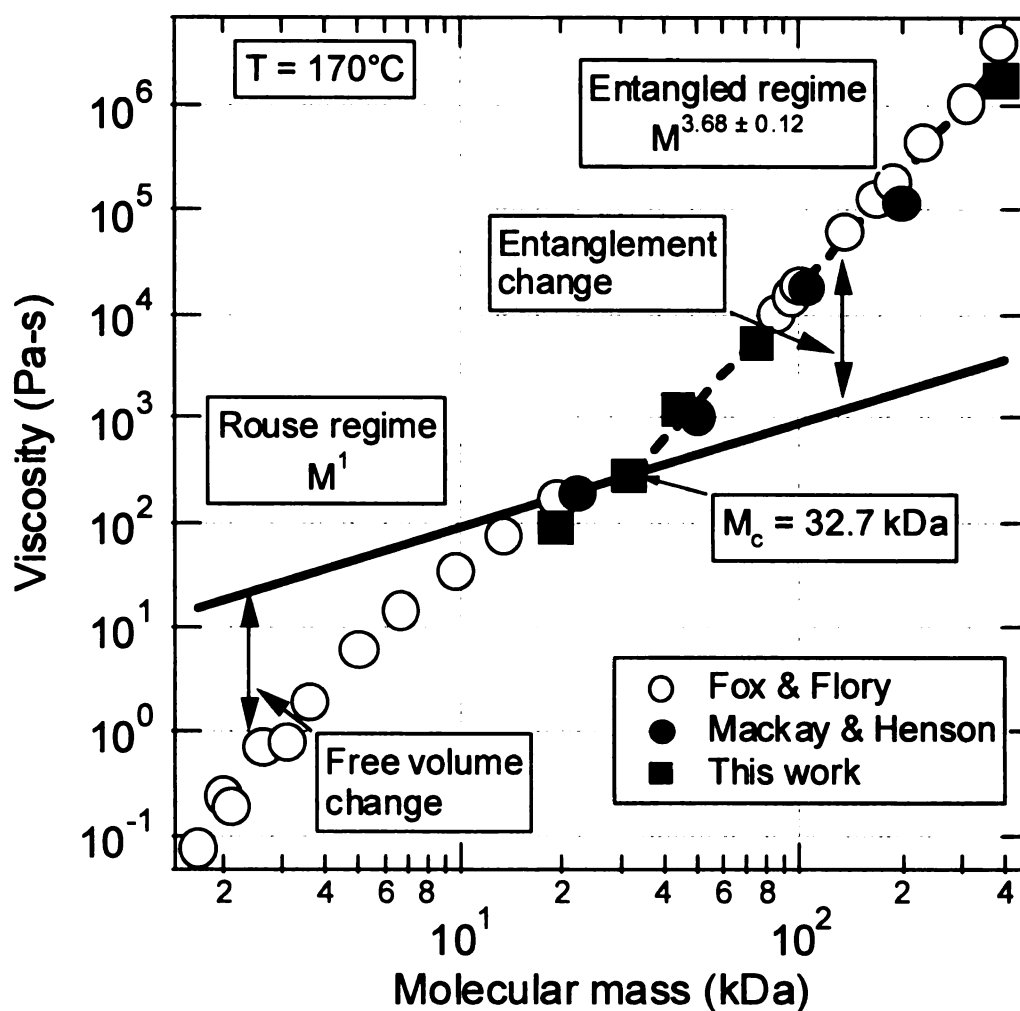


**Figure 5.1.** Viscosity as a function of molecular mass ( $M$ ) for polystyrene melts at 170°C. Data from Fox and Flory<sup>2,3</sup>, Mackay and Henson<sup>5</sup> and this work are used to show how, below the critical molecular mass for entanglement coupling ( $M_c$ ) the Rouse model is followed, except from deviations caused by a free volume change. Above  $M_c$  the entangled regime results with a much larger power law exponent of viscosity with  $M$ . Changes in the entanglement structure or dynamics could reduce the viscosity to the Rouse limit.

It is conjectured that thin polymer films next to hard surfaces<sup>158 159</sup> change polymer entanglement<sup>160</sup> with minimal change in the radius of gyration ( $R_g$ ) parallel to the substrate.<sup>161</sup> So it was hypothesized by us that nanoparticle inclusion could affect polymer flow in a more robust manner compared to precipitation techniques discussed

above due to the introduction of a vast number of hard surfaces by the nanoparticles. Yet, addition of particulates to polymer melts demonstrates complicated behavior,<sup>137</sup> although continuum relations provide methods to data correlation. In Einstein's seminal manuscript,<sup>33</sup> it was shown that the viscosity increase Brownian particles provide scales with the particle volume fraction,  $\phi$  ( $\eta = \eta_s [1 + 2.5\phi]$ , where  $\eta$  is the solution viscosity and  $\eta_s$  is the solvent viscosity). A viscosity increase has been observed in many systems<sup>100</sup> even when small ( $\sim 260$  nm) polystyrene latex particles<sup>162</sup> and nanoparticles ( $\sim 56$  nm) made of silica<sup>163</sup> were studied. These systems have particle sizes much larger than the suspending fluids' molecular size and so continuum expectations introduced by Einstein are followed.

Of course, when the particle becomes molecular in size it is possible to see deviations. Edward<sup>164</sup> surveyed the literature to find when the Stokes-Einstein (SE) relation could not be applied to diffusion of molecular penetrants in simple fluids such as water and carbon tetrachloride. When the penetrant's radius ( $a$ ) became 2-3 times that of the suspending liquids' then deviations from the SE relation were evident. This is equivalent to stating that the numerical factor for the friction coefficient  $\zeta$  ( $\equiv 6\pi \eta_s a$ ) is no longer 6 and decreased in value when very small penetrants were considered.

Deviations from the SE relation have been observed in diffusion of tracer spheres in polymer solutions.<sup>165</sup> In this case, however, the most significant deviation occurred at high polymer concentration with large spheres ( $a \sim 1 \mu\text{m}$ ) rather than smaller ( $a \sim 20$  nm). The explanation given was that shear thinning influenced the diffusivity. More recent work has concentrated on this effect to determine the microrheology or local viscosity of polymer solutions (see *e.g.* Lu and Solomon<sup>166</sup>). This phenomenon is argued

as related to local scale heterogeneity of the polymer solution. Further, larger particles were found to diffuse faster than smaller and this may be akin to the principle of size exclusion chromatography as the larger particles take a less circuitous route through the heterogeneous structure.

The situation is different in polymer melts such as poly(dimethyl siloxane) or PDMS. Roberts et al.<sup>167</sup> showed that a larger silicate nanoparticle ( $a = 2.8$  nm) followed the SE relation as long as an adsorption layer of PDMS was considered. The 5 kDa polymer's radius of gyration ( $R_g$ ) was 2.0 nm and so the particle and polymer were of the same size. Of course, the particle is much larger than the PDMS monomer unit. When a smaller nanoparticle was investigated ( $a = 0.44$  nm), which is closer in size to the monomer unit and much smaller than the polymer as a whole, anomalous behavior was observed and the particle appeared smaller than its true size, at least in a hydrodynamic sense. The authors state that this smaller nanoparticle behaved like a solvent while the larger as a colloidal particle. Note  $M_c$  for PDMS is 24.5 kDa<sup>13</sup> and so all the studies by Roberts et al. were conducted in an **unentangled** polymer melt.

Recently, Zhang and Archer<sup>168</sup> studied the effect of the nanoparticle-polymer interaction parameter, in blends of poly(ethylene oxide) (PEO) and silica nanoparticles (~12 nm diameter). Pure silica nanoparticles are strongly interacting (physisorption) with PEO. It was seen that even a very small addition of nanoparticles caused a large increase in viscosity of an **entangled** PEO system, probably by formation of a polymer-nanoparticle network in the melt. When the nanoparticle surface was chemically modified by grafting an oligomeric PEO terminated with a trimethoxy silanyl group, no network

formation was found. Further, there was no change in the viscosity of the polymer melt on nanoparticle addition.

The above provides a brief introduction to the complicated dynamics of polymer melts and highlights that the size and scale of nanoparticles compared to polymer molecules could yield interesting behavior. The nanoparticles used in this work have a size between 5 – 10 nm which is much larger than a monomer unit ( $\sim 0.3$  nm). Polymers in contrast to simple fluids, like water, have an equilibrium configuration that spans 10 – 20 nm and so the nanoparticles are smaller than the polymer molecules. Further, the size associated with entanglement coupling is approximately 5 – 10 nm and is of the same size as the nanoparticles. Clearly, the nanoscopic size chosen here could disrupt the polymer dynamics.

In our previous study,<sup>8</sup> we investigated the effect of polystyrene nanoparticles<sup>11</sup> on the flow properties of **entangled** polystyrene melts. This is an ideal system since the particle and polymer are chemically equivalent, and have a similar refractive index, thereby reducing if not eliminating dispersion forces.<sup>169</sup> Thus, the system was equivalent to hard spheres dispersed in an entangled polymer melt.

The terminal (zero shear) viscosities of the systems were always found to decrease upon nanoparticle addition, paralleling the reduction of the glass transition temperature ( $T_g$ ). The plateau modulus ( $G_N^0$ ) was not affected and so it was argued that the entanglement density<sup>13, 150</sup> was not affected. Further, a graph of the terminal viscosity with temperature ( $T$ ) above  $T_g$ , or  $T - T_g$ , resulted in a master curve suggesting that the nanoparticles caused a glass transition temperature decrease and the viscosity reduction related to a free volume change. Evidently the free volume change of unentangled melts,

concomitant with the excess viscosity reduction below the Rouse limit, is translated to entangled melts (see Fig. 5.1).

Free volume could be readily incorporated by nanoparticles through their high surface area to volume ratio.<sup>10</sup> Assuming an excluded volume layer of thickness  $\Delta$  exists around each nanoparticle, the fractional free volume ( $f$ ) within the linear polystyrene matrix is increased by  $\sim 3\phi\Delta/a$ . The free volume increase can be quite large for nanoparticles; assuming a volume fraction of 0.1, exclusion layer thickness of 0.1 nm and radius of 3 nm results in an  $f$  increase of 0.01 which is a 10-20% increase in free volume at typical melt temperatures. A colloidal scale particle ( $a \sim 300$  nm) produces a much smaller fractional free volume increase, 0.0001.

It was anticipated by Mackay et al.<sup>8</sup> that the viscosity decrease was a much more complicated phenomenon than a mere free volume increase. This became evident when the average interparticle half gap ( $h$ ) was determined. Twice this distance represents the average distance separating particles and is approximated by

$$h/a = [\phi_m/\phi]^{1/3} - 1 \quad (5.1)$$

where  $\phi_m$  is the maximum random packing volume fraction ( $\sim 0.638$ ). Since the half gap scales with nanoparticle radius, this variable can become quite small at modest loadings. For example, a 3 nm radius nanoparticle at a volume fraction of 0.1 suspended in a liquid results in an average half gap of  $\sim 2.5$  nm and is much smaller than the entangled linear polymer's  $R_g$ . Thus, it appears easy to confine linear polymers between nanoparticles at moderate volume fractions as long as they don't agglomerate (depletion flocculation). The systems discussed by Mackay et al. were all confined (*i.e.*  $h < R_g$ ) and the linear polymer had masses above  $M_c$ .



We were able to confirm through small angle neutron scattering (SANS) that our system did not significantly agglomerate even at volume fractions of 0.5. This result agrees with Cosgrove et al.'s study<sup>144</sup> for a poly(ethylene oxide) - water system containing silica nanoparticles ( $a = 8$  nm). They found that negligible particle clustering was evident possibly because the nanoparticles are smaller than the linear polymer ( $R_g \sim 10 - 35$  nm). It can be hypothesized that continuum arguments<sup>170</sup> are no longer valid in nanosystems and when  $R_g/h$  approaches and exceeds one that phase separation and agglomeration does not occur.

In the present study we extend our results to gain further insight into this unique phenomenon of a viscosity reduction when nanoparticles are added to polymer melts. The ratio  $R_g/h$  was greater than one in the previous study<sup>8</sup> indicating that the linear macromolecules in the continuous phase were always confined. Here the ratio is made less than one to determine the effect of this variable under different conditions. In addition, a wider range of nanoparticle sizes and polymer molecular masses are used to elucidate the effect of size and molecular architecture on the flow properties of polymer melts.

## Experimental

**Materials and synthesis.** Linear polystyrene (PS) was purchased from Scientific Polymer Products at molecular masses of 19.3, 31.6, 75.7 and 393.4 kDa. Details of these polymers are given in Table 5.1. The radius of gyration was determined by a relation developed from data of Cotton et al.<sup>171</sup> ( $R_g(\text{nm}) = 0.87 \sqrt{M(\text{kDa})}$ ), a deuterated polymer

has a prefactor of 0.84) The nanoparticles (NPs) were synthesized by intramolecular crosslinking, details of the process are provided elsewhere.<sup>11</sup> All the nanoparticles used in this work were tightly crosslinked (20 mol% intramolecular crosslinking). It should be pointed out that the solubility parameter for the polystyrene nanoparticles matched that for linear polystyrene (9.1 - 9.2 (cal/cm<sup>3</sup>)<sup>1/2</sup>) determined by measuring the hydrodynamic radius in various solvents via dynamic light scattering. The solvent producing the largest radius is assumed to have the same solubility parameter as the polymer. All solvents were purchased from Sigma-Aldrich and used as received.

**Table 5.1.** Polystyrene materials used in this study.

Sample	M <sub>w</sub> (kDa) <sup>a</sup>	M <sub>n</sub> (kDa) <sup>a</sup>	Condition
PS 19kDa	19.3	18.1	Linear
PS 31kDa	31.6	28.9	Linear
PS 75kDa	75.7	64.7	Linear
PS 393kDa	393.4	339.1	Linear
d-PS 155kDa	155.8	130.9	Linear
25 kDa NP	27.3 <sup>b</sup>	25.3 <sup>b</sup>	Crosslinked
52 kDa NP	61.3 <sup>b</sup>	52.0 <sup>b</sup>	Crosslinked
135 kDa NP	162.0 <sup>b</sup>	135.0 <sup>b</sup>	Crosslinked

<sup>a</sup> M<sub>w</sub> is the weight average mass and M<sub>n</sub> is the number average molecular mass.

<sup>b</sup> Based on the assumption that a single chain collapses to give a single nanoparticle. The masses for the linear chains were determined by GPC.

**Sample Preparation.** Blends of the PS nanoparticles with linear PS were prepared through co-dissolution in THF and rapid precipitation with methanol,<sup>8, 116</sup> followed by drying in vacuum at 50°C for at least a week to ensure complete solvent removal. The powder was then molded by compression, under vacuum, in a pellet press

(8 mm diameter) to ensure that no trapped air remained in the sample. The samples were aged at 130–170°C, under vacuum, for several hours to ensure homogeneity.

**Rheology measurements.** The 8-mm diameter discs obtained from the pellet press were placed on the 8-mm parallel plates fixture of a Rheometrics ARES rheometer set at a gap of approximately 0.4 mm. Measurements were done in the dynamic (oscillatory) mode. Frequency sweeps in the range 0.1-100 rad/sec were performed at various temperatures. These were then combined using time-temperature superposition<sup>87</sup> to yield a master curve at 170°C (all quoted temperatures refer to the surface temperature of the lower plate). The strain during the dynamic shear test was kept small enough to ensure that all response was in the linear viscoelastic region. A dwell time of 8-10 mins. was allowed at each temperature for the samples to attain a uniform melt temperature, before commencing measurements.

**Differential scanning calorimetry (DSC) measurements.** A TA instruments Q-1000 DSC was used to perform all glass transition measurements. Each sample was subjected to at least three heating - cooling cycles, where each cycle consisted of heating the sample from 0°C – 200°C, at a rate of 5°C / min, followed by cooling back to 0°C, also at 5°C / min. The inflection point for the heat flow as a function of temperature was taken as the glass transition temperature for a particular cycle. The glass transition temperatures reported in this work are the mean of the glass transition temperatures obtained from the second and the third run cycle.

**Relaxation spectra.** The RSI Orchestrator software available with the ARES rheometer was used to evaluate the continuous relaxation spectra, using both the  $G'$  (storage modulus) and  $G''$  (loss modulus) data. An algorithm developed by Mead<sup>172, 173</sup>

was used to model the relaxation modulus as a discrete  $N$  element Maxwell line spectrum. In such a case the storage and loss moduli for a system are given as

$$G'(\omega) = \sum_{i=1}^N G_i \frac{(\omega t_i)^2}{1 + (\omega t_i)^2} \quad (5.2.a)$$

$$G''(\omega) = \sum_{i=1}^N G_i \frac{\omega t_i}{1 + (\omega t_i)^2} \quad (5.2.b)$$

where  $\omega$  is the frequency,  $t_i$  are the time constants and  $G_i$  the corresponding moduli. The discrete relaxation spectra are converted to a continuous relaxation spectrum based on the work of Baumgaertel and Winter.<sup>174</sup> They developed the ‘parsimonious’ model to mimic a continuous relaxation spectrum, based on the idea that the discrete relaxation times should be freely adjustable so as to converge to the characteristic relaxation values for the material under study. Then, for a system having equally log-spaced time constants, the continuous  $H(t_i)$  and the discrete spectra are related by a simple scale factor

$$G_i = H(t_i) \log(R) \quad (5.3)$$

where  $R$  is the ratio of successive time constants.

**Small Angle Neutron scattering (SANS).** The SANS experiments were performed on the compression molded samples at the SAND instrument of IPNS at Argonne National Laboratory.<sup>175</sup> Neutrons are produced at IPNS with a pulse frequency of 30 Hz and wavelengths ( $\lambda$ ) in the range 1.4 - 14 Å. The instrument has a fixed detector distance of 2 m, which results in an instrument  $q$  range of 0.005-0.6 Å<sup>-1</sup> ( $q = 4\pi/\lambda \sin(\theta/2)$ , where  $\theta$  is the scattering angle). The instrument detector was a 40 × 40 cm<sup>2</sup> area sensitive <sup>3</sup>He detector with 128 × 128 channels. The scattering time for the samples was 2 hours.

The raw data were absolutely calibrated using a silica standard, following the described procedure at IPNS.<sup>176</sup> All samples were also run in transmission mode for 15 minutes to aid in the calibration.

**Kratky plots.** The description of scattering from polymer chains in their theta condition (second virial coefficient,  $A_2 = 0$ ) was first postulated by Debye.<sup>17</sup> For a Gaussian distribution of segment density within the coil the scattering function (or differential cross-section)  $I(q)$  is given as<sup>18,177</sup>

$$I(q) = \phi \times V (\Delta\rho)^2 \left\{ 2(\exp(-(qR_g)^2) + (qR_g)^2 - 1)/(qR_g)^4 \right\} \quad (5.4)$$

Here,  $\phi$  is the volume fraction of scattering centers,  $V$ , the volume of a single scattering center and  $(\Delta\rho)^2$ , the difference in the scattering length densities between solvent and scatterer (or the contrast). In the high  $q$  limit (practically  $q > 5R_g^{-1}$ ),<sup>18</sup> eq. 5.4 reduces to

$$I(q) \times q^2 = 2\phi \times V (\Delta\rho)^2 / (R_g^2) \quad (5.5)$$

The plot showing the variation of  $I(q) \times q^2$  with  $q$  is known as a Kratky plot. For any given sample,  $\phi$ ,  $V$ ,  $\Delta\rho$ ,  $R_g$  are constant, thus, from eqs. 4 and 5, for an ideal, Gaussian coil the Kratky plot should asymptotically approach a constant value (plateau) at high  $q$  values.

The Kratky plot is a good indicator of the polymer's inherent molecular architecture as it reflects the short-range interactions acting along the polymer chain from neighbor to neighbor, such as bond forces and hindrance of rotation. Deviations from the asymptotic behavior (as observed for a polymer coil) in the Kratky plot indicates non-ideal arrangement of the polymer segments. A constant density sphere has no plateau and

a series of ever decreasing peaks is seen. Both ring and star polymers have a peak (maximum) prior to the asymptote revealing different distributions than linear polymers.<sup>84</sup>

## Results and Discussion

SANS serves as an important tool to determine the degree of dispersion as well as the molecular architecture of polymer nanoparticles, both in solution and melt states. This technique is especially useful for this system as there is no optical or mass contrast between the PS nanoparticles and linear PS, eliminating the possible use of light or x-ray scattering, as well as electron microscopy, for characterization.

Fig. 5.2.a shows the Kratky plot for a 2% blend (by mass) of the 52 kDa NP in deuterated-155 kDa linear polystyrene. The background was deuterated-polystyrene, and hence the data shows scattering from the nanoparticles. The peak in the Kratky plot is immediately apparent, indicating that the intramolecular crosslinking induces a particle like nature to the molecules.<sup>142</sup>

Fig. 5.2.b shows the scattering intensity from the same sample as a function of the wave vector  $q$ . It can be seen that the intensity is not a power law function of  $q$ , instead the intensity goes to a plateau in the low  $q$  regime, confirming the absence of phase separation (depletion flocculation) of the nanoparticles, which has been a common problem with other nanoparticle-polymer blends.<sup>178, 179</sup>

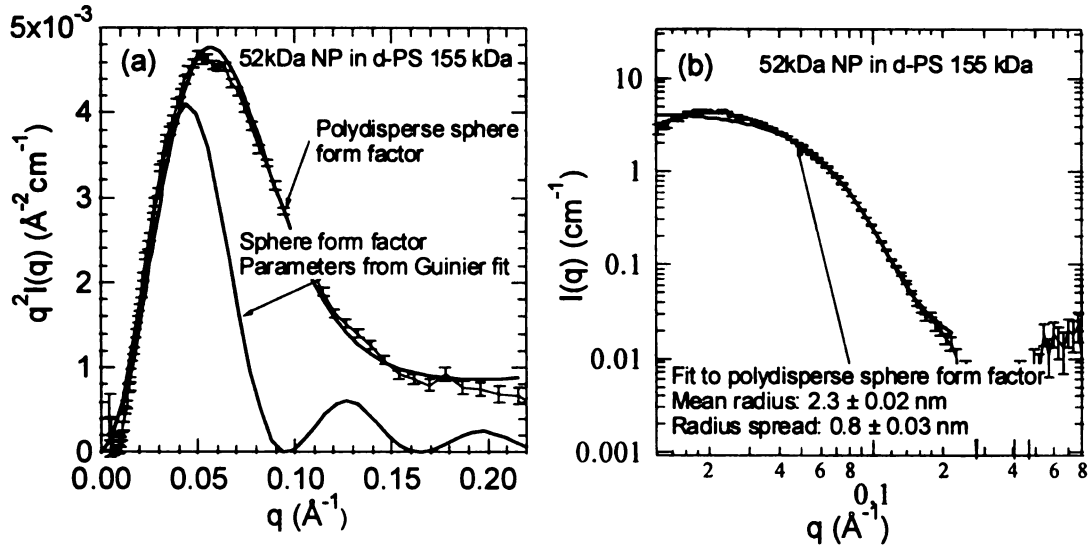


**Figure 5.2.** (a) Neutron scattering intensity ( $I$ ) multiplied by the wave vector ( $q$ ) squared as a function of wave vector (Kratky plot) for 2 wt% 52 kDa NP blended with d-PS 155 kDa. The peak is associated with globular objects and the associated Schulz polydisperse hard sphere fit reasonably represents the data (mean radius of  $2.3 \pm 0.02$  nm with a radius spread of  $0.8 \pm 0.03$  nm). The other curve is the result of a simulation assuming a monodisperse system of spheres with a radius given by the Guinier result ( $4.0 \text{ nm} = \sqrt{(5/3) \times 3.1 \text{ nm}}$ ). (b) Log-log graph of intensity versus wave vector for the same system and the associated polydisperse hard sphere fit.

Also, shown in Fig. 5.2.a, is the Kratky profile for a monodisperse hard sphere system having the same radius of gyration as the nanoparticles determined with the Guinier technique. The Guinier approximation is applied in the low  $q$  scattering regime, when  $q \times R_g$  is small and can be written as

$$\log I(q) = \log I(0) - \frac{(qR_g)^2}{3} \quad (5.6)$$

where  $I(0)$  is given by  $\phi V(\Delta\rho)^2$ . The Guinier plot,<sup>86</sup>  $\log(I(q))$  versus  $q^2$ , allows determination of  $R_g$  and, further, can be used as a concentration check through the neutron intensity at zero wave vector, which we have done.

The parameters determined from the Guinier fit do not represent the data well due to the slight sample polydispersity. This becomes apparent when the scattering data are fitted to a polydisperse hard sphere model by assuming a Schulz distribution<sup>180</sup> arriving at a mean radius ( $\langle a \rangle$ ) of  $2.3 \pm 0.0_2$  nm and a radius spread of  $0.8 \pm 0.0_3$  nm; the fit is shown in Fig. 5.2 to be reasonably representative of the data. These values yield a radius polydispersity index (rPDI) of 1.12 and polydispersity parameter of 8.3 ( $k$ ,  $\text{rPDI} = [k+1]/k$ ). The z-average radius can be found to be  $2.9 \pm 0.6$  nm ( $[k+2]/k \times \langle a \rangle$ ) while the radius found from the Guinier analysis is  $4.0 \pm 0.9$  nm (for a hard sphere  $a = \sqrt{(5/3)} \times R_g$ ). Since the Guinier technique yields the z-average size, agreement between these two values is expected, while deviations between them may occur from errors in either regression and/or because the polydispersity is not accurately described by the Schulz distribution. Polydispersity is expected through the nature of the polymerization reaction as well as the crosslinking process itself which may produce molecular dimers, trimers, etc. We use a radius calculated from the expected number average molecular mass for the NPs (Table 5.1) assuming a density (1.04 g/cc) equivalent to bulk polystyrene.

Since homogeneous blends can be produced, different molecular mass nanoparticles were blended with linear polystyrene having molecular mass below  $M_c$  (unentangled), near  $M_c$  and above  $M_c$  (entangled). Fig. 5.3.a shows the ratio of the terminal (zero shear) viscosity of the nanoparticle blends with PS 19.3 kDa to the terminal viscosity of pure PS 19.3 kDa, as a function of  $R_g/h$  (see eq 5.1). When the ratio  $R_g/h$  is less than 1, the interparticle separation between the nanoparticles is greater than the radius of gyration of the linear polymer coil. With increasing particle loading, the interparticle gap becomes less than the radius of the polymer, causing confinement. It is



important to point out that none of the viscosity data discussed here show a master curve when correlated with particle volume fraction (see appendix).

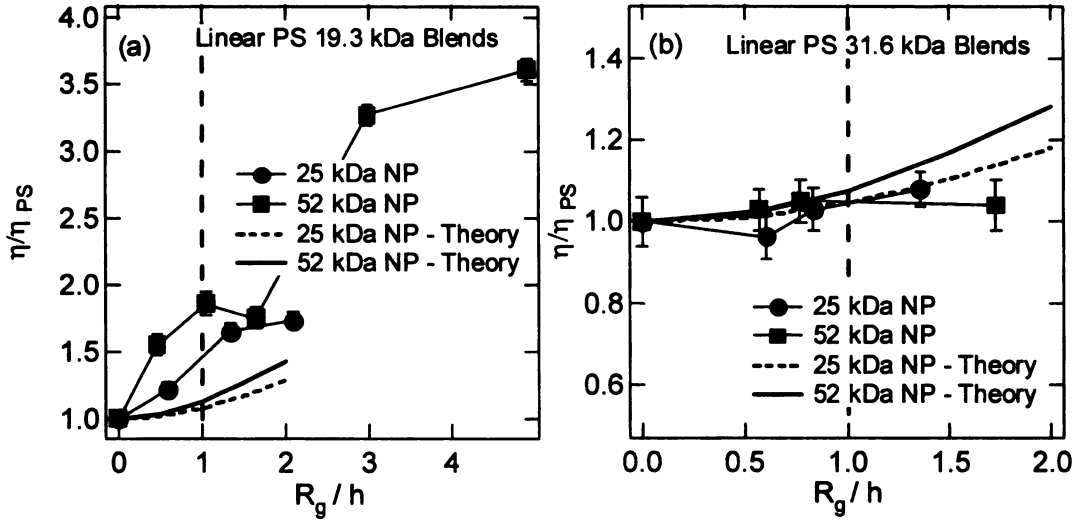


**Figure 5.3.** Viscosity ratio of the nanoparticle blends with respect to pure polystyrene, with polystyrene below (19.3 kDa) (a) and near (31.6 kDa) (b) the critical entanglement molecular mass at 170°C. The curves labeled theory are the values predicted by Batchelor's relation for this system, ending at the limit of the relation's applicability ( $\phi \sim 0.1$ ). It can be seen that the blend viscosity is much greater than the predicted value for the blend below  $M_c$ , however, when the polymer is near  $M_c$ , the viscosity hardly varies with addition of nanoparticles, again contradicting the Einstein and Batchelor predictions.

From Fig. 5.3.a it can be seen that addition of both the 25kDa and the 52kDa nanoparticles causes a sharp increase in the viscosity of the polymer melt. The curves labeled 'theory' are predictions from Batchelor's relation,<sup>148</sup> which is a modification of Einstein's relation, and includes the effect of hydrodynamic interactions in the system with increasing concentration,

$$\eta = \eta_s(1 + 2.5\phi + 6.2\phi^2) \quad (5.7)$$

The  $\phi^2$  correction improves the limit of applicability of Batchelor's relation to  $\phi \sim 0.1$  as compared to Einstein's relation whose limit is  $\phi \sim 0.02$ . From Fig. 5.3.a, it can be

seen that addition of nanoparticles increases the viscosity of unentangled polymers and this increase is much greater than predicted by either Einstein or Batchelor. Also, the increase in viscosity caused by the addition of 52 kDa NP's is greater than caused by the 25 kDa NP's, suggesting that the viscosity increase in the polymer is affected by nanoparticle size.

Fig. 5.3.b shows the effect of nanoparticle addition on linear polystyrene near  $M_c$ . In this case it can be seen that there is essentially no change in the viscosity of the linear polymer on the addition of nanoparticles, even with particle volume fractions as high as 0.1 (the standard deviation in the measured viscosity for all samples was  $< 5\%$ ). This surprising result holds true for both the 25 kDa and 52 kDa nanoparticles. It was also seen that the complex viscosity ( $\eta^*$ ), storage modulus ( $G'$ ) and loss modulus ( $G''$ ) curves (not shown here) for all the nanoparticle blends completely overlaid with the pure linear polymer curve at all frequencies. This observation is in stark contrast to what is seen for the unentangled and the entangled polymers, as will be shown below.

Entangled polystyrene samples with molecular mass 75 kDa and 393 kDa, were blended with the nanoparticles at various concentrations, and as shown in Fig. 5.4.a, the viscosity ratio for PS 75 kDa is a complicated function of  $R_g/h$ . It is immediately apparent that the behavior of the entangled system is different to the previous two cases that were considered. For both the 52 kDa and the 135 kDa NP it can be seen that when  $R_g/h$  is less than 1 (no confinement), the viscosity increases sharply. Here the increase in viscosity is much greater than that predicted by either Einstein's or Batchelor's relation. However, as soon as  $R_g/h$  is greater than 1 (confinement), there is an abrupt decrease in viscosity. For example, the 52 kDa nanoparticle system has a viscosity ratio change from 1.6 to 0.6 as

the  $R_g/h$  value changes from 0.9 ( $\phi = 0.01$ ) to 2.1 ( $\phi = 0.05$ ). In all the different nanoparticle systems, for values of  $R_g/h$  greater than one, it can be seen that the viscosity ratio is either close to 1 or is greatly reduced. Thus, the confinement of the linear chain leads to a reduction in the melt viscosity, even as the particle volume fraction is increased. It is also important to point out the reduction in viscosity does not scale with the volume fraction (see appendix for this chapter) of the added nanoparticles, as mentioned above. This suggests that the mixing rule for viscosity is not applicable for this system.

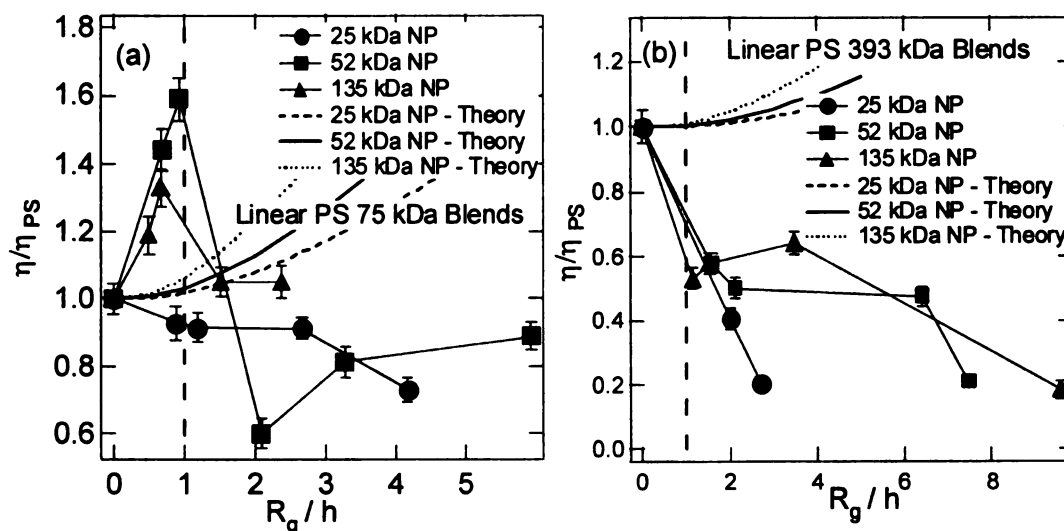


**Figure 5.4.** Viscosity ratio of the nanoparticle blends with respect to pure polystyrene for two different entangled systems, PS 75 kDa (a) and PS 393 kDa (b) at 170°C. The curves labeled theory are the values predicted by Batchelor's relation and these end at the limit of the relation's applicability ( $\phi \sim 0.1$ ). The viscosity falls precipitously when the radius of gyration is greater than the inter-particle half-gap for the entangled systems.

The viscosity variation for the PS 393 kDa blends is shown in Fig. 5.4.b. In this case all the blends considered had an  $R_g/h$  value  $>1$ , and as was seen for the PS 75 kDa blends, the viscosity is decreased for all the nanoparticle blends at all concentrations. It is

interesting to note addition of just 1% ( $R_g/h = 2.8$ ) of the 25 kDa NP causes an 80% reduction in the melt viscosity. It was difficult to produce a blend with  $R_g/h < 1$  for this system because of the very low concentration of nanoparticles required.

The complex viscosity profiles for the pure polystyrene (PS 393 kDa), pure 52 kDa nanoparticles, as well as their blends, as a function of frequency, are presented in Fig. 5.5.a. It is observed that the pure nanoparticle system does not have a terminal viscosity and instead behaves like a yield stress material, having an infinite viscosity at zero shear rate (frequency). This behavior is similar to the rheological behavior of some intramolecularly crosslinked polystyrene microgels studied by Antonietti et. al.<sup>141, 181</sup>

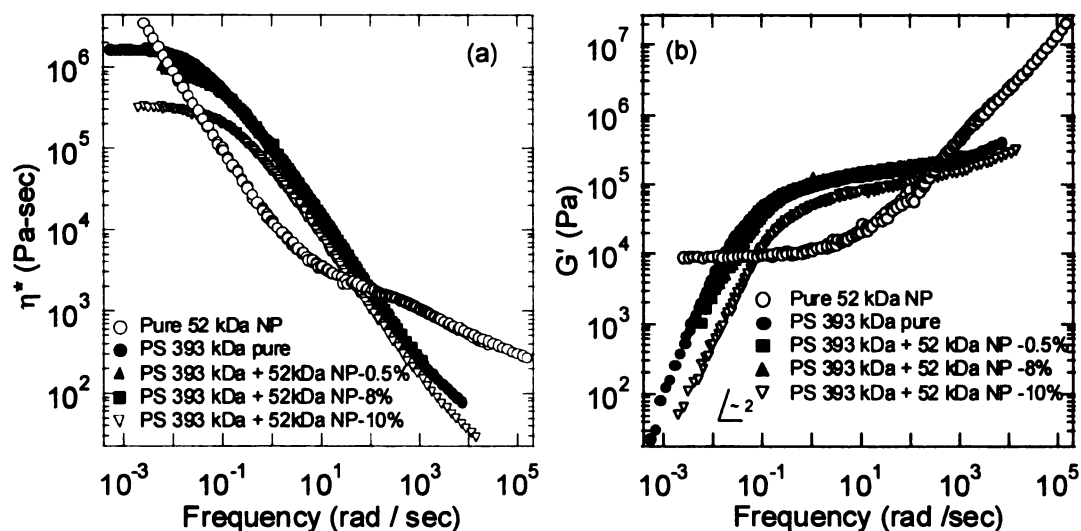


**Figure 5.5.** (a) Complex viscosity as a function of frequency for PS 393 kDa, 52 kDa NP and their blends at 170°C. It can be seen that the pure nanoparticles display a gel like behavior with an infinite terminal viscosity. All the blends however have a distinct terminal viscosity which is lower than the pure component. (b) Storage modulus variation with frequency for the same systems at 170°C. Blends with a nanoparticle concentration below 10% have a plateau modulus equivalent to the virgin polymer while the 10% blend has a reduced modulus and complex viscosity at all frequencies.

In contrast, both the pure linear polymer and the nanoparticle blends have a finite terminal viscosity. From Fig. 5.5.a, it can also be seen addition of nanoparticles at low concentrations (up to  $\phi \sim 0.08$ ), only affects the terminal region, demonstrated by a lower zero shear viscosity. Above a critical frequency ( $\sim 10^{-1}$  rad/s in this case) the viscosity curves for all the blends merge with the pure polystyrene curve. However, further addition of nanoparticles causes a viscosity reduction at all frequencies, as can be seen with the 10% blend.

The same trend is observed for the storage modulus curves of the pure components and the blends (Fig. 5.5.b). Traditionally the storage modulus for the polymer blends relates directly to the storage modulus of its components.<sup>182, 183</sup> In this case, however,  $G'$  variation for the blends is governed by the  $G'$  for the linear polymer, with the nanoparticles providing a reduction in the terminal region. As was seen earlier, after a frequency  $\sim 10^{-1}$  rad/s, all the  $G'$  curves (up to  $\phi \sim 0.08$ ) merge with the pure PS 393 kDa curve.

For all the blends discussed above, the minima in  $G''/G'$  ( $\tan \delta$ ) occurred near a frequency of 10 rad/s. The value of  $G'$  corresponding to the minima in  $\tan \delta$  is taken as the plateau modulus ( $G_N^0$ ).<sup>99</sup> As all the  $G'$  curves overlay near this frequency, it was concluded that the plateau modulus of the polymer is unaffected by addition of nanoparticles, up to  $\phi = 0.08$  (the  $G_N^0$  values are listed in Table 5.2). This observation is contrary to the rule of mixing for athermal systems as postulated by both Tsengoglou<sup>184</sup> and Wu,<sup>185</sup> where the plateau modulus for the blend scales with the plateau modulus of its components.

**Table 5.2.** The plateau modulus for pure PS 393 kDa and its blends with various nanoparticles at 170°C

Sample	Plateau Modulus (MPa)
PS 393 kDa	0.167±0.015
PS 393 kDa + 25kDa NP -0.5% blend	0.165±0.019
PS 393 kDa + 25kDa NP -1% blend	0.078±0.009 <sup>a</sup>
PS 393 kDa + 52kDa NP -0.5% blend	0.171±0.009
PS 393 kDa + 52kDa NP -1% blend	0.161±0.020
PS 393 kDa + 52kDa NP -8% blend	0.180±0.014
PS 393 kDa + 52kDa NP-10% blend	0.103±0.005 <sup>a</sup>
PS 393 kDa + 135kDa NP-0.5% blend	0.192±0.016
PS 393 kDa + 135kDa NP-1% blend	0.184±0.014
PS 393 kDa + 135kDa NP-20% blend	0.061±0.015 <sup>a</sup>

<sup>a</sup> The viscosity for these blends was reduced at all frequencies on nanoparticle addition, as compared to the neat polymer.

It is interesting to compare the effect of nanoparticle size on the complex viscosity profile for PS 393 kDa. Addition of 52 kDa NP ( $R_g = 3.1$  nm; Fig. 5.5.a) caused an effect only in the terminal region at low volume fractions with a decreased viscosity at all frequencies at higher volume fractions ( $\phi \sim 0.1$ ). In comparison, the addition of 25 kDa NP ( $R_g = 2.2$  nm) causes a decrease in viscosity at all frequencies with particle volume fractions as low as 0.01, as shown in Fig. 5.6.a. The addition of 135 kDa NP ( $R_g = 4.0$  nm, Fig 5.6.b), again affects only the terminal region at low volume fraction, while at higher volume fractions ( $\phi \sim 0.2$ ), the viscosity is decreased at all frequencies. Note the polymer is confined for all these systems, i.e.  $R_g/h > 1$ .

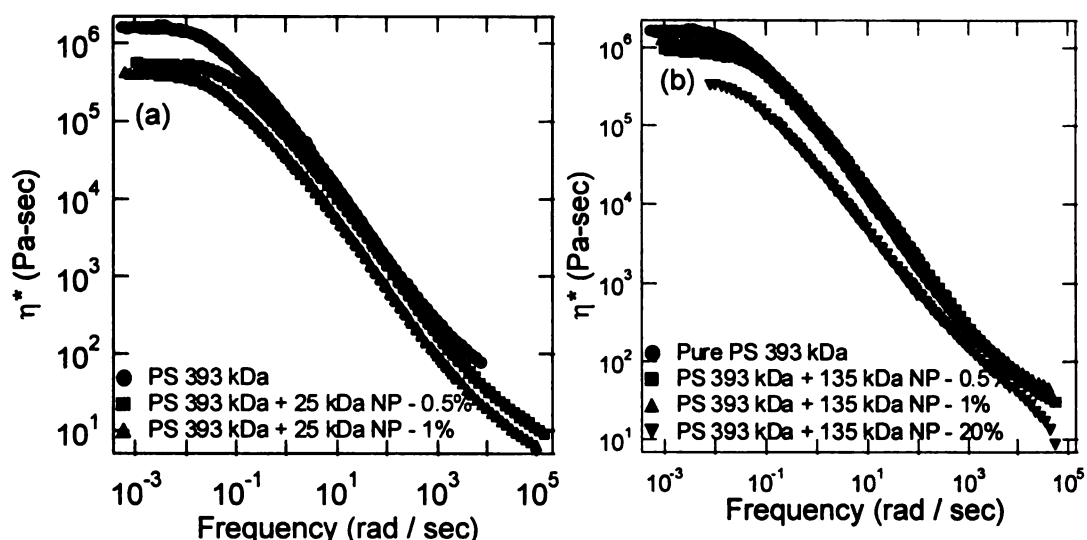


**Figure 5.6.** (a). Complex viscosity as a function of frequency for pure PS 393 kDa and its blends with 25 kDa NP at 170°C. In this case, the viscosity is decreased at all frequencies. A large viscosity reduction is apparent with just 1% addition of the nanoparticles. (b) Complex viscosity as a function of frequency for the blends of 135 kDa NP with PS 393 kDa also at 170°C. Here, only the terminal viscosity is reduced with nanoparticle addition until the concentration reaches 20%.

This differing viscosity behavior can be related to the total number of nanoparticles present in the blend, at least to first order. As the molecular weight of the nanoparticles decreases, for the same volume fraction, the total number of nanoparticles in the blend increases. For  $\phi = 0.01$ , the number of 25 kDa NP is  $2.3 \times 10^{14}$  NP/mg; for the 52 kDa NP, with  $\phi = 0.1$ , the number of nanoparticles is  $9 \times 10^{14}$  NP/mg, while for the 135 kDa NP, at  $\phi = 0.2$ , the number of nanoparticles is  $8.6 \times 10^{14}$  NP/mg. Thus, when the total number of nanoparticles present in the blend are below a certain threshold ( $\sim 10^{15}$  NPs/mg), only the zero shear viscosity is reduced; however on the addition of more nanoparticles, a reduction in viscosity at all frequencies is seen. We find that the number of polymer chains in these blends are also  $\sim 10^{15}$  chains/mg and so by this empirical observation the data suggests that the chain dynamics are severely affected and the

viscosity is decreased at all frequencies when the number of polymer chains approximately equals the number of nanoparticles..

The complex viscosity and the storage modulus for the blends of PS 19.3 kDa and 52 kDa NP as a function of frequency are shown in Fig. 5.7. It can be seen that both the viscosity and storage modulus increase at all frequencies on the addition of the nanoparticles. Also, the increase in these properties scales with the concentration of the added nanoparticles. The effects observed here may be due to a density increase (Fig. 5.8.a) and free volume decrease ( $T_g$  increases, Table 5.3) provided by the nanoparticles. Interestingly, a zero shear viscosity can be observed for all the blends measured, even though the pure nanoparticles behave as a gel (as seen in Fig. 5.5). On comparing the data in Fig. 5.7 with the data shown in Fig. 5.5 for an entangled polymer, the importance of chain entanglements in the polymer is again emphasized.

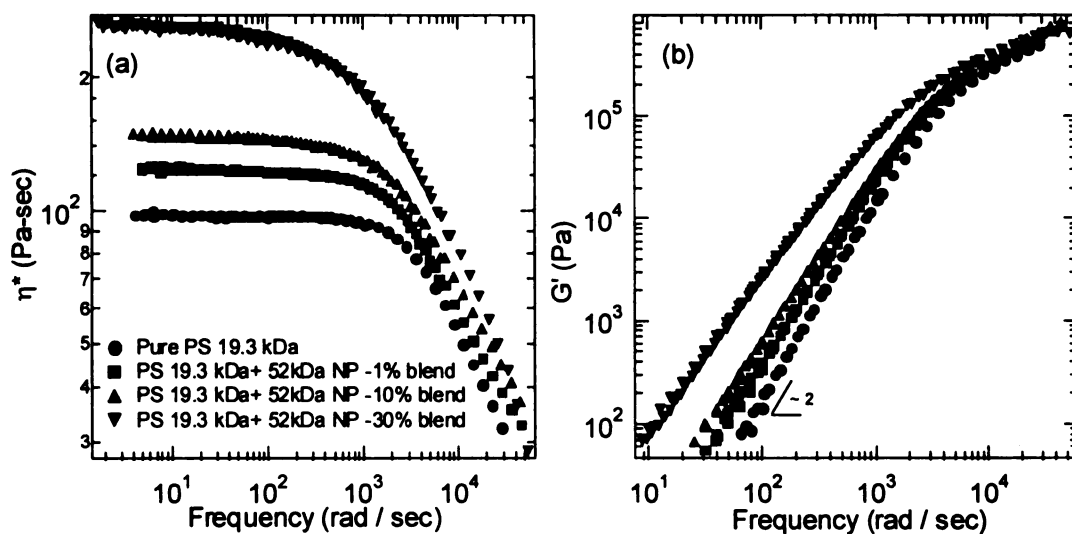


**Figure 5.7.** Complex viscosity (a) and storage modulus (b) data for pure PS 19.3 kDa and its blends with 52 kDa NP at 170°C. Both these properties increase at all frequencies upon nanoparticle addition. Same symbols used in each graph.



The molecular mass between chain entanglements,  $M_e$ , for narrow dispersity polymer melts can be estimated by using the equation,<sup>13, 14</sup>

$$M_e = \rho RT/G_N \quad (5.8)$$

where  $\rho$  is the bulk density of the material at temperature  $T$ , and  $R$  is the ideal gas constant. The bulk density values for the various PS 19.3 kDa and PS 393 kDa blends are shown in Fig. 5.8. It can be seen that the addition of the nanoparticles may cause a very small reduction in the bulk density for PS 393 kDa blends, particularly for the smaller nanoparticles (Fig. 5.8.b). From Table 5.2, it is observed that the plateau modulus is unaffected by the 52 kDa and 135 kDa nanoparticle addition at lower volume fractions. Hence, for those samples, the relation in eq. 5.8 implies that  $M_e$  remains unaffected by nanoparticle addition. From Fig. 5.4.b, it can be seen that for the 52 kDa NP at  $\phi=0.08$ , the terminal viscosity decreases by about 60% with nanoparticle addition. Thus, even with this large reduction in viscosity, the polymer entanglements are not affected, at least in the way entanglements are thought of traditionally. This is surprising behavior, as the effects on viscosity produced by nanoparticle addition are strongly dependent on the presence or absence of entanglements (Fig. 5.1).

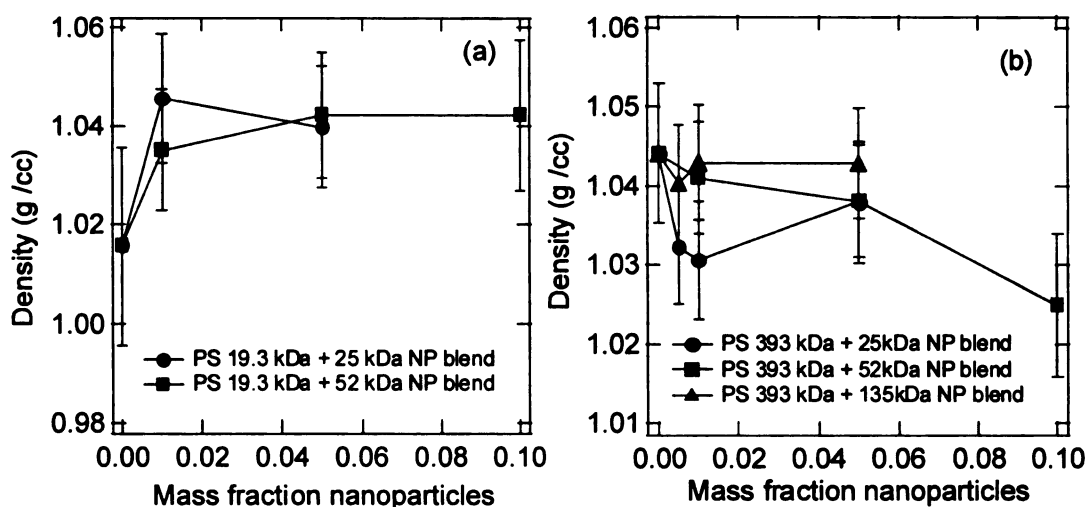


**Figure 5.8.** Bulk density variation as a function of nanoparticle concentration for PS 19.3 kDa blends (a) and PS 393 kDa blends (b) at 25°C. For polymer molecular below  $M_c$ , the density increases, and when it is above  $M_c$ , the density decreases or remains constant, on nanoparticle addition.

In Figs. 5.9.a and 5.9.b, the  $G''(\omega)$  data was used to obtain the continuous relaxation spectrum for PS 393 kDa and its blends with the 52 kDa NP (up to  $\phi = 0.1$ ), as described in the experimental section. It can be seen that the relaxation spectra for pure polystyrene as well as the blends, have a peak near  $\lambda \approx 30$ secs indicative of a narrow molecular mass distribution in the polymer sample.<sup>186</sup> It should be noted that the pure nanoparticles have an infinite terminal relaxation time, suggesting that the relaxation properties of the nanoparticle-polymer blend are distinct and not a distribution of the individual relaxation times of its components. This observation is in contrast to what is generally observed for blends of low and high molecular mass polystyrene.<sup>186</sup> In addition, as no separate relaxation times are seen for the pure nanoparticles, there is no nanoparticle structure formation within the polymer melt as has been seen in a few previous nanoparticle-polymer systems.<sup>168, 187</sup>

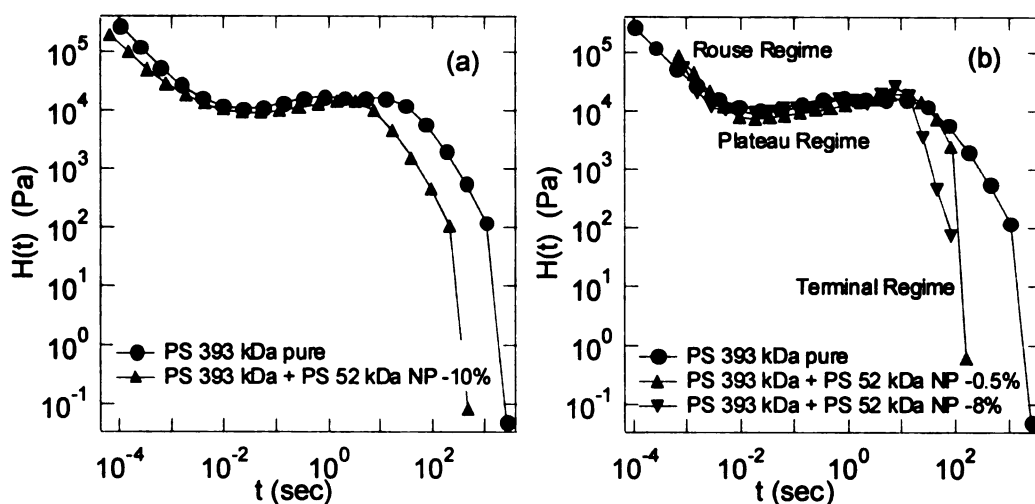


**Figure 5.9.** Relaxation spectra for pure PS 393 kDa and its blends with 52 kDa NP up to concentrations of up to 8% (a) and for a concentration of 10% (b). The Rouse, Plateau and Terminal regimes are also shown. It can be seen that the nanoparticles only affect the terminal regime, by reducing the longest relaxation time, at lower concentrations while at higher concentrations, a reduction occurs at all relaxation times.

For  $\phi = 0.1$  (Fig. 5.9.b), it can be seen that the relaxation modulus for the blends is reduced, when compared to the relaxation modulus for the pure polymer, at all relaxation times. This could be attributed to a dilution effect with the nanoparticles acting as plasticizers.<sup>9, 188-190</sup> However, addition of the nanoparticles at low volume fractions (up to  $\phi = 0.08$ , Fig. 5.9.a), quite unexpectedly, does not significantly affect the Rouse or the plateau regime of the relaxation spectra. Instead, nanoparticle addition reduces only the longest relaxation times (terminal region) for the polymer chain, causing a fall in the terminal viscosity. These are the relaxations caused by the reptation<sup>15, 67</sup> of a polymer chain in the polymer melt.

There are several mechanisms that may cause this curious behavior. We hypothesized in our previous publication that a reduction in viscosity is produced by an increase in free volume, for a given temperature, due to a reduction in the glass transition

temperature found in many of the blends discussed here. This is part of the reason for the viscosity decrease, however, as seen in Table 5.3 a clear correlation between glass transition temperature and viscosity reduction is not apparent with this expanded data set. Further, there is no clear glass transition reduction when  $R_g/h$  is greater than one, see Fig. 5.4.a, and a viscosity reduction is evident. Thus, another mechanism must exist to explain the viscosity reduction and possibly operate in tandem to the free volume change (see fig. 5.8.b).

**Table 5.3.** The viscosity ratio, under terminal conditions, glass transition temperature and degree of confinement for the pure nanoparticles, linear polystyrenes and their blends.

Nanoparticle Blend	Viscosity Ratio	T <sub>g</sub> (°C)	R <sub>g</sub> /h	Nanoparticle Blend	Viscosity Ratio	T <sub>g</sub> (°C)	R <sub>g</sub> /h
PS 25.3 kDa NP	-	96.8	-	PS 75 kDa	1.0	106.3	0
PS 52 kDa NP	-	107.5	-	PS 75 kDa + 0.5% 25 kDa NP	0.93	106.2	0.88
PS 135 kDa NP	-	131.5	-	PS 75 kDa + 1.0% 25 kDa NP	0.91	106.0	1.19
PS 19.3 kDa	1.0	99.5	0	PS 75 kDa + 5.0% 25 kDa NP	0.91	106.5	2.66
PS 19.3 kDa + 1.0% 25 kDa NP	1.22	101.4	0.60	PS 75 kDa + 10% 25 kDa NP	0.73	106.6	4.16
PS 19.3 kDa + 5.0% 25 kDa	1.65	101.4	1.34	PS 75 kDa + 0.5% 52 kDa NP	1.44	105.0	0.69
PS 19.3 kDa + 10% 25 kDa NP	1.73	102.0	2.10	PS 75 kDa + 1.0% 52 kDa NP	1.59	106.1	0.93
PS 19.3 kDa + 1.0% 52 kDa NP	1.55	101.4	0.47	PS 75 kDa + 5.0% 52 kDa NP	0.60	104.7	2.10
PS 19.3 kDa + 5.0% 52 kDa NP	1.86	101.3	1.05	PS 75 kDa + 20% 52 kDa NP \	0.89	104.0	5.93
PS 19.3 kDa + 10% 52 kDa NP	1.75	100.9	1.65	PS 75 kDa + 0.5% 135 kDa NP	1.19	104.4	0.50
PS 19.3 kDa + 30% 52 kDa NP	3.61	103.4	4.91	PS 75 kDa + 1.0% 135 kDa NP	1.33	106.5	0.68
PS 31.6 kDa	1.0	104.5	0	PS 75 kDa + 5.0% 135 kDa NP	1.05	106.3	1.52
PS 31.6 kDa + 0.5% 25 kDa NP	0.97	103.0	0.61	PS 393 kDa	1.0	106.9	0
PS 31.6 kDa + 1.0% 25 kDa NP	1.03	104.2	0.83	PS 393 kDa + 0.5% 25 kDa NP	0.41	106.1	2.02
PS 31.6 kDa + 5.0% 25 kDa NP	1.08	104.0	1.36	PS 393 kDa + 1.0% 25 kDa NP	0.20	104.1	2.72
PS 31.6 kDa + 1.0% 52 kDa NP	1.03	103.2	0.58	PS 393 kDa + 0.5% 52 kDa NP	0.58	105.9	1.58
PS 31.6 kDa + 2.0% 52 kDa NP	1.05	103.3	0.77	PS 393 kDa + 1.0% PS 52 kDa NP	0.50	104.9	2.13
PS 31.6 kDa + 5.0% 52 kDa NP	1.04	103.4	1.73	PS 393 kDa + 8.0% PS 52 kDa NP	0.48	96.7	6.40
				PS 393 kDa + 10% 52 kDa NP	0.21	106.2	7.47
				PS 393 kDa + 0.5% 135 kDa NP	0.53	103.5	1.15
				PS 393 kDa + 1.0% 135 kDa NP	0.58	106.0	1.55
				PS 393 kDa + 5.0% 135 kDa NP	0.64	106.6	3.48
				PS 393 kDa + 20% 135 kDa NP	0.18	106.0	9.60

We hypothesize that these phenomena are related to the double reptation<sup>191, 192</sup> or constraint release<sup>35</sup> phenomenon introduced by the nanoparticles. In this model, constraints are released due to movement of surrounding molecules constituting the entanglement mesh (tube<sup>67</sup>). This has the effect of reducing the relaxation time, yet, not the modulus, as we observe experimentally.

The physics of the mechanism introduced by the nanoparticles will certainly depend on the relative diffusion time scales of the nanoparticle and polymer. As evident from Fig. 5.9, the pure 393 kDa polymer relaxation time is of order 10-50 s. Assuming the nanoparticles follow the SE model one can estimate a diffusion time, through a distance  $a$ , as  $\sim 50$  s ( $= \zeta a^2/k_B T$ ,  $k_B$  is Boltzmann's constant) which is the same order as the polymer relaxation time. One may expect a viscosity reduction if the nanoparticles diffuse much more rapidly than the linear polymer so they can not contribute to the entanglement mesh. So, the continuum SE relation may not be valid for nanoparticles diffusing through the polymer (temporary) network to allow this hypothesized mechanism. Diffusion of neutrally interacting NPs in entangled melts is certainly worthy of further study and here we merely (tentatively) hypothesize that the NPs invoke constraint release noting inconsistencies of this model with some of the data.

Yet, once there are approximately the same number of nanoparticles and polymer molecules per unit volume the viscosity falls at all frequencies. Clearly, under this condition, the entanglement network or tube of constraints has suffered to great extent and the plateau modulus is seen to decrease. However, this curious phenomenon occurs in the high frequency Rouse regime that is not affected at all until this nanoparticle concentration. So, once the entanglement network is severely affected, to reduce the

plateau modulus and viscosity at all frequencies, the Rouse regime is similarly affected. We find all these observations remarkable and postulate that what we interpret as independent free volume and constraint release mechanisms in fact operate in concert to generate the flow property modification.

## **Conclusion**

We have shown that addition of polystyrene nanoparticles to linear polystyrene produces peculiar and unique behavior with a viscosity reduction only when the polymer molecule is entangled and confined. In fact, there appears to be critical behavior at the characteristic molecular mass for entanglements where the viscosity does not change, within experimental error. Further, when there is approximately one nanoparticle present for each polymer molecule, an abrupt viscosity decrease is present at all frequencies.

In our previous study,<sup>8</sup> we demonstrated that the increase in free volume, signaled by a glass transition temperature decrease, accounted for the viscosity reduction at a given temperature. Here we have extended the data set to realize the phenomenon is much more complicated with a viscosity increase present when the polymer molecule is not confined then a precipitous drop occurs upon molecular confinement. Further, the plateau modulus is not initially affected suggesting no change in the number of entanglements. We hypothesize that the nanoparticles induce constraint release affecting the longest relaxation modes thereby producing a terminal viscosity decrease without reduction in the plateau modulus. However, as the nanoparticle concentration is increased, until there is approximately one nanoparticle for every polymer molecule, the





viscosity at all frequencies falls, as does the plateau modulus, suggesting a drastic change in the entanglement structure. Yet, the Rouse regime is similarly affected promoting the idea that the single molecule as well as the entanglement dynamics are similarly changed.

In Fig. 5.1 we showed that when no entanglements are present then the viscosity can deviate from the Rouse prediction due to free volume effects, while reduction of entanglements above the critical molecular weight can yield a viscosity change. It appears this explanation where the two regimes are considered separately may be too simple. Above the critical molecular weight one may have free volume and entanglement changes induced by nano-objects which are not easily reconciled under existing theoretical considerations. It is clear, however, that this is a nanoscale effect and larger particle sizes will not produce any of this behavior.

### **Appendix for Chapter 5**

Here we present the viscosity ratio for the blends given in Figs. 5.3 and 5.4 as a function of volume fraction in Fig. 5.10. It is clear there is no scaling with volume fraction as expected for suspensions.

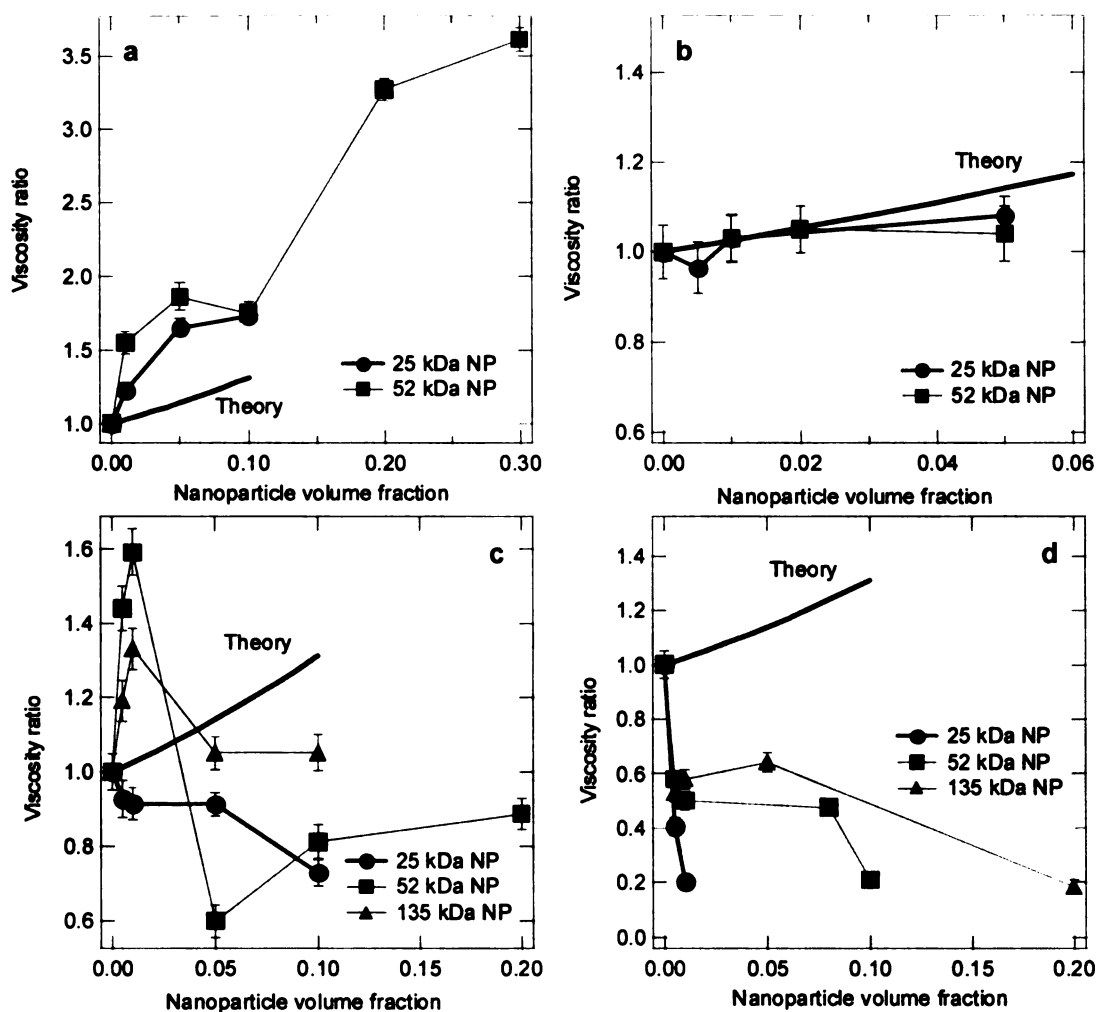


**Figure 5.10.** Viscosity ratio of the nanoparticle blends with respect to pure polystyrene as a function of nanoparticle volume fraction, with different molecular weight linear polystyrenes' at 170°C: (a) 19.3 kDa, (b) 31.6 kDa, (c) 75 kDa, (d) 393 kDa. The curves labeled theory are the values predicted by Batchelor's relation for this system, ending at the limit of the relation's applicability ( $\phi \sim 0.1$ ).

## CHAPTER 6

### BREAKDOWN OF THE CONTINUUM STOKES-EINSTEIN RELATION FOR NANOSCALE INCLUSIONS IN POLYMER MELTS

---

#### Introduction

The assembly of inorganic nanoparticles in polymer matrices and block copolymers has been widely studied with the aim of tailoring their magnetic, mechanical, electrical or optical properties.<sup>23, 36-38</sup> Other nanoparticles found in nature (bionanoparticles) including tobacco mosaic virus and cowpea mosaic virus have also now been functionalized with various synthetic polymers with the objective of directing them into self assembled ordered structures to tailor vehicles for drug delivery.<sup>39, 40</sup> In addition, the movement of proteins, DNA and other naturally occurring nanoparticle – like systems, either inside or outside the cell are expected to emulate the nanoparticle – polymer matrix interaction. So, any study targeting the assembly or diffusion of nanostructures requires an understanding of the nanoparticle dynamics, spatial arrangement and ordering kinetics within the polymer matrix. Moreover, with many important experimental techniques moving towards smaller length scales and sample volumes, such as microrheology<sup>41, 42</sup> which uses the generalized Stokes – Einstein (SE) relation to determine the shear modulus and viscosity, an accurate description of nanoscale dynamics becomes essential for data interpretation. Further, we<sup>48, 49</sup> and others<sup>188</sup> found that addition of nanoparticles to polymer melts causes an unexpected

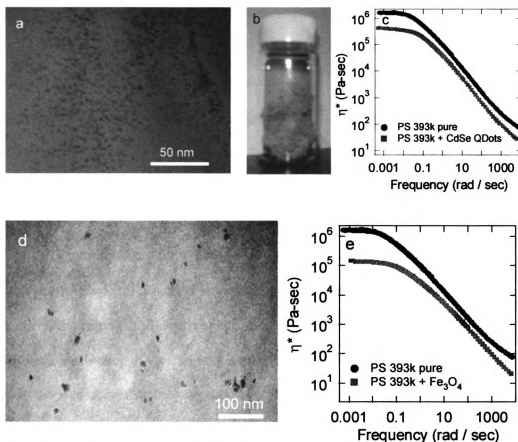
reduction in their viscosity, contradicting Einstein's prediction for a viscosity increase and so it is suspected that the nanoparticle dynamics contributes to this phenomenon.

The observed reduction in viscosity for many systems required that the nanoparticles diffuse faster than the prediction from the SE relation ( $D = k_B T / 6\pi\eta a$ , here  $D$  is the diffusion coefficient,  $k_B$  is the Boltzmann constant,  $\eta$  is the bulk polymer melt viscosity,  $T$  is the temperature and  $a$  is the radius of the particle) for the system.<sup>49</sup> In this work, we report the results for the first successful, measurements to our knowledge of the diffusion coefficients of nanoparticles in polymer melts, using X-ray photon correlation spectroscopy (XPCS or dynamic X-ray scattering)<sup>43, 44</sup> and to directly determine the nanoparticle diffusivity. The measured diffusion coefficients were found to be dependent on the molecular mass of the polymer, but were independent of the temperature. However, for all the different cases studied, we found that the diffusion coefficient was larger than the prediction from the SE relation by up to a factor of 100.

## Results and Discussion

Recently, addition of quantum dots (QD) to polymers has received the attention of a number of research groups, mainly because of their extraordinary range of potential applications, including electronic materials<sup>193, 194</sup> and biosensors.<sup>195, 196</sup> Most synthesized quantum dots have a covering of tri-*n*-octylphosphine oxide (TOPO) ligands on their surface. However, the dispersion of these quantum dots in various polymer matrices has proven to be quite difficult, unless the TOPO ligands are replaced by either the matrix polymer or another polymer that is miscible with the matrix polymer.

In our recent work <sup>34</sup> we showed that dispersion of organic nanoparticles is possible in various polymer matrices despite chemical dissimilarity, as long as the radius of the nanoparticle is less than the radius of gyration ( $R_g$ ) of the matrix polymer. That work is extended here for dispersing inorganic nanoparticles i.e. oleic acid covered CdSe quantum dots <sup>197</sup> in polystyrene (PS) as shown in Fig. 6.1.a. The radius of the quantum dots is 6 nm (as determined through dynamic light scattering in Toluene at 35°C), with a QD core radius of 2 nm, as can be seen from the TEM micrograph; while the  $R_g$  of the polystyrene is  $\sim 17$  nm. The quantum dots are miscible up to a very high mass fraction ( $\sim 38$  wt% in Fig. 6.1.a) and the dispersion of the quantum dots within the polymer matrix has been achieved without any chemical modification of the oleic acid covered surface. Indeed linear oleic acid is expected to have an unfavorable interaction with the polystyrene matrix causing phase separation. However, it is believed that this unfavorable process is offset by an enthalpy gain due to an increase in molecular contacts at dispersed nanoparticle surfaces.<sup>34</sup> It should be pointed out that the method of blend preparation (rapid precipitation here) is quite critical to ensure the dispersion of nanoparticles.<sup>34</sup> A picture of the as prepared PS-QD blend can be seen in Fig. 6.1.b. The blend is colored pink because of the dispersion of the quantum dots, in comparison, pure PS is white. Also, as was the case with the organic nanoparticles,<sup>48, 49</sup> the addition of the quantum dots to polystyrene also causes a large reduction ( $\sim 60\%$ ) in the melt viscosity (Fig. 6.1.c) of the nanocomposite, even at this high mass fraction.



Images in this dissertation are presented in color.

**Figure 6.1. Inorganic nanoparticles can be dispersed in polymer matrices by the process of rapid precipitation and cause a large reduction in the polymer melt viscosity.** a. TEM micrograph of a 38wt.% blend of oleic acid capped quantum dots dispersed in polystyrene (molecular mass 393kDa). Based on the nanoparticle concentration and size, as well as the sample size, there should be several thousands of nanoparticles visible in the micrograph, as seen. The dispersion of inorganic nanoparticles is possible in polymers as long as the  $R_g$  of polymer > radius of nanoparticles. b. An optical picture of the QD-PS blend, showing the pink color of the blend. c. The complex viscosity as a function of frequency for pure PS and the PS-QD blend. The melt viscosity reduces by ~ 60% on the addition of quantum dots even at this high weight loading, contradicting Einstein's prediction for a viscosity increase. d. A TEM micrograph of the 5 wt% blend of the magnetite nanoparticles in PS (molecular mass 393kDa). There should be several tens of nanoparticles in this micrograph, as is clearly seen. e. The complex viscosity as a function of frequency for pure PS and the PS-magnetite nanoparticle blend. The addition of just 5 wt% of the magnetite nanoparticles causes ~ 90% reduction in the melt viscosity of pure polystyrene.

see methods in Chapter 7 for more details) in polystyrene. The magnetite nanoparticles are quite polydisperse with a radius varying between 5-10 nm (as obtained from dynamic light scattering in Benzene at 35°C), and can be readily dispersed in the high molecular weight polystyrene ( $R_g \sim 17$  nm), as shown in Fig. 6.1.d (the PS-magnetite nanoparticle blend is yellow in color as compared to the pink PS-QD blend). The addition of  $\sim 5$  wt.% of the magnetite nanoparticles causes an  $\sim 90\%$  reduction in the melt zero shear viscosity (Fig. 6.1.00e).

The mechanism for the unusual and important decrease in viscosity on the addition of nanoparticles, first seen for the ideal case of polystyrene nanoparticles in linear polystyrene<sup>48</sup> and observed here again for the addition of quantum dots as well as the magnetite nanoparticles, has not been understood so far. However, from our previous work, it was clear that the reduction in viscosity was only seen in entangled systems, while for the unentangled systems, addition of nanoparticles causes a viscosity increase. It was postulated then that the nanoparticles must diffuse faster than predicted by the continuum SE relation and hence not contribute to the entanglement network, to cause the observed reduction in viscosity.<sup>49</sup>

Deviations from the SE relation have been observed before, especially when the particle radius came close to the size of the solvent molecules. The continuum SE relation is ideally applicable only for  $a \gg \zeta$  (correlation length for a polymer, generally taken as the size of a monomer / polymer segment). However, there have been differing findings on the region of applicability of the SE relation. Edward<sup>164</sup> reviewed the literature and found that the SE relation could not be applied to diffusion of molecular penetrants' in simple fluids such as water and carbon tetrachloride. Indeed, when the penetrants' radius

became 2-3 times that of the suspending liquids' then deviations from the SE relation were quite evident. Similarly, Somoza et al.<sup>198</sup> found the local viscosity for rotation of dissolved anthracene ( $\sim 0.6$  nm in radius) to be orders of magnitude lower than the bulk viscosity for PDMS. However, previous simulations report the applicability of the SE relation on the atomic level.<sup>199</sup> More recently, Vergeles et. al.<sup>200</sup> showed that the SE relation can serve as a qualitative approximation for particle sizes comparable to the solvent; while simulations from Heyes et al.<sup>201</sup> predicted that the translational diffusion coefficients for nanoparticles in polymer solutions are lower than the SE predictions, while the rotational diffusion coefficients are higher than the predictions from the SED (Stokes-Einstein-Debye) relation. Also, XPCS, the technique used in this work, was used to measure the translational diffusion coefficient of  $\sim 70$  nm PS spheres in glycerol for various volume fractions of the particles.<sup>43</sup> The measured diffusion coefficient in this case was found to match well with the predicted value from the SE relation. However, as we stated before, direct measurement of the diffusion coefficient of nanoparticles in polymer melts has not been performed before. It is also important to note that in this work the nanoparticles are larger than the correlation length but smaller than the  $R_g$  of the polymer.<sup>202, 203</sup>

Our XPCS measurements were carried out at the 8-ID-I beamline at the Advanced Photon Source (APS). Both the nanoparticle systems used in this work (quantum dots and magnetite nanoparticles) were ideal for the study as they provided a large contrast for the X-ray diffraction. XPCS is a relatively new technique for the determination of condensed matter dynamics, and is in essence the extension of dynamic light scattering into the X-ray regime.<sup>204</sup> The primary requirement for the technique is the availability of a high



brilliance synchrotron radiation source and the x-ray beam has to be made partially coherent with the detector size matched to the size of the coherent speckles scattered by the sample.<sup>205</sup> Fluctuations in the speckle intensity are then directly related to the sample dynamics as discussed elsewhere.<sup>43</sup>

Dynamical properties of the melts were characterized via autocorrelation of sequences of CCD images, like the one shown in Fig. 6.2.a, and normalized to the circular average of the CCD scattering at each wave vector. This allowed for the determination of the normalized intensity – intensity autocorrelation function,  $g_2(q, t)$ , which is related to the field autocorrelation function,  $g_1(q, t)$ , by

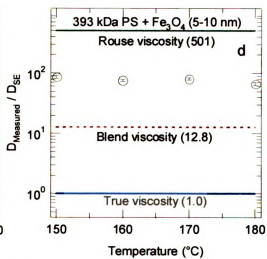
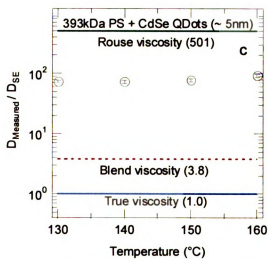
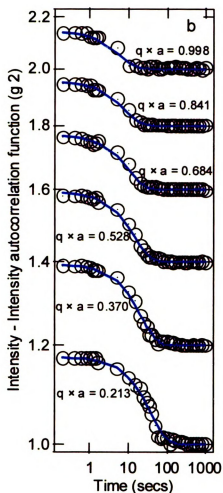
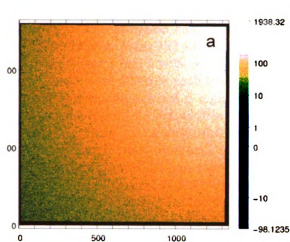
$$g_2(q, t) = 1 + \alpha (g_1(q, t))^2 \quad (6.1)$$

here  $t$  is the delay time,  $q$  is the wave vector ( $= 4\pi/\lambda \sin(\theta/2)$ ,  $\lambda$  is the wavelength of the X rays and  $\theta$  is the scattering angle) and  $\alpha$  is the setup dependent instrument contrast ( $\sim 0.15$  for these measurements), with

$$g_1(q, t) = \exp(-t/\tau_r) \quad (6.2)$$

where  $\tau_r = 1 / (q^2 D)$ .

Typical data obtained for the intensity-intensity autocorrelation function as a function of the delay time is shown in Fig. 6.2.b. This data could be well fitted to a single exponential (the solid blue lines in Fig. 6.2.b) with  $\alpha$  and  $\tau_r$  as the two fitting parameters. By definition, a plot of  $1/\tau_r$  versus  $q^2$  is a straight line, whose slope gives us the diffusion coefficient. This was found under all conditions demonstrating normal Brownian motion.



Images in this dissertation are presented in color.

**Figure 6.2. The diffusion coefficients of quantum dots and magnetite nanoparticles in PS (molecular mass 393 kDa). a.** A single frame (CCD image) obtained from the X-ray diffraction of the 5 wt% magnetite nanoparticles in PS. For each sample, 400-500 such frames were taken at each temperature, at intervals of 0.1 secs. **b.** Each frame was divided into equally spaced  $q$  regimes, based on their angular distance from the upper right hand corner of the frame (the centre of the X-ray beam). The scattering from these regimes was used to calculate the intensity-intensity autocorrelation function ( $g_2(q,t)$ ) using the mean  $q$  value from each regime. The data from 6 of those  $q$  values can be seen here ( $a$  is the radius of the nanoparticle = 5 nm; the sample is at 160°C). Each data set has been offset with respect to the previous data set by 0.2, starting from  $q \times a = 0.370$ , to allow for easier visibility (so the data set for  $q \times a = 0.370$  has been offset by 0.2, while the data set for  $q \times a = 0.998$  has been offset by 1). The data is then fitted to a single exponential (the solid blue line), to obtain  $\tau_r$  as a function of  $q$ . **c.** The ratio of the measured diffusion coefficient to the diffusion coefficient calculated from the SE relation for the quantum dots in PS. **d.** The same ratio for the magnetite nanoparticles in PS.

Fig. 6.2.c and Fig. 6.2.d show the ratio  $D_{\text{measured}} / D_{\text{SE}}$  for the CdSe Quantum dots and the magnetite nanoparticles in linear PS as a function of temperature (it should be noted that the glass transition temperature for PS is 106°C). This ratio would be 1 if the measured diffusion coefficient matched the prediction from the SE relation based on the viscosity of pure PS. Because the addition of the nanoparticles causes a reduction in the melt viscosity, the red dotted line shows the value of the ratio if the blend viscosity is used to calculate  $D_{\text{SE}}$  instead of the viscosity of pure PS. If the polymer had no entanglements then the viscosity would be equal to the so called Rouse viscosity,<sup>151</sup> and the system should follow the solid green line shown on the graph. It should be pointed out here that for the calculation of  $D_{\text{SE}}$  for the magnetite nanoparticles, we have used a radius of 5 nm, which is the size of the smallest particles and gives the highest value for  $D_{\text{SE}}$ , while a radius of 5 nm was used for the QD's, yielding the highest value of  $D_{\text{SE}}$ .

It is immediately clear that both the nanoparticle systems diffuse almost a 100 times faster than the prediction from the SE relation based on the viscosity of pure PS,

contrary to MD simulations for the system.<sup>201</sup> This is equivalent to stating that the local viscosity experienced by nanoparticles is much less than the viscosity macroscopically measured.

The size and shape of the particles are expected to be critical<sup>206</sup> to their diffusion. For example, the nanoparticles are about the same size as the tube diameter or the entanglement mesh length,<sup>14</sup> in entangled polystyrene (~ 8-9 nm). In fact, the quantum dots are smaller than the tube diameter, while some of the magnetite nanoparticles are larger, however, for both cases, the measured diffusion coefficients are much faster than the SE prediction. Clearly, both the systems diffuse regardless of the entanglement network and their size, leading to this extremely high diffusion coefficient. Quite significantly, the diffusivity ratio is almost independent of temperature for both the systems, suggesting that an activated process other than that associated with the polymer melt is not present. The XPCS measurements were repeated for the addition of these nanoparticles to a lower molecular weight PS matrix (molecular mass of 115 kDa), as discussed below, to find  $D_{\text{measured}} / D_{\text{SE}}$  was approximately 10 for all temperatures tested suggesting a molecular mass dependence.

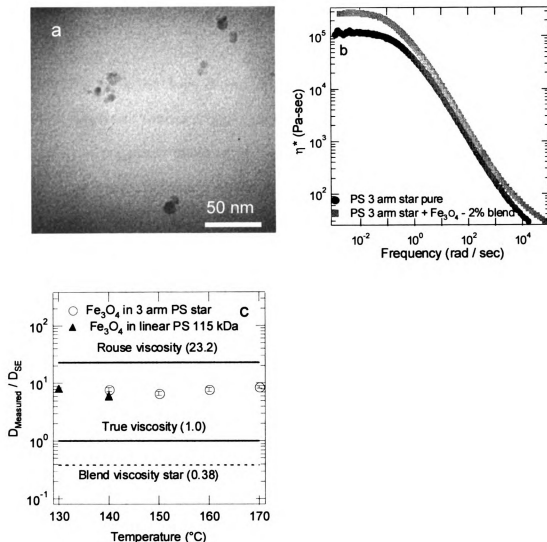
The nanoparticles' fast diffusion suggests that the physical mechanism for the viscosity decrease seen in nanoparticle-polymer blends is through the constraint release phenomena.<sup>15, 35</sup> In this model, constraints are released due to movement of surrounding molecules constituting the entanglement mesh or tube<sup>67</sup>. This has the effect of reducing the polymer blend viscosity, yet, not the modulus, as we observe experimentally<sup>49</sup>. This hypothesis is clearly dependent on the relative time scales of diffusion for the linear chain and the nanoparticles. From our calculations and experimental data<sup>49</sup> the relaxation time

for the PS linear chain is  $\sim 10$ -50 secs., which is about 10-100 times slower than the diffusion time for the nanoparticles through a distance equivalent to their radius or the tube diameter. Thus, we hypothesize that the nanoparticles diffuse rapidly, without participating in the entanglement mesh and their occupied volume provides the constraint release. However, this would suggest a simple dependence of viscosity on the nanoparticle concentration, which we do not see, suggested that complicated polymer and nanoparticle dynamics contribute to the observed reduction in viscosity.

To confirm our hypothesis that constraint release contributes to the viscosity decrease, we extend our work to study the effect of nanoparticle addition on the viscosity of star polymers. Star polymers do not relax by reptation or constraint release but only by primitive path fluctuations,<sup>15, 207</sup> since the star cannot move back and forth as a whole.<sup>150</sup> If constraint release is the cause of the viscosity decrease in linear polymers, the viscosity of star polymers should not decrease on the addition of nanoparticles, which is what we observe.

A TEM micrograph is shown in Fig. 6.3.a, for the 2 wt% dispersion of magnetite nanoparticles in a 3 arm PS star (molecular mass of each arm  $\sim 108$  kDa), clearly demonstrating that the magnetite nanoparticles are well dispersed. The complex viscosity as a function of frequency for the pure 3 arm star as well its 2 wt% blend with the magnetite nanoparticles is shown in Fig. 6.3.b, showing a viscosity increase. In fact a 60% increase in the zero shear viscosity can be observed, even at this low weight fraction of the nanoparticles. Significantly, XPCS measurements on this sample indicate that the diffusion coefficient of the nanoparticles, even in this case, is almost 10 times the larger than diffusion coefficient predicted from the SE relation based on the pure 3 arm star

viscosity (Fig. 6.3.c). Since the viscosity of the blend is greater than the viscosity for the pure 3 arm star, the ratio of diffusion coefficients obtained by using the blend viscosity is less than one, as shown in the figure. It should be noted that the ratio obtained by using the measured diffusion coefficient still lies within the limits of the ratios obtained by using the pure 3 arm star viscosity and that obtained by using the Rouse viscosity, based on the arm length. Also, the diffusion occurs at the same rate as a linear polymer with mass equal to that of an arm (Fig. 6.3.c) demonstrating that the star architecture does not influence the diffusion, rather it is the lower molecular mass of the arm which is important.



Images in this dissertation are presented in color.

**Figure 6.3. Addition of magnetite nanoparticles to 3-arm PS stars.** **a.** A TEM micrograph showing the dispersion of magnetite nanoparticles (2 wt% or 0.4 vol%) in a 3 arm PS star (molecular mass of each arm  $\sim 108$  kDa). Based on the nanoparticle concentration and the sample size there should be 5-10 nanoparticles in this figure, as can be seen here. **b.** The complex viscosity as a function of frequency for the pure 3 arm star as well as its blend with the magnetite nanoparticles. It can be seen that the addition of the nanoparticles causes a large increase in the viscosity of the star, in contrast to the viscosity decrease seen on the addition of the same nanoparticles to linear PS. **c.** The ratio of the measured diffusion coefficient (from XPCS data) to the diffusion coefficient from the SE relation for the magnetite nanoparticles dispersed in the 3 arm star and linear PS with molecular mass of 115 kDa. Even though the addition of the magnetite nanoparticles causes an increase in the melt viscosity, their diffusion coefficient is almost an order of magnitude higher than the prediction from the SE relation.





## Conclusion

With this work we have shown that it is possible to disperse inorganic nanoparticles in polymer matrices at high mass fractions without surface modification, as long as the  $R_g$  of polymer  $>$  radius of the nanoparticles. We also, for the first time, successfully measured the diffusion coefficients of different nanoparticles in an entangled polystyrene matrix. The diffusion coefficients of the nanoparticles were found to be as much as 100 times faster than the predictions from the continuum Stokes - Einstein relation based on the bulk viscosity, in contrast to previous simulations. This suggests that the local viscosity in the case of nanoparticles is much lower than the bulk viscosity, as the nanoparticles do not feel all of the entanglements in the system. The faster nanoparticle diffusion coefficients lead to an overall decrease in the bulk viscosity of the polymer melt, contradicting Einstein's century old prediction and common observation of a viscosity increase on the addition of particles to solutions and melts. This unusual decrease in viscosity can be explained by a faster mode of polymer relaxation as compared to reptation, constraint release, introduced by the fast diffusion of the nanoparticles. The importance of constraint release was tested by studying the dynamics of nanoparticle addition to 3 arm stars, which can only relax by primitive path fluctuations. As anticipated, the addition of nanoparticles increases the melt viscosity of the 3 arm stars, in spite of the fact that the nanoparticles diffuse almost 10 times faster than the SE prediction for the system.

## CHAPTER 7

### DESIGNING MULTIFUNCTIONAL NANOCOMPOSITES

---

#### Introduction

Nanomaterials hold the promise of providing new properties that far exceed traditional material performance. However, in many instances, significant improvements in material properties of nanocomposites have not yet been achieved,<sup>7, 45, 46</sup> mainly because the factors affecting nanoparticle dispersion are poorly understood. In our recent work, we demonstrated various strategies for the dispersion of organic nanoparticles in polymers.<sup>208</sup> Here we extend that work and define the dispersion techniques as well as the polymer and nanoparticles parameters, including the polymer molecular mass ( $M_p$ ), its radius of gyration ( $R_g$ ), nanoparticle shape, concentration as well as its radius ( $a$ ), required to cause simultaneous enhancements in multiple material properties and hence produce truly multifunctional nanocomposites, with both organic and inorganic nanoparticles.

Recently, fullerenes ( $C_{60}$  or bucky balls, diameter  $\sim 0.7$  nm) have received much attention as nanofillers, with pure fullerenes and their derivatives being used to impart fascinating photonic, electronic and biomedical properties, which could prove useful for a gamut of future applications, including solar cells,<sup>28, 209</sup> superconductive materials<sup>210, 211</sup> and drug delivery.<sup>212</sup> However, the dispersion of fullerenes in polymers has proven quite difficult.<sup>24, 213, 214</sup> To improve the compatibility of fullerenes with bulk polymers, various

techniques, including the modification of fullerene structure and direct attachment of fullerenes to the polymer backbone by covalent bonds, have been tried. These methods, apart from being resource intensive, can not be used to produce fully miscible blends.<sup>47</sup>

To determine whether dispersion of fullerenes is possible, a reasonable estimate of the ultimate solubility in polymers can be made with the Flory theory<sup>26, 208</sup> to arrive at the solvent binodal volume fraction ( $\phi_B$ ) of:  $-\ln(\phi_B) \approx 1 + \chi$ ; in the limit of small nanoparticle concentration. Since the *chi* parameter ( $\chi$ ) is related to the molecular insertion energy on a lattice ( $\epsilon$ ) and given by:  $\chi = z\epsilon/k_B T$ , where  $z$  is the coordination number,  $k_B$ , the Boltzmann constant and  $T$ , the temperature; one expects its value to be of order 1 – 10, allowing one to predict soluble concentrations of up to ~ 10 vol%. Even with the basic Flory theory suggesting the possible dispersion of fullerenes, previous studies in the literature have been unsuccessful.<sup>24, 213, 214</sup>

## Experimental

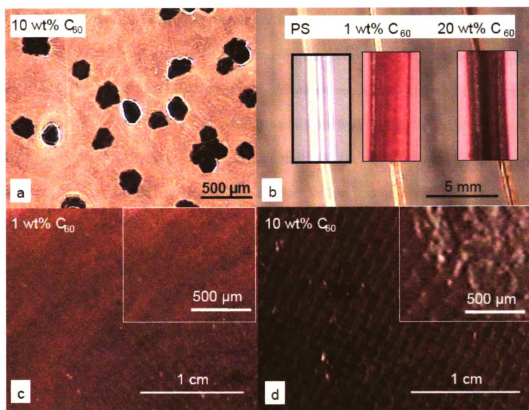
Nanocomposites of fullerenes and polystyrene were prepared through co-dissolution in toluene followed by precipitation into methanol. The solids were filtered from methanol and dried in vacuum at 50°C for at least a week to ensure complete solvent removal. For rheological measurements, 8-mm diameter discs were pressed under vacuum in a specially designed pellet press and were used with the 8-mm parallel plates fixture of a Rheometrics ARES rheometer set at a gap of approximately 0.4 mm. Frequency sweeps in the range 0.1-100 rad/sec were performed at various temperatures and then combined using time-temperature superposition to yield a master curve at

170°C. The strain during the dynamic shear test was kept small enough to ensure that all response was in the linear viscoelastic region. The magnetite ( $\text{Fe}_3\text{O}_4$ ) nanoparticles were obtained from the Ferrotec Corporation. The particles are coated with a stabilizing dispersing agent (surfactant) to enable their solubility in organic solvents. The disks obtained from the pellet press were also used to make films by compression in a Wabash compression molding press at 160°C. Steel spacers were used to obtain the desired film thickness. After compression the films were aged at 170°C for 3–4 hours to ensure homogeneity and then samples were cut from the film for dynamic mechanical analysis with a Rheometrics RSA III. The phase separated films were produced by co-dissolution of polystyrene and fullerenes in toluene followed by casting onto a glass slide. All these films were then used as samples for dynamic mechanical analysis, wide angle X-ray diffraction and electrical conductivity tests. Thermal analysis was performed using a TA instruments Q1000 DSC. Samples were heated and cooled at 5°C/min. Thermogravimetric analysis (TGA) was carried out using a TA instruments Q50 TGA. Here, the samples were heated at 20°C/min from room temperature to 330°C and held isothermally for up to 24 hours.

## **Results and Discussion**

In our previous work,<sup>208</sup> we showed that the polymer radius of gyration ( $R_g$ ) must be greater than the nanoparticle radius ( $a$ ) to ensure nanoparticle dispersion. However, even when the dispersed state is thermodynamically stable, it may be inaccessible unless the correct processing method is employed for nanoparticle dispersion. We find that rapid

precipitation (see methods for details) can be used to produce miscible fullerene – polystyrene nanocomposites up to a maximum concentration of ~ 2 vol% in linear, monodisperse polystyrene. In comparison, gradual solvent evaporation (a method typically employed for nanoparticle dispersion by various researches) leads to large scale phase separation (Fig. 7.1.a) of the bucky balls. The formation of these phase separated structures relates directly to the difference in solubility between the linear polymer and the fullerenes which causes the fullerenes to precipitate from solution before the linear polymer. However, using rapid precipitation, a more homogeneous blend can be obtained,<sup>8, 116</sup> as the nanoparticle and the polymer separate out of solution together. These nanocomposites can then be drawn into fibers, Fig. 7.1.b, and no large scale aggregates are apparent. They can also be compression molded to form thin films, as shown in Fig. 7.1.c and 7.1.d. A color shift from light to dark brown with increasing concentration of fullerenes can be clearly seen in these pictures. In comparison, the pure polystyrene film is colorless.



**Images in this dissertation are presented in color.**

**Figure 7.1. It is possible to disperse fullerenes in polystyrene by rapid precipitation.** Fullerene-polystyrene nanocomposites developed through solvent evaporation produce large phase separated domains **a**, while rapid precipitation yields homogeneous blends that allow melt spinning of fibers **b**. The nanocomposites can also be compression molded to prepare free standing thin films as shown in the optical micrographs **c**, and **d**. Markings on the films are from the platens.

At this point, it is important to consider the average interparticle half gap ( $h$ ) between the dispersed fullerenes. Twice this distance represents the average distance between particles and is approximated by;  $h/a = [\phi_m/\phi]^{1/3} - 1$ , where  $\phi_m$  is the maximum random packing volume fraction ( $\sim 0.638$ ). At a fullerene weight fraction of 0.01, the average interparticle half gap is  $\sim 1.3$  nm which is much smaller than the 393 kD polystyrene's radius of gyration ( $R_g$ ) ( $\sim 17$  nm), considered above, in Fig. 1.<sup>171</sup> Thus, it

can be imagined that the linear polymer would be severely distorted from its equilibrium conformation because of confinement caused by the presence of fullerenes.<sup>95</sup> Higher particle loadings would probably enhance this distortion considering that the interparticle gap would decrease to  $\sim 0.4$  nm at a fullerene weight fraction of 0.1. At this volume fraction, the interparticle gap is comparable to the fullerene equilibrium separation in a single crystal<sup>215</sup> and the polystyrene monomer size! And so it is quite remarkable that we get good dispersion of fullerenes in polystyrene up to  $\sim 2$  vol% or  $\sim 3.5$  wt%.

From differential scanning calorimetry (DSC) measurements, a first order transition from simple cubic structure to face centered cubic structure around  $-15^{\circ}\text{C}$  was observed for pure fullerenes.<sup>215</sup> This transition is clearly visible in Fig. 7.2.a and is also apparent in the 10 wt% blend produced by solvent evaporation (the inset shows an expanded view of the DSC data obtained for the 10 wt% blend prepared by solvent evaporation). Note the glass transition for polystyrene is also apparent at  $\sim 105^{\circ}\text{C}$ . In contrast, the 10 wt% blend prepared by rapid precipitation shows a single transition near the glass transition temperature of pure polystyrene, suggesting the absence of large phase separated fullerene domains or that the simple cubic to face center cubic transition does not occur in this case.

In Fig. 7.2.b, we show the intensity (obtained from wide angle x-ray scattering, WAXS) as a function of  $d$  spacing, for the various nanocomposites prepared by rapid precipitation, where  $d = 2\pi/q$ ,  $q$  is the wave vector defined as  $4\pi/\lambda \times \sin(\theta/2)$  with  $\lambda$ , the X-ray wavelength (1.54 Å) and  $\theta$ , the scattering angle. No peaks are present in the WAXS intensity profile for the 1 wt% nanocomposite, confirming the absence of phase separated fullerene domains,<sup>216</sup> however, at higher concentrations, peaks in the WAXS

intensity can be clearly seen. These match well with those seen for fullerene single crystals,<sup>215</sup> as shown in the figure, and are probably the result of scattering from phase separated crystallites in the higher concentration blends.

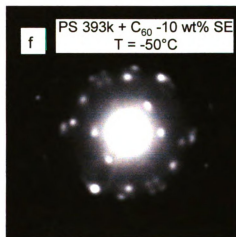
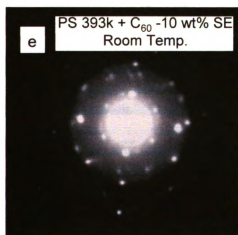
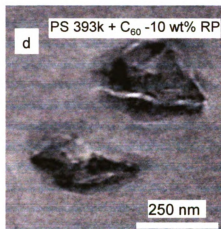
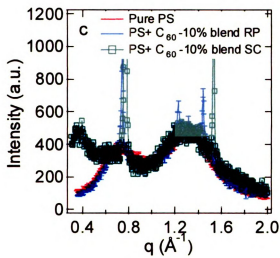
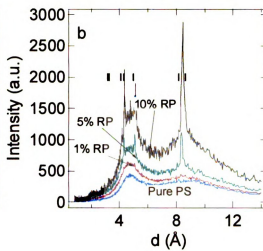
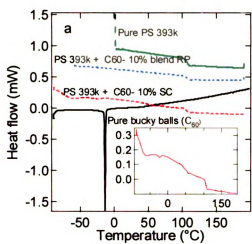
The same WAXS intensity data is plotted as a function of the wave vector in Fig. 7.2.c, together with the data for the 10 wt% blend prepared by solvent evaporation. It can be seen that the blend prepared by gradual solvent evaporation displays a large degree of low  $q$  scattering, clearly indicating large scale phase separation,<sup>18</sup> which is absent in the blends prepared by rapid precipitation. Subsequent TEM experiments on the blends prepared by rapid precipitation did, however, uncover some phase separated regions approximately 200 – 300 nm in size (Fig. 7.2.d) for concentrations above 1 wt%. However, it is clear that the ubiquitousness of the phase separated regimes is greatly reduced by employing the rapid precipitation method as evidenced by the lack of low  $q$ -vector scattering. It should be noted that all of the samples were annealed for ~ 24 hrs, at 170°C, before performing the TEM and WAXS experiments, to make sure that rapid precipitation does not lead to a kinetically trapped metastable state. These aging conditions are above the glass transition temperature of polystyrene (106°C) and the relaxation or reptation time is about 40 sec. at 170°C, ensuring the polymer molecules have explored many configurations; while the RMS diffusion distance of the nanoparticles is on the order of 100's nm also ensuring that they have explored sufficient space within the sample to achieve an equilibrium.

To ascertain whether the transition in the fullerene packing (seen for the pure fullerenes around – 15°C) occurs in these phase separated structures, electron diffraction patterns at different temperatures from the fullerene crystallites produced by both solvent



evaporation and rapid precipitation were obtained. Fig. 7.2.e shows the diffraction pattern for the fullerene crystallites produced by solvent evaporation at room temperature. It can be seen that the diffraction pattern has hexagonal symmetry, as expected. A clear change in the diffraction pattern and hence the crystal structure can be observed on lowering the temperature to  $-50^{\circ}\text{C}$  (Fig. 7.2.f), which can be related to a transition from face center cubic packing to simple cubic.

The much smaller crystallites present in the 5 wt% and 10 wt% samples produced by rapid precipitation also showed a diffraction pattern with hexagonal symmetry at room temperature (similar to Fig. 7.2.e); however, quite surprisingly no change was observed in the diffraction pattern on lowering the temperature to as much as  $-70^{\circ}\text{C}$ <sup>217</sup> (which was the limit of temperature control in the TEM). Thus, rapid precipitation provides, in essence, a method for ‘freezing’ the crystal structure of the fullerene crystals, which could prove to be very important for future electronic application of both fullerenes and their derivatives.<sup>217</sup> We suspect the transition does not occur as the small crystallites are tightly encased by the surrounding polystyrene not allowing an expansion to the simple cubic structure. It should be noted here that for the 1 wt% blend and regions where there are no crystallites for higher concentration samples, there was no equivalent electron diffraction pattern. Thus, long range order in the homogeneous blend, or in the regions outside the nanocrystals, is not present.





**Images in this dissertation are presented in color.**

**Figure 7.2. Dispersion of 1 wt% fullerenes is possible, however, higher concentration mixtures tend to have slight phase separation with small crystallite formation.** **a**, Dispersion of 10 wt% fullerenes in 393 kDa polystyrene via rapid precipitation leads to a single (glass) transition of the nanocomposite (PS – 10 wt% C<sub>60</sub> RP) with a glass transition that is slightly greater than that for pure polystyrene (Pure 393 kDa PS). Pure fullerenes have a crystal structure transition around -15°C (Pure C<sub>60</sub>) which is absent in the nanocomposite produced by rapid precipitation, but is present in the phase separated film produced by solvent evaporation (PS – 10 wt% C<sub>60</sub> SE), as can be seen more clearly in the inset. **b**, The change in the polystyrene WAXS intensity profile (Pure 393 kDa PS) with the addition of fullerenes for mixtures produced with rapid precipitation can be significant. At 5 and 10 wt% fullerenes (5 wt% RP and 10 wt% RP) evidence of a crystalline structure becomes clear while the amorphous halo for polystyrene is only slightly changed through addition of 1 wt% fullerenes (1 wt% RP). The lines at an intensity of 2000 are positions of the structure peaks seen for a fullerene single crystal plotted as a function of  $d$ -spacing. **c**, The WAXS intensity profiles, as a function of  $q$ -vector, for 10 wt% fullerene – polystyrene mixtures produced via rapid precipitation (PS – 10 wt% C<sub>60</sub> RP) and solvent evaporation (PS – 10 wt% C<sub>60</sub> SE) are vastly different with the latter showing low  $q$  scattering indicative of large scale phase separation. The data for the sample prepared by rapid precipitation agrees well with that for pure polystyrene (Pure 393 kDa PS) at low  $q$ -vector. **d**, A TEM micrograph for the 10 wt% fullerene mixture produced by rapid precipitation shows some phase separated crystallites. **e**, An electron diffraction pattern from a crystallite (present in a blend prepared by solvent evaporation) at room temperature demonstrating six-fold symmetry. **f**, Electron diffraction pattern from another crystallite, from the same sample, at -50°C.

In our previous work,<sup>8</sup> we reported for the first time that the addition of intramolecularly crosslinked polystyrene nanoparticles to linear polystyrene, quite surprisingly, caused a *decrease* in the polymer melt viscosity, contradicting Einstein's century old relation. It was postulated that the viscosity decrease observed in these nanocomposites was directly related to the increase in the melt free volume caused by nanoparticle addition.<sup>10</sup> However, subsequent experiments<sup>95</sup> revealed that a change in free volume does not account for all of the effects observed in this system, with a viscosity decrease only present for entangled and confined ( $h < R_g$ ) systems. Indeed, addition of nanoparticles led to a viscosity increase in unentangled polymers. This

provides us two design parameters to cause a viscosity *reduction* in nanocomposites: the polymer must be entangled ( $M_p > M_c$ , where  $M_c$  is the critical molecular mass critical mass for entanglement coupling<sup>13</sup>) and the interparticle half gap  $h < R_g$  of the polymer. It should also be pointed out that the shape of the nanoparticles is extremely important as so far only spherical nanoparticles have been shown to provide a viscosity decrease, with other nanofillers like nanoclays<sup>138</sup> and carbon nanotubes<sup>218, 219</sup> producing a large increase in the viscosity of the polymer melt, leading to more challenging processing conditions.

From Fig. 7.3.a, it can be seen that the unusual viscosity decrease first seen in the ideal polystyrene nanoparticle - linear polystyrene system is repeated here for the fullerene - polystyrene system. The addition of fullerenes, at all the mass fractions considered, causes a large decrease in the terminal viscosity of polystyrene as shown in Fig. 7.3.a (PS 393 kD is entangled,  $R_g$  of polymer  $\sim 17$  nm hence  $R_g > a$ , and for all these nanoparticle concentrations  $h < R_g$ ). Indeed an 80% reduction in the melt viscosity can be observed by addition of 10 wt% fullerenes! This is one of the largest reductions in viscosity on the addition of nanoparticles reported in the literature. It is known that phase separated structures (crystallites) are present with the 5 and 10 wt% samples (Fig. 7.2), at least at room temperature, and so it is interesting that the viscosity continues to decrease even under this condition. However, it can be seen that the viscosity does not change at the same rate at concentrations above 1 wt% and so, apparently, the small, phase separated, crystallites, should they be present in the melt, slow the viscosity decrease.

Due to the gradual color change in the nanocomposites (Fig. 7.1) we suspect there may be more fullerenes dissolved in the polystyrene phase for the 10 wt% rapidly precipitated blend than at the initial concentration where phase separation was detected ( $\sim$

2 vol%). This may account for the continued viscosity decrease despite the potential introduction of crystallites. Note, the 10 wt% fullerene phase separated system prepared via solvent evaporation (Fig. 7.1.a) shows a large viscosity **increase** above pure polystyrene and in fact no terminal (zero shear) viscosity is observed for the system.

Viscoelastic materials are also fast gaining popularity in damping applications,<sup>220</sup> however, issues like poor thermal stability, reliability and high weight penalty have severely affected their large scale development. Recently, Suhr et al.<sup>221</sup> showed addition of multiwalled carbon nanotubes (MWNT) to epoxy can greatly improve its mechanical damping properties.<sup>222</sup> This unique observation of increasing the damping properties, without any detrimental effects on the polymer strength, was expected to be related to the large surface area to volume ratio present in these nanoscale fillers.<sup>221</sup>

The MWNT's have a interfacial contact area of  $\sim 100 \text{ m}^2/\text{g}$ , in comparison, the fullerenes have an interfacial contact area of  $\sim 1300 \text{ m}^2/\text{g}$  (a high interfacial area is expected for all spherical nanofillers). It was hypothesized by us that this large fullerene contact area would allow for large frictional dissipation of energy, leading to excellent damping properties. From Fig. 7.3.b, it can be seen that this is indeed the case. A five fold increase in the loss modulus ( $E''$ ) of the fullerene – polystyrene nanocomposite can be observed without significantly affecting the elastic modulus ( $E'$ ). Indeed a slight increase in the elastic modulus is observable. We note that Suhr et al. used 50 vol% of MWNT to achieve  $\sim 3$ -times enhanced damping while the loss modulus we have measured with the 50 wt% ( $\sim 37$  vol%) fullerene nanocomposite shows  $\sim 5$  fold increase and a similar increase in damping is expected. It should be pointed out that this is the first

example of a spherical nanoparticle causing significant improvements in the damping properties of polymers.

The weight loss with time for the various fullerene - polystyrene nanocomposites prepared by solvent evaporation and rapid precipitation are shown in Fig. 7.3.c. All the samples were kept isothermally at 330°C under a nitrogen atmosphere. It can be seen addition of fullerenes causes a significant reduction in the degradation rate of polystyrene, suggesting their usage as possible fire retardants (other experiments under an air atmosphere also show a significant improvement in thermal stability on fullerene addition). It should be noted here that the weight fraction of the samples remaining at the end of each experiment equals the weight fraction of fullerenes in the nanocomposites, as fullerenes do not degrade at 330°C.

Nanocomposites have shown great promise as effective fire retardants for some types of materials.<sup>223</sup> Typically, research on the thermal stability of nanocomposites has focused on the use of graphite sheets<sup>224</sup> and layered silicates,<sup>225</sup> where the spacing between the layers is in the nanometer range. It has been proposed that enhanced barrier properties are related to the observed improvement in thermal stability. Barrier properties take into consideration both the thermal barrier, which reduces the polymer temperature, as well as mass transport barrier which makes it difficult for the degradation products to leave the polymer, and for oxygen to diffuse into the polymer. However, such a mechanism for thermal stability might not extend to our case as unusual permeability results have been reported in the case of nanoparticle filled polymers. It was seen that nanoscale, fumed silica particles when blended with poly(4-methyl-2-pentyne) simultaneously and rather surprisingly enhance both membrane permeability and

selectivity for large organic molecules over small permanent gases.<sup>10</sup> Such an effect in our case would probably enhance the thermal degradation of the polymer by decreasing the mass transport barrier.

In more recent work, it has been postulated that the formation of a jammed network of nanofillers is essential for causing an improvement in the thermal degradation properties of nanocomposites containing nanotubes and carbon black.<sup>219</sup> However, in our case we see significant improvements in the thermal properties coupled with a large viscosity *decrease* (Fig. 7.3.a), clearly indicating the absence of a jammed or gel-like network of nanoparticles within the polymer melt. Indeed the formation of a gel-like network in the case of carbon black particles would indicate their phase separation from the polymer, especially if the radius of the carbon black particles is greater than the radius of gyration of the linear polymer ( $R_g < a$ ).<sup>208</sup>

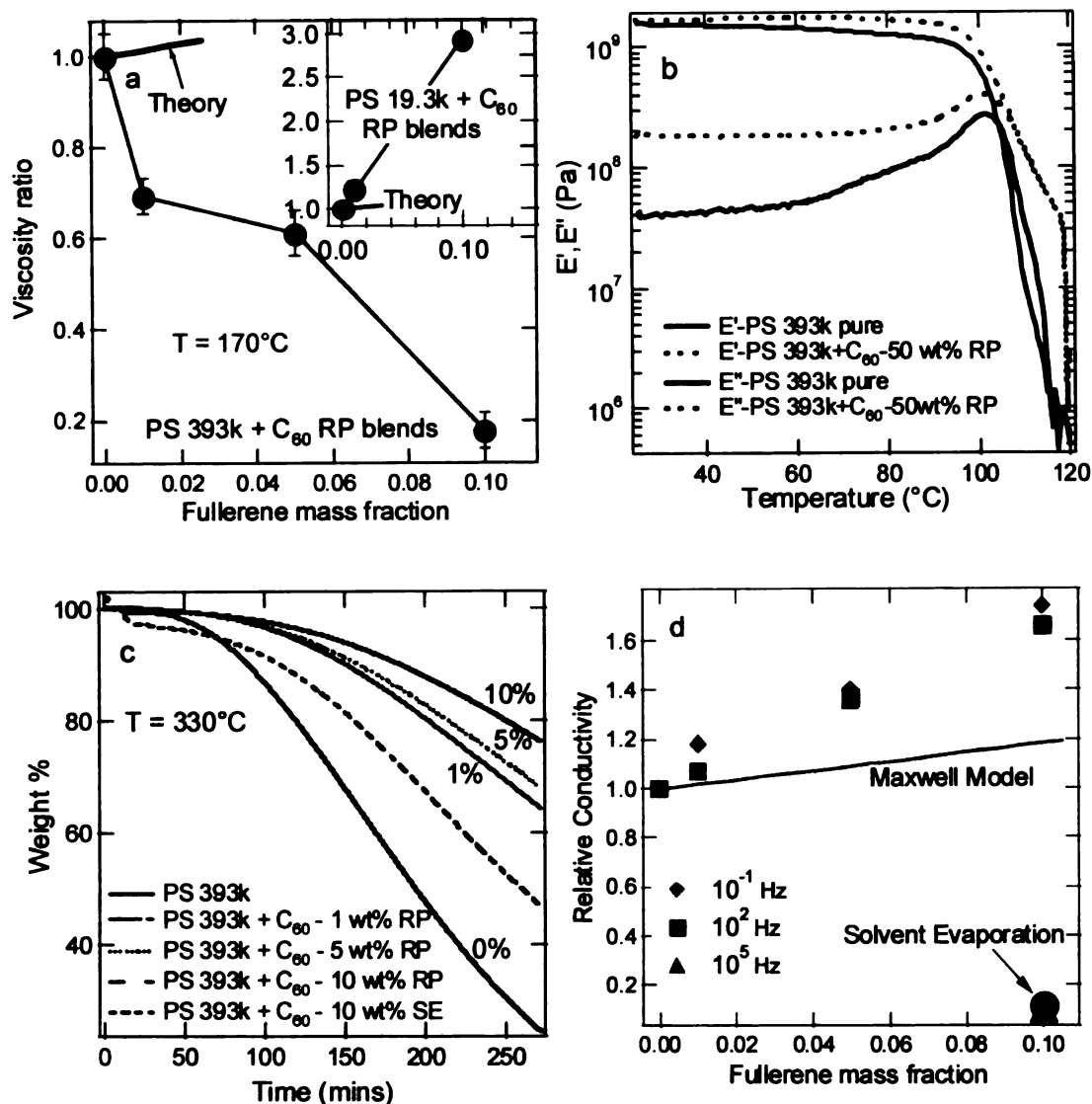
Improvement in thermal stability for our case may then be related to the overall free energy of the system. It can be imagined that a large increase in the system's entropy, because of the fullerene dispersion, leads to a negative overall free energy for the system (this is the reason why the fullerenes stay dispersed).<sup>208</sup> Removal of the linear chain through thermal degradation (the fullerenes do not degrade at 330°C) in this case would lead to a gain in the overall free energy (make it positive) of the system and could be the reason for slowing down the degradation of the composite. In other words, the polymer and its degradation products might condense within the nanoparticles' interstices and on their surfaces to remain thermodynamically stable until the overall entropy is increased by the low molecular mass degradation products leaving the system. It should be pointed out that this gain in free energy on the dispersion of particles is truly a



nanoscale phenomenon since addition of larger particles leads to an adverse free energy effect.<sup>208</sup> So again  $R_g$  must be greater than  $a$  to cause improvements in the thermal stability of the nanocomposite.

The electrical conductivity of the fullerene-polystyrene nanocomposites was also determined. As has been seen before with the addition of nanoscale fillers to thermoplastics<sup>226, 227</sup> and polymer electrolytes,<sup>228</sup> addition of fullerenes (with the rapid precipitation technique) also causes an increase in the conductivity of polystyrene (Fig. 7.3.d). It is interesting that this increase in conductivity, even though small, is much greater than Maxwell's predicted increase<sup>50</sup> for an infinitely conductive spherical filler. This unusual increase in conductivity is expected to be related to the small interparticle gap ( $2h$ ) in the nanocomposite. This small gap would allow charge transfer by electron hopping between electronegative fullerenes<sup>229, 230</sup> (if they are close enough) and may even allow for ballistic electron transfer.<sup>231</sup> Indeed the formation of small fullerene nanoclusters (in the higher fullerene concentration samples) may enhance the nanocomposite conductivity even more.<sup>231</sup> In comparison, the nanocomposite prepared by solvent evaporation has a lower conductivity than neat polystyrene (Fig. 7.3.d).

Thus, we have successfully designed a truly multifunctional<sup>7</sup> nanocomposite with enhanced damping properties, better thermal stability, greater electrical conductivity coupled with a much reduced melt viscosity allowing for easier melt processing and the development of finer features, using existing industrial technologies like injection molding and extrusion. It is also the first time that all of these improvements in the bulk properties have been shown to occur simultaneously in any nanocomposite.



Images in this dissertation are presented in color.

**Figure 7.3. Addition of fullerenes to linear polystyrene has multifunctional effects on the properties including a viscosity reduction, increase in dissipation, increase in degradation time and increase in conductivity. a,** The addition of fullerenes to polystyrene leads to a sharp decrease in the melt viscosity as long as the samples are prepared by rapid precipitation. This behavior directly contradicts Einstein's prediction (theory) of a viscosity increase in such a system. The inset shows the effect of fullerene addition on the viscosity of unentangled polystyrene ( $M_w = 19.3$  kDa). The blend was prepared by rapid precipitation. **b,** Minimal changes are seen in the storage ( $E'$ ) modulus on the addition of fullerenes while a five fold increase is observed in the loss ( $E''$ ) modulus, indicating a significant improvement in the damping properties of the composite. The samples are pure 393 kDa polystyrene (Pure 393 kDa PS) and the same

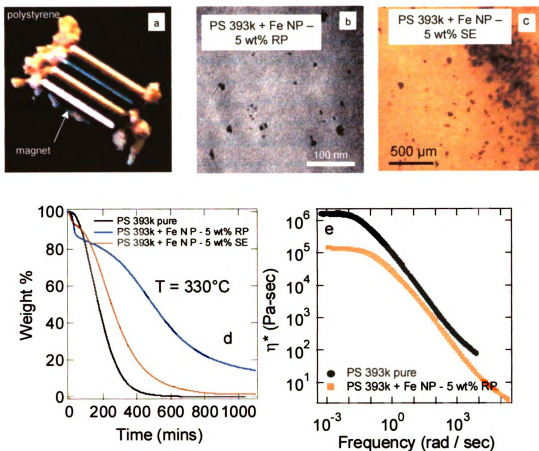
polystyrene containing 50 wt% fullerenes produced by rapid precipitation (PS- 50 wt% C<sub>60</sub> RP). **c**, The addition of fullerenes, when well dispersed, greatly reduce the rate of thermal decomposition of the nanocomposite as shown by weight loss curves obtained by heating the samples to 330°C, under a nitrogen atmosphere. The samples containing 1 and 10 wt% C<sub>60</sub> samples were produced by rapid precipitation (labeled RP) and when compared to pure 393 kDa polystyrene (Pure 393 kDa PS) have a much greater time to degrade. For comparison, phase separated fullerenes perform much worse and a 10 wt% blend prepared by solvent evaporation (PS – 10 wt% C60 SE) only slightly increases the degradation time. **d**, Conductivity of C<sub>60</sub> - 393 kDa polystyrene nanocomposites, relative to pure polystyrene. When fullerenes are well dispersed in polystyrene, prepared by rapid precipitation the conductivity rises above the Maxwell model prediction for an infinitely conducting particle. In comparison a sample containing phase separated structures produced by solvent evaporation has a relative conductivity that is ~ 90% lower than pure polystyrene. Conductivity was measured at a variety of frequencies and only the 10<sup>-1</sup>, 10<sup>2</sup> and 10<sup>5</sup> Hz data are shown.

To test if our design parameters (spherical nanoparticle, entangled polymer,  $R_g > a$ ,  $h < R_g$  and using rapid precipitation for dispersion; the various design parameters and the properties they affect have been summarized in Table 7.1) can be used to produce multifunctional nanocomposites with inorganic nanoparticles as well, we study the effects of adding magnetite nanoparticles (see methods) to polystyrene ( $M_w = 393$  kD). A picture of the nanocomposite prepared by rapid precipitation, attracted to a permanent magnet, is shown in Fig. 7.4.a, showing that the incorporation of the nanoparticles has made the nanocomposite ferromagnetic. Again, rapid precipitation and the condition that  $R_g$  is larger than  $a$ , enables good dispersion of the nanoparticles as evidenced by the TEM image shown in Fig. 7.4.b. Image analysis shows that the nanoparticles are quite polydisperse with their radius varying between 5-10 nm. The good dispersion of the magnetic nanoparticles, at this high density, opens up plethora of possible future applications including electro-magnetic shielding, high density memory, magnetic recording, drug delivery and separation aids<sup>232-234</sup> (this is an additional benefit which was of course not seen with the fullerenes). Again, as was the case with fullerenes, solvent

evaporation leads to large scale phase separation (Fig. 7.4.c, note the change in the scale bar compared to Fig. 7.4.b) due to the large difference in solubility between the nanoparticles and the polymer in the common solvent (benzene). The incorporation of the ferromagnetic nanoparticles using rapid precipitation also improves the thermal stability (Fig. 7.4.d) of the nanocomposite. Again the thermal stability of the rapidly precipitated blend is better than the blend prepared by solvent evaporation. The initial, rapid weight loss for time less than 100 sec is most likely due to the steric stabilizing layer leaving the system. The magnetite addition also simultaneously causes a massive reduction in the melt viscosity (Fig. 7.4.e). It is quite surprising that just 5 wt% (or  $\sim 1$  vol%) of the magnetite nanoparticles can cause an  $\sim 90\%$  reduction in the polymer melt viscosity, which is again one of the largest viscosity decreases reported on the addition of nanoparticles. It would thus appear that the improvement in thermal stability and the viscosity decrease seen in the fullerene - linear polystyrene blends can transcend to other nanoparticle - polymer systems and is not the result of some peculiar chemical or physical interaction.

**Table 7.1.** Design parameters for nanoparticle dispersion and producing multifunctional nanocomposites.

<b>Parameter</b>	<b>Parameter values to enhance bulk properties</b>
Method for nanoparticle dispersion	Rapid precipitation provides a better technique for nanoparticle dispersion.
Polymer molecular mass ( $M_p$ )	$M_p > M_c$ for nanoparticles to cause a reduction in viscosity; $M_p$ also determines $R_g$ .
Polymer $R_g$	$R_g > a$ for nanoparticle dispersion and for improving thermal stability; $R_g > h$ for viscosity reduction.
Nanoparticle shape	So far, only spherical nanoparticles have been shown to cause a viscosity decrease; spherical nanoparticles also have higher interfacial contact area leading to better damping properties.
Nanoparticle radius ( $a$ )	$R_g > a$ for nanoparticle dispersion and improving thermal stability.
Nanoparticle concentration	Determines the interparticle half gap, $h$ ; $R_g > h$ for viscosity reduction.



Images in this dissertation are presented in color.

**Figure 7.4.** It is possible to disperse ferromagnetic nanoparticles in linear polystyrene (393 kDa) to make a ferromagnetic polymeric material. **a**, Polystyrene is slightly colored by the dispersed magnetite nanoparticles which cause the sample to be attracted to a permanent magnet. **b**, A TEM micrograph showing the nanoparticle dispersion with gross phase separation. **c**, Nanoparticle - polystyrene blends developed through solvent evaporation produce large phase separated domains. Also, as shown for the fullerene nanoparticles, the magnetite nanoparticles at 5 wt% reduce the amount of degradation (**d**) and the melt viscosity at all frequencies (**e**). The degradation experiment was performed at 330 °C under a nitrogen atmosphere and the viscosity was measured at multiple temperatures and shifted to a reference temperature of 170 °C.

## Conclusion

In conclusion, as long as we follow certain critical design parameters (spherical nanoparticle, entangled polymer,  $R_g > a$ ,  $h < R_g$  and using rapid precipitation for dispersion), we can create multifunctional nanocomposites with both *organic and inorganic* nanoparticles having the desired electrical or magnetic properties, coupled with enhanced mechanical damping, greater thermal stability and a much reduced melt viscosity.

## CHAPTER 8

### CONCLUSION

---

In this work we aimed to provide a better understanding of nanoparticle-polymer blends. There were some significant findings through the course of the project which not only helped us proceed with the project but will also prove useful to other researchers working in the area. Some of those findings and their implications have been detailed below.

First, we started out by comparing the various methods used in the literature for nanoparticle dispersion. One of the most common methods in the literature was solvent evaporation,<sup>24</sup> which entailed the mixing of the polymer and the nanoparticle in a common solvent, followed by the evaporation of the solvent. Differences in the solubility's of the nanoparticles and the polymer typically led to phase separation in this case. To overcome this difficulty, we used the 'rapid precipitation' technique<sup>34, 48</sup> (Chapters 4 and 7). In this case, as both the nanoparticles and the polymer are insoluble in the non-solvent, they precipitate out together.

With the understanding of the importance of the technique used for nanoparticle dispersion, we studied the various parameters responsible for the miscibility or phase stability of nanoparticles in linear polymers. One of the most important findings of this work is the establishment of a thumb rule for phase stability in nanoparticle-polymer blends. In Chapter 3 we showed that it is possible to disperse chemically dissimilar nanoparticles in various polymer matrices as long as the  $R_g$  of the polymer > radius of



nanoparticle. This simple parameter has allowed us to disperse both organic (like polyethylene in polystyrene or polystyrene in poly(methylmethacrylate)) and inorganic nanoparticles (like magnetite nanoparticles or Cd-Se quantum dots in polystyrene) in dissimilar polymer matrices.

Another important finding highlighted in Chapter 3 is that linear chains get stretched on the addition of nanoparticles. This has been an extremely controversial subject in the literature. Multiple simulation<sup>124, 235-242</sup> and some experimental studies<sup>126, 243</sup> have tried to provide a conclusive answer to the issue. However, their findings are almost equally divided, with half of the studies suggesting that there should be an increase in the chain dimensions on nanoparticle addition while the other half concluding that the nanoparticles do not affect the chain dimensions at all. Our experimental work, using SANS, conducted on the ideal system of polystyrene nanoparticles in linear polystyrene, conclusively shows that linear chains do indeed get stretched on the addition of nanoparticles, and that the chain stretching is directly proportional to the volume fraction of the added nanoparticles.

Another objective of this work was the study of the effects of nanoparticle addition on the flow properties of polymer melts. This work has been detailed in chapters 4 and 5. It was seen that the addition of nanoparticles to unentangled polymers led to a sharp increase in their viscosity, in comparison, the addition of nanoparticles to a polymer near its critical molecular weight for entanglement had almost no effect on the viscosity of the polymer melt. When extended to entangled polymers, it was seen that the addition of nanoparticles to a constrained (Chapter 5) and entangled polymer melt caused a large *decrease* in the viscosity of polymer melts. This unusual viscosity decrease was

seen for various inorganic and organic nanoparticle – polymer systems (Chapters 5 and 6). In certain cases as much as 80 - 90% reduction in the polymer melts' viscosity was observed with just 1-5% by volume addition of the nanoparticles. This surprising behavior has recently been confirmed for a variety of nanoparticle – polymer systems by various other research groups.<sup>216, 244-248</sup>

To understand the reasons for the viscosity reduction caused by the addition of nanoparticles, we recently measured the diffusion coefficients of various nanoparticles in an entangled polystyrene matrix (Chapter 7). It was seen that in certain cases the diffusion coefficient of the nanoparticles was almost 100 times larger than the diffusion coefficient calculated from the Stokes-Einstein relation based on the bulk polymer viscosity. We hypothesize that this fast nanoparticle diffusion provides another mode for polymer relaxation based on the mechanism of constraint release. To confirm this hypothesis we also measured the viscosity of a nanoparticle – 3 arm star blend. Stars can only relax by primitive path fluctuations, and as expected, the addition of nanoparticles caused an increase in the melt viscosity of the stars.

The final objective of this work was to build up materials utilizing the various important findings in this work. We have taken the first steps in that direction by creating one of the first 'multifunctional'<sup>7</sup> polymer – nanoparticle composites (Chapter 7). It was seen that the addition of fullerenes ( $C_{60}$ ) and magnetite nanoparticles can impart specific electrical or magnetic properties to the polymer coupled with simultaneous improvements in the mechanical, thermal and rheological properties.

It is clear in the end that the addition of nanoparticles to polymers can create some unexpected property enhancements like miscibility despite chemical dissimilarity and a

reduction in the polymer melt viscosity, which are not expected with the addition of micron or colloidal scale fillers. It has to be expected then that there still remain a lot of fascinating discoveries to be made in this area, which should definitely provide impetus to a future batch of researchers.

## LIST OF PUBLICATIONS

The following publications were made as a direct result of the research carried out for this project.

### Published and accepted journal articles:

- 1) "Nanoscale effects leading to non-Einstein-like decrease in viscosity", Michael E. Mackay, Tien T. Dao, Anish Tuteja, Derek L. Ho, Brooke van Horn, Ho-Cheol Kim, Craig J Hawker, *Nature Materials*, 2003, 2(11), 762-766.
- 2) "Effect of ideal, organic nanoparticles on the flow properties of linear polymers; non-Einstein-like behavior", Anish Tuteja, Michael E. Mackay, Brooke van Horn, Craig J. Hawker, *Macromolecules*, 2005, 38, 8000-8011.
- 3) "General strategies for nanoparticle dispersion ", Michael E. Mackay, Anish Tuteja, Phil M. Duxbury, Craig J. Hawker, Brooke van Horn, Zhibin Guan, R.S. Krishnan, *Science*, 2006, 311, 1740-1743.
- 4) "The molecular architecture and rheological characterization of novel intramolecularly crosslinked polystyrene nanoparticles", Anish Tuteja, Michael E. Mackay, Brooke van Horn, Craig J. Hawker, Derek L. Ho, 2006, *Journal of Polymer Science – Part B – Polymer Physics*, 44, 1930-1947.

### Journal articles submitted for review or in preparation:

- 1) "Multifunctional nanocomposites: nanoparticle induced enhancements in the thermal, mechanical, magnetic, electrical and rheological properties of polymers." Anish Tuteja, Michael. E. Mackay.
- 2) "Nanoparticles induced expansion in linear polymer coils", Anish Tuteja, Michael E. Mackay, Brooke van Horn, Craig J. Hawker.
- 3) "Breakdown of the Stokes-Einstein relation for nanoscale inclusions in polymer melts", Anish Tuteja, Michael E. Mackay, Suresh Narayanan, Michael Wong.

## REFERENCES

1. Krishnamoorti, R.; Vaia, R. A., ACS: Washington, DC, 2002; Vol. 804.
2. Chapman, R.; Mulvaney, P. *Chem. Phys. Lett.* **2001**, 349, (5-6), 358-362.
3. Wilson, O.; Wilson, G. J.; Mulvaney, P. *Adv. Mater.* **2002**, 14, (13-14), 1000-+.
4. Yoon, P. J.; Fornes, T. D.; Paul, D. R. *Polymer* **2002**, 43, (25), 6727-6741.
5. Lagaly, G. *Appl. Clay Sci.* **1999**, 15, (1-2), 1-9.
6. Luckham, P. F.; Rossi, S. *Adv. Colloid Interface Sci.* **1999**, 82, (1-3), 43-92.
7. Vaia, R. A.; Wagner, H. D. *Materials Today* **2004**, 7, 32-37.
8. Mackay, M. E.; Dao, T. T.; Tuteja, A.; Ho, D. L.; Horn, B. v.; Kim, H.-C.; Hawker, C. J. *Nature Mat.* **2003**, 2, 762-766.
9. Roberts, C.; Cosgrove, T.; Schmidt, R. G.; Gordon, G. V. *Macromolecules* **2001**, 34, 538-543.
10. Merkel, T. C.; Freeman, B. D.; Spontak, R. J.; He, Z.; Pinnau, I.; Meakin, P.; Hill, A. J. *Science* **2002**, 296, 519-522.
11. Harth, E.; VanHorn, B.; Lee, V. Y.; Germack, D. S.; Gonzales, C. P.; Miller, R. D.; Hawker, C. J. *J. Am. Chem. Soc.* **2002**, 124, 8653-8660.
12. Antonietti, M.; Pakula, T.; Bremser, W. *Macromolecules* **1995**, 28, (12), 4227-4233.
13. Ferry, J. D., *Viscoelastic properties of polymers*. 3rd ed.; J. Wiley & Sons: New York, 1980.
14. Graessley, W. W., *The Entanglement Concept in Polymer Rheology*. Springer-Verlag: New York, 1974; Vol. 16.
15. Larson, R. G., *The Structure and Rheology of Complex Fluids*. Oxford University Press: New York, 1999.
16. deGennes, P. G. *The Journal of Chemical Physics* **1971**, 55, (2), 572-579.
17. Debye, P. *Phys. Coll. Chem.* **1947**, 51, 18-32.
18. King, S. M., Small-angle neutron scattering. In *Modern Techniques for Polymer Characterisation*, Pethrick, R. A.; Dawkins, J. V., Eds. John Wiley & Sons: New York, 1999.
19. Burchard, W. *Advances in Polymer Science* **1999**, 143, 113-195.

20. Schmidt, M.; Burchard, W. *Macromolecules* **1981**, 14, 210-211.
21. Schweizer, K. S. *J. Chem. Phys.* **1989**, 91, (9), 5822-5839.
22. Schweizer, K. S. *J. Non-Cryst. Solids* **1991**, 131, 643-649.
23. Lin, Y.; Boker, A.; He, J. B.; Sill, K.; Xiang, H. Q.; Abetz, C.; Li, X. F.; Wang, J.; Emrick, T.; Long, S.; Wang, Q.; Balazs, A.; Russell, T. P. *Nature* **2005**, 434, (7029), 55-59.
24. Weng, D.; Lee, H. K.; Levon, K.; Mao, J.; Scrivens, W. A.; Stephens, E. B.; Tour, J. M. *European Polymer Journal* **1999**, 35, 867-878.
25. Ginzburg, V. V. *Macromolecules* **2005**, 38, 2362-2367.
26. Flory, P. J., *Principles of Polymer Chemistry*. Cornell University Press: Ithaca, 1953.
27. Du, F. M.; Fischer, J. E.; Winey, K. I. *Journal Of Polymer Science Part B-Polymer Physics* **2003**, 41, (24), 3333-3338.
28. Sariciftci, N. S.; Smilowitz, L.; Heeger, A. J.; Wudl, F. *Science* **1992**, 258, 1474-1477.
29. Sariciftci, N. S.; Heeger, A. J. *Synthetic Metals* **1995**, 70, (1-3), 1349-1352.
30. Siegel, R. W. *Phys Today* **1993**, 46-Oct, 64-68.
31. Mayo, M. J.; Siegel, R. W.; Narayanasamy, A.; Nix, W. D. *J. Mat. Res.* **1990**, 5, 1073-1082.
32. Mayo, M. J.; Siegel, R. W.; Liao, Y. X.; Nix, W. D. *J. Mat. Res.* **1992**, 7, 973-979.
33. Einstein, A. *Ann. d. Phys. Leipzig* **1906**, 19, 371-381.
34. Mackay, M. E.; Tuteja, A.; Duxbury, P. M.; Hawker, C. J.; Van Horn, B.; Guan, Z.; Chen, G.; Krishnan, R. S. *Science* **2006**, 311, (5768), 1740-1743.
35. Tsenoglou, C. *Macromolecules* **1991**, 24, (8), 1762-1767.
36. Lopes, W. A.; Jaeger, H. M. *Nature* **2001**, 414, (6865), 735-738.
37. Li, M.; Schnablegger, H.; Mann, S. *Nature* **1999**, 402, (6760), 393-395.
38. Bockstaller, M. R.; Lapetnikov, Y.; Margel, S.; Thomas, E. L. *Journal Of The American Chemical Society* **2003**, 125, (18), 5276-5277.

39. Raja, K. S.; Wang, Q.; Gonzalez, M. J.; Manchester, M.; Johnson, J. E.; Finn, M. G. *Biomacromolecules* **2003**, 4, (3), 472-476.
40. Johnson, J. E.; Chiu, V. *Current Opinion in Structural Biology* **2000**, 10, (2), 229-235.
41. Chen, D. T.; Weeks, E. R.; Crocker, J. C.; Islam, M. F.; Verma, R.; Gruber, J.; Levine, A. J.; Lubensky, T. C.; Yodh, A. G. *Physical Review Letters* **2003**, 90, (10), 108301.
42. Papagiannopoulos, A.; Waigh, T. A.; Fluerasu, A.; Fernyhough, C.; Madsen, A. *Journal of Physics: Condensed Matter* **2005**, 17, (25), L279.
43. Lurio, L. B.; Lumma, D.; Sandy, A. R.; Borthwick, M. A.; Falus, P.; Mochrie, S. G. J.; Pelletier, J. F.; Sutton, M.; Regan, L.; Malik, A.; Stephenson, G. B. *Physical Review Letters* **2000**, 84, (4), 785-788.
44. Narayanan, S.; Lee, D. R.; Guico, R. S.; Sinha, S. K.; Wang, J. *Physical Review Letters* **2005**, 94, (14), -.
45. Gao, F. *Materials Today* **2004**, 7, 50-55.
46. Curtin, W. A.; Sheldon, B. W. *Materials Today* **2004**, 7, 44-49.
47. Martensa, T.; D'Haenb, J.; Muntersa, T.; Beelena, Z.; Gorisb, L.; Mancab, J.; D'Olieslaegerb, M.; Vanderzandea, D.; Scheppera, L. D.; Andriessenc, R. *Synthetic Metals* **2003**, 138, 243-247.
48. Mackay, M. E.; Dao, T. T.; Tuteja, A.; Ho, D. L.; Van Horn, B.; Kim, H. C.; Hawker, C. J. *Nature Materials* **2003**, 2, (11), 762-766.
49. Tuteja, A.; Mackay, M. E.; Hawker, C. J.; Van Horn, B. *Macromolecules* **2005**, 38, (19), 8000-8011.
50. Maxwell, J. C., *A Treatise on Electricity and Magnetism*. 2nd Ed. ed.; Oxford University Press: Cambridge, 1904.
51. Mackay, M. E.; Dao, T. T.; Tuteja, A.; Ho, D. L.; Horn, B. v.; Kim, H.-C.; Hawker, C. J. *Nature Materials* **2003**, 2, 762-766.
52. Xia, Y. G., B; Yin, Y; Lu, Y. *Adv. Mater.* **2000**, 12, 693.
53. Kuhn, W.; Balmer, G. *J. Poly. Sci.* **1962**, 57, 311-319.
54. Longi, P. G., F; Rossi, U. *Makromol. Chem* **1969**, 129, (157).
55. Martin, J. E.; Eichinger, B. E. *Macomolecules* **1983**, 16, 1345-1350.
56. Martin, J. E.; Eichinger, B. E. *Macromolecules* **1983**, 16, 1350-1358.

57. Eichinger, B. E. *Macromolecules* **1980**, 13, (1), 1-11.
58. Antonietti, M.; Sillescu, H.; Schmidt, M.; Schuch, H. *Macromolecules* **1988**, 21, (3), 736-742.
59. Antonietti, M.; Ehlich, D.; Folsch, K. J.; Sillescu, H.; Schmidt, M.; Lindner, P. *Macromolecules* **1989**, 22, (6), 2802-2812.
60. Antonietti, M.; Bremser, W.; Schmidt, M. *Macromolecules* **1990**, 23, (16), 3796-3805.
61. Antonietti, M.; Bremser, W.; Pakula, T. *Acta Polymerica* **1995**, 46, (1), 37-44.
62. Roland, C. M.; Santangelo, P. G.; Antonietti, M.; Neese, M. *Macromolecules* **1999**, 32, (7), 2283-2287.
63. Fox, T. G.; Flory, P. J. *J. Am. Chem. Soc.* **1948**, 70, 2384-2395.
64. Fox, T. G.; Flory, P. J. *J. Poly. Sci.* **1954**, 14, 315-319.
65. Berry, G. C.; Fox, T. G. *Adv. Poly. Sci.* **1968**, 5, 261-357.
66. Edwards, S. F. *Proc Phys Soc* **1967**, 92:9.
67. deGennes, P. G. *J. Chem. Phys.* **1971**, 55, (2), 572-579.
68. Lodge, T. P.; Rotstein, N. A.; Prager, S. *Adv. Chem. Phys.* **1990**, 79, 1-132.
69. McKenna, G. B.; Hadziioannou, G.; Lutz, P.; Hild, G.; Strazielle, C.; Straupe, C.; Rempp, P.; Kovacs, A. J. *Macromolecules* **1987**, 20, (3), 498-512.
70. Fetters, L. J.; Kiss, A. D.; Pearson, D. S.; Quack, G. F.; Vitus, F. J. *Macromolecules* **1993**, 26, (4), 647-654.
71. Antonietti, M.; Sillescu, H. *Macromolecules* **1986**, 19, (3), 798-803.
72. Koppi, K. A.; Tirrell, M.; Bates, F. S.; Almdal, K.; Mortensen, K. *J. Rheo.* **1994**, 38, (4), 999-1027.
73. Kornfield, J. A.; Fuller, G. G.; Pearson, D. S. *Macromolecules* **1989**, 22, (3), 1334-1345.
74. Doi, M.; Pearson, D.; Kornfield, J.; Fuller, G. *Macromolecules* **1989**, 22, (3), 1488-1490.
75. Ylitalo, C. M.; Kornfield, J. A.; Fuller, G. G.; Pearson, D. S. *Macromolecules* **1991**, 24, (3), 749-758.



76. Mackay, M. E.; Dao, T. T.; Tuteja, A.; Ho, D. L.; Horn, B. v.; Kim, H.-C.; Hawker, C. J. *Nat. Mater.* **2003**, 2, 762-766.
77. Huggins, M. L. *J. Am. Chem. Soc.* **1942**, 64, 2716.
78. Kraemer, E. O. *Ind. Eng. Chem.* **1938**, 30, 1200.
79. Brandrup, J.; Immergut, E. H., *Polymer Handbook*. Third Edition ed.; John Wiley & Sons: New York, 1989.
80. In pp The hydrodynamic radius ( $R_h$ ) and viscosimetric radius ( $R_\eta$ ), determined from the viscosimetric volume, are almost equivalent.  $R_h$  is measured in a homogeneous flow field and  $R_\eta$  within a shear flow field. As long as the molecular distortion is not too great they appear to be practically the same.
81. Yamakawa, H., *Modern Theory of Polymer Solutions*. Harper and Row: London, 1971.
82. Munch, J. P.; Hild, G.; Candau, S. *Macromolecules* **1983**, 16, (1), 71-75.
83. Brown, W. *Macromolecules* **1985**, 18, (9), 1713-1719.
84. Higgins, J. S.; Benoît, H. C., *Polymers and neutron scattering*. Clarendon Press: Oxford, 2002.
85. Kajiwara, K.; Burchard, W. *Polymer* **1981**, 22, 1621-1628.
86. Guinier, A. F., G, *Small angle scattering of X-rays*. Wiley: New York, 1955.
87. Horio, M.; Fujii, T.; Onogi, J. *Phys. Chem.* **1964**, 68, 778.
88. Staudinger, H.; Heuer, W. *Ber.* **1930**, 63, (B), 222-234.
89. Jeong, M.; Mackay, M. E.; Hawker, C. J.; Vestberg, R. *Macromolecules* **2001**, 34, 4927-4936.
90. Kuhn, W.; Majer, H. *Makromol. Chem* **1955**, 18/19, 239-253.
91. Wedemeyer, W. J.; Xu, X. B.; Welker, E.; Scheraga, H. A. *Biochemistry* **2002**, 41, 1483-1491.
92. Ueberreiter, K.; Kanig, G. *J. Chem. Phys.* **1950**, 18, (4), 399-406.
93. Glans, J. H.; Turner, D. T. *Polymer* **1981**, 22, (11), 1540-1543.
94. Nielsen, L. E. *Journal of Macromolecular Science-Reviews in Macromolecular Chemistry* **1969**, C 3, (1), 69-&.

95. Tuteja, A.; Mackay, M. E.; Hawker, C. J.; Horn, B. V. *Macromolecules* **2005**, *38*, 8000-8011.
96. Krishnan, R. S.; Mackay, M. E.; Hawker, C. J.; Van Horn, B. *Langmuir* **2005**, *21*, (13), 5770-5776.
97. Dee, G. T.; Sauer, B. B. *Advance in Physics* **1998**, *47*, 161-205.
98. Mackay, M. E.; Henson, D. J. *J. Rheology* **1998**, *42*, 1505-1517.
99. Lomellini, P. *Polymer* **1992**, *33*, (6), 1255-1260.
100. Russel, W. B.; Saville, D. A.; Schowalter, W. R., *Colloidal Dispersions*. Cambridge University Press: Cambridge, 1989.
101. Shah, S. A.; Chen, Y. L.; Schweizer, K. S.; Zukoski, C. F. *J. Chem. Phys.* **2003**, *119*, 8747-8760.
102. O'Hern, C. S.; Silbert, L. E.; Liu, A. J.; Nagel, S. R. *Phys. Rev. E* **2003**, *68*, (1), 011306-1 - 011306-19.
103. Zimm, B. H. *J. Chem. Phys.* **1948**, *16*, 1099-1116.
104. Utracki, L. A., *Polymer Alloys and Blends*. Hanser Publishers: New York, 1990.
105. Cragg, L. H.; Hammerschlag, H. *Chem. Rev.* **1946**, *39*, 79-135.
106. Utracki, L. A.; Schlund, B. *Polymer Engineering and Science* **1987**, *27*, (20), 1512-1522.
107. Lin, Y.; Boker, A.; He, J. B.; Sill, K.; Xiang, H. Q.; Abetz, C.; Li, X. F.; Wang, J.; Emrick, T.; Long, S.; Wang, Q.; Balazs, A.; Russell, T. P. *Nature* **2005**, *434*, 55-59.
108. Hooper, J. B.; Schweizer, K. S.; Desai, T. G.; Koshy, R.; Keblinski, P. *J. Chem. Phys.* **2004**, *121*, 6986-6997.
109. Hooper, J. B.; Schweizer, K. S. *Macromolecules* **2005**, *38*, 8858-8869.
110. Sariciftci, N. S.; Smilowitz, L.; Heeger, A. J.; Wudl, F. *Science* **1992**, *258*, (5087), 1474-1476.
111. Sariciftci, N. S.; Heeger, A. J. *Syn.Met.* **1995**, *70*, (1-3), 1349-1352.
112. Guan, Z.; Cotts, P.; McCord, E.; McLain, S. *Science* **1999**, *283*, 2059-2062.
113. Starr, F. W.; Schröder, T. B.; Glotzer, S. C. *Physical Review* **2001**, *64*, 021802-1 - 021802-5.

114. Weng, D.; Lee, H. K.; Levon, K.; Mao, J.; Scrivens, W. A.; Stephens, E. B.; Tour, J. M. *Eur. Poly. J.* **1999**, 35, (5), 867-878.
115. Flory, P. J., *Principles of Polymer Chemistry*. Cornell University Press: Ithaca, 1953; p 672.
116. Du, F. M.; Fischer, J. E.; Winey, K. I. *J. Poly. Sci. Part B-Poly. Phys.* **2003**, 41, 3333-3338.
117. Bezmel'nitsyn, V. N.; Eletsii, A. V.; Okun', M. V. *Phys. - Uspekhi* **1998**, 41, (11), 1091-1114.
118. Utracki, L. A., *Polymer Alloys and Blends*. Hanser Publishers: New York, 1990; p 356.
119. Bates, F. S.; Wignall, G. D. *Phys. Rev. Letters* **1986**, 57, 1429-1432.
120. Lauter-Pasyuk, V.; Lauter, H. J.; Ausserre, D.; Gallot, Y.; Cabuil, V.; Hamdoun, B.; Kornilov, E. I. *Physica B* **1998**, 248, 243-245.
121. Thompson, R. B.; Ginzburg, V. V.; Matsen, M. W.; Balazs, A. C. *Science* **2001**, 292, (5526), 2469-2472.
122. Ginzburg, V. V. *Macromolecules* **2005**, 38, (6), 2362-2367.
123. Gallas, J. M.; Littrell, K. C.; Seifert, S.; Zajac, G. W.; Thiyagarajan, P. *Biophys. J.* **1999**, 77, 1135-1142.
124. Sharaf, M. A.; Mark, J. E. *Polymer* **2004**, 45, (11), 3943-3952.
125. Vacatello, M. *Macromolecules* **2002**, 35, 8191-8193.
126. Nakatani, A. I.; Chen, W.; Schmidt, R. G.; Gordon, G. V.; Han, C. C. *Polymer* **2001**, 42, (8), 3713-3722.
127. Kruse, W. A.; Kirste, R. G.; Haas, J.; Schmitt, B. J.; Stein, D. J. *Makrom. Chem. - Macrom. Chem. Phys.* **1976**, 177, (4), 1145-1160.
128. Russell, T. P.; Stein, R. S. *J. Poy. Sci. B-Poly. Phys.* **1982**, 20, (9), 1593-1607.
129. Zoller, P.; Walsh, D. J., *Standard Pressure-Volume-Temperature Data for Polymers*. Technomic Publishing: Lancaster, 1995.
130. Dee, G. T.; Sauer, B. B. *Colloid and Interface Science* **1992**, 152, 85-103.
131. Mackay, M. E.; Carmezini, G.; Sauer, B. B.; Kampert, W. *Langmuir* **2001**, 17, 1708-1712.

132. vanKrevelen, D. W., *Properties of Polymers, Their Estimation and Correlation with Chemical Structure*. 2 ed.; Elsevier Scientific Pub. Co: 1976; p 620.
133. Marrucci, G. *Transactions of the Society of Rheology* **1972**, 16, (2), 321-330.
134. Park, S. Y.; Barrett, C. J.; Rubner, M. F.; Mayes, A. M. *Macromolecules* **2001**, 34, (10), 3384-3388.
135. Huh, J.; Ginzburg, V. V.; Balazs, A. C. *Macromolecules* **2000**, 33, (21), 8085-8096.
136. VanDerWerff, J. C.; Kruif, C. G. d. *Physical Review A* **1989**, 39, (2), 795-807.
137. Metzner, A. B. *J. Rheology* **1985**, 29, (6), 739-775.
138. Krishnamoorti, R.; Ren, J.; Silva, A. S. *J. Chem. Phys.* **2001**, 114, 4968-4973.
139. Siegel, R. *Physics Today* **1993**, 64-68.
140. O'Brien, V. T.; Mackay, M. E. *Langmuir* **2000**, 16, 7931-7938.
141. Antonietti, M.; Pakula, T.; Bremser, W. *Macromolecules* **1995**, 28, 4227-4233.
142. Tande, B. M.; Wagner, N. J.; Mackay, M. E.; Hawker, C. J.; Vestberg, R.; Jeong, M. *Macromolecules* **2001**, 34, 8580-8585.
143. Burchard, W.; Kajiwara, K.; Neger, D. *Journal of Polymer Science: Polymer Physics Edition* **1982**, 20, 157-171.
144. Cosgrove, T.; Griffiths, P. C.; Lloyd, P. M. *Langmuir* **1995**, 11, 1457-1463.
145. Krieger, I. M.; Dougherty, T. J. *Transactions of The Society of Rheology* **1959**, III, 137-152.
146. Starr, F. W.; Schröder, T. B.; Glotzer, S. C. *Macromolecules* **2002**, 35, 4481-4492.
147. Varnik, F.; Baschnagel, J.; Binder, K. *Phys. Rev. E* **2002**, 65, 021507-1-021507-14.
148. Batchelor, G. K. *J. Fluid Mech* **1977**, 83, (1), 97-117.
149. Xue, G.; Lu, Y.; Shi, G.; Dai, Q. *Polymer* **1994**, 35, (4), 892-894.
150. Doi, M.; Edwards, S. F., *The theory of polymer dynamics*. Clarendon Press: Oxford, 1986.
151. Rouse, P. E. *J. Chem. Phys.* **1953**.

152. Lodge, T. P.; Rotstein, N. A.; Prager, S. *Adv. Chem. Phys.* **1990**, 79, 1-132.
153. Kotliar, A. M.; Kumar, R.; Back, R. A. *J. Poly. Phys.: Part B: Poly. Phys.* **1990**, 28, 1033-1045.
154. Liu, C.-Y.; Morawetz, H. *Macromolecules* **1988**, 21, (2), 515-518.
155. Farrington, P. J. Polymer structure, dynamics and viscoelasticity. PhD, The University of Queensland, Brisbane, 1996.
156. Tsenoglou, C. *Macromolecules* **2001**, 34, (7), 2148-2155.
157. Ianniruberto, G.; Marrucci, G. *J. Non-Newt. Fluid Mech.* **2000**, 95, (2-3), 363-374.
158. Zax, D. B.; Yang, D. K.; Santos, R. A.; Hegemann, H.; Giannelis, E. P.; Manias, E. *J. Chem. Phys.* **2000**, 112, (6), 2945-2951.
159. Anastasiadis, S. H.; Karatasos, K.; Vlachos, G.; Manias, E.; Giannelis, E. P. *Phys. Rev. Lett.* **2000**, 84, (5), 915-918.
160. Brown, H. R.; Russell, T. P. *Macromolecules* **1996**, 29, (2), 798-800.
161. Jones, R.; Kumar, S.; Ho, D.; Briber, R.; Russell, T. *Macromolecules* **2001**, 34, 559-567.
162. Cheng, P. Y.; Schachman, H. K. *J. Poly. Sci.* **1955**, 16, 19-30.
163. VanDerWerff, J. C.; Kruif, C. G. d. *J. Rheology* **1989**, 33, (3), 421-454.
164. Edward, J. T. *J. Chem. Educ.* **1970**, 47, 261-270.
165. Lin, T.-H.; Philies, G. D. J. *Macromolecules* **1984**, 17, 1686-1691.
166. Lu, Q.; Solomon, M. J. *Phys. Rev. E* **2002**, 66, (6), 061504.
167. Roberts, C.; Cosgrove, T.; Schmidt, R.; Gordon, G. *Macromolecules* **2001**, 34, 538-543.
168. Zhang, Q.; Archer, L. A. *Langmuir* **2002**, 18, 10435-10442.
169. Israelachvili, J. N., *Intermolecular and Surface Forces*. 2nd ed.; Academic Press: New York, 1992; p 450.
170. Lekkerkerker, H. N. W.; Poon, W. C.-K.; Pusey, P. N.; Stroobants, A.; Warren, P. B. *Europhys. Lett.* **1992**, 20, (6), 559-564.
171. Cotton, J. P.; Decker, D.; Benolt, H.; Farnoux, B.; Higgins, J.; Jannink, G.; Ober, R.; Picot, C.; desCloizeaux, J. *Macromolecules* **1974**, 7, (6), 863-872.

172. Mead, D. W. *J. Rheology* **1994**, 38, (6), 1769-1795.
173. Mead, D. W. *J. Rheology* **1997**, 40, (4), 633-661.
174. Baumgaertel, M.; Winter, H. H. *J. Non-Newtonian Fluid Mech.* **1992**, 44, 15-36.
175. Thiyagarajan, P. U., V.; Littrell, K.; Ku, C.; Wozniak, D. G.; Belch, H.; Vitt, R.; Toeller, J.; Leach, D.; Haumann, J. R.; Ostrowski, G. E.; Donley, L. I.; Hammonds, J.; Carpenter, J. M.; Crawford, R. K. *ICANS XIV-The Fourteenth Meeting of the International Collaboration on Advanced Neutron Sources; June 14-19, 1998, Starved Rock Lodge, Utica, IL* **1998**, 2, 864-878.
176. Thiyagarajan, P.; Epperson, J. E.; Crawford, R. K.; Carpenter, J. M.; Klippert, T. E.; Wozniak, D. G. *J. Appl. Cryst.* **1997**, 30, 280-293.
177. Glasstone, S.; Laidler, K. J.; Eyring, H., *The theory of rate processes*. McGraw-Hill Book Co.: New York, 1941.
178. Weng, D.; Lee, H. K.; Levon, K.; Mao, J.; Scrivens, W. A.; Stephens, E. B.; Tour, J. M. *Eur. Polym. J.* **1999**, 35, 867-878.
179. Cole, D.; Shull, K.; Baldo, P.; Rehn, L. *Macromolecules* **1999**, 32, 771-779.
180. Griffith, W. L.; Triolo, R.; Compere, A. L. *Phys. Rev. A* **1987**, 35, (5), 2200-2206.
181. Antonietti, M.; Bremser, W.; Muschenborn, D.; Rosenauer, C.; Schupp, B.; Schmidt, M. *Macromolecules* **1991**, 24, 6636.
182. Onogi, S.; Masuda, T.; Kitagawa, K. *Macromolecules* **1970**, 3, (2), 109-115.
183. Onogi, S.; Kato, H.; Ueki, S.; Ibaragi, T. *Journal of Polymer Science: Part C* **1966**, 15, 481-494.
184. Tsenoglou, C. *J. Polym. Sci. - Part B: Polymer Physics* **1988**, 26, 2329.
185. Wu, S. *Polymer* **1987**, 28, 1144.
186. Masuda, T.; Kitagawa, K.; Inoue, T.; Onogi, S. *Macromolecules* **1970**, 3, 116-125.
187. Bohm, G. G. A.; Nguyen, M. N. *Journal of Applied Polymer Science* **1995**, 55, 1041-1050.
188. Kopesky, E. T.; Haddad, T. S.; Cohen, R. E.; McKinley, G. H. *Macromolecules* **2004**, 37, 8992-9004.
189. Nuel, L.; Denn, M. M. *Rheologica Acta* **1991**, 30, 65-70.
190. Lakdawala, K.; Salovey, R. *Polymer Engineering and Science* **1987**, 27, 1043-1049.

191. des Cloizeaux, J. D. *Europhys. Lett.* **1988**, 5, 437–442.
192. Cloizeaux, J. d. *Makromol. Chem., Macromol. Symp.* **1991**, 45, 153-167.
193. Huynh, W. U.; Peng, X. G.; Alivisatos, A. P. *Advanced Materials* **1999**, 11, (11), 923-+.
194. Lee, J.; Sundar, V. C.; Heine, J. R.; Bawendi, M. G.; Jensen, K. F. *Advanced Materials* **2000**, 12, (15), 1102-+.
195. Pathak, S.; Choi, S. K.; Arnheim, N.; Thompson, M. E. *Journal Of The American Chemical Society* **2001**, 123, (17), 4103-4104.
196. Michalet, X.; Pinaud, F. F.; Bentolila, L. A.; Tsay, J. M.; Doose, S.; Li, J. J.; Sundaresan, G.; Wu, A. M.; Gambhir, S. S.; Weiss, S. *Science* **2005**, 307, (5709), 538-544.
197. Asokan, S.; Krueger, K. M.; Alkhawaldeh, A.; Carreon, A. R.; Mu, Z. Z.; Colvin, V. L.; Mantzaris, N. V.; Wong, M. S. *Nanotechnology* **2005**, 16, (10), 2000-2011.
198. Somoza, M. M.; Sluch, M. I.; Berg, M. A. *Macromolecules* **2003**, 36, (8), 2721-2732.
199. Alder, B. J.; Gass, D. M.; Wainwrig, Te. *Journal Of Chemical Physics* **1970**, 53, (10), 3813-&.
200. Vergeles, M.; Koblinski, P.; Koplik, J.; Banavar, J. R. *Physical Review E* **1996**, 53, (5), 4852-4864.
201. Heyes, D. M.; Nuevo, M. J.; Morales, J. J. *Journal of the Chemical Society-Faraday Transactions* **1998**, 94, (11), 1625-1632.
202. Pryamitsyn, V.; Ganesan, V. *Macromolecules* **2006**, 39, (2), 844-856.
203. Kim, J.; Keyes, T. J. *Phys. Chem. B* **2005**, 109, (45), 21445-21448.
204. Grubel, G.; Zontone, F. *Journal of Alloys and Compounds* **2004**, 362, (1-2), 3.
205. Sutton, M.; Mochrie, S. G. J.; Greytak, T.; Nagler, S. E.; Berman, L. E.; Held, G. A.; Stephenson, G. B. *Nature* **1991**, 352, (6336), 608.
206. Gisser, D. J.; Johnson, B. S.; Ediger, M. D.; Vonmeerwall, E. D. *Macromolecules* **1993**, 26, (3), 512-519.
207. deGennes, P. G. *Le Journal de Physique* **1975**, 36, 1199-1203.
208. Mackay, M. E.; Tuteja, A.; Duxbury, P. M.; Hawker, C. J.; Horn, B. V.; Guan, Z.; Chen, G.; Krishnan, R. S. *Science* **2006**, 311, (5768), 1740-1743.

209. Hoppe, H.; Sariciftci, N. S. *Journal of Material Research* **2004**, 19, (7), 1924-1945.
210. A. F. Hebard; Rosseinsky, M. J.; Haddon, R. C.; Murphy, D. W.; Glarum, S. H.; Palstra, T. T. M.; Ramirez, A. P., A. R. K. *Nature* **1991**, 350, 600.
211. Tanigaki, K.; Ebbesen, T. W.; Saito, S.; Mizuki, J.; Tsai, J. S.; Kubo, Y.; Kuroshima, S. *Nature* **1991**, 352, 222.
212. Chen, B.-X.; Wilson, S. R.; Das, M.; Coughlin, D. J.; Erlanger, B. *Proc. Nat'l Acad. Sci* **1998**, 95, 10809-10813.
213. Brabec, C. J.; Dyakonov, V.; Sariciftci, N. S.; Graupner, W.; Leising, G.; Hummelen, J. C. *Journal of Chemical Physics* **1998**, 109, (3), 1185-1195.
214. Lu, Z.; He, C.; Chung, T.-S. *Polymer* **2001**, 42, 5233-5237.
215. Heiney, P. A.; Fischer, J. E.; Mcghie, A. R.; Romanow, W. J.; Denenstein, A. M.; Mccauley, J. P.; Smith, A. B.; Cox, D. E. *Phys. Rev. Lett.* **1991**, 66, (22), 2911-2914.
216. Kopesky, E. T.; Haddad, T. S.; Cohen, R. E.; McKinley, G. H. *Macromolecules* **2004**, 37, (24), 8992-9004.
217. Fischer, J. E.; Heiney, P. A.; Mcghie, A. R.; Romanow, W. J.; Denenstein, A. M.; Mccauley, J. P.; Smith, A. B. *Science* **1991**, 252, (5010), 1288-1290.
218. Kharchenko, S. B.; Douglas, J. F.; Obrzut, J.; Grulke, E. A.; Migler, K. B. *Nature Materials* **2004**, 3, (8), 564-568.
219. Kashiwagi, T.; Du, F. M.; Douglas, J. F.; Winey, K. I.; Harris, R. H.; Shields, J. R. *Nature Materials* **2005**, 4, (12), 928-933.
220. Biggerstaff, J. M.; Kosmatka, J. B. *Journal of Composite Materials* **1999**, 33, (15), 1457-1469.
221. Suhr, J.; Koratkar, N.; Keblinski, P.; Ajayan, P. *Nature Materials* **2005**, 4, (2), 134-137.
222. Koratkar, N.; Wei, B. Q.; Ajayan, P. M. *Advanced Materials* **2002**, 14, (13-14), 997-+.
223. Porter, D.; Metcalfe, E.; Thomas, M. J. K. *Fire and Mater.* **2000**, 24, 45-52.
224. Nyden, M. R.; Gilman, J. W. *Computational and Theoretical Polymer Science* **1997**, 7, (3-4), 191-198.
225. Zhu, J.; Morgan, A. B.; Lamelas, F. J.; Wilkie, C. A. *Chemistry of Materials* **2001**, 13, (10), 3774-3780.



226. Charati, S. G.; Dibakar, D. D.; Elkovitch, M.; Ghosh, S.; Mutha, N.; Rajagopalan, S.; Shaikh, A. A. Electrically conductive compositions and method of manufacture thereof. 7,026,432, 2006.
227. Thompson, C. M.; Herring, H. M.; Gates, T. S.; Connell, J. W. *Composites Science and Technology* **2003**, 63, (11), 1591-1598.
228. Croce, F.; Appetecchi, G. B.; Persi, L.; Scrosati, B. *Nature* **1998**, 394, (6692), 456-458.
229. Arici, E.; Sariciftci, N. S.; Meissner, D., Hybrid Solar Cells. In *Encyclopedia of Nanoscience and Nanotechnology*, Nalwa, H. S., Ed. American Scientific Publishers: Valencia, 2004.
230. Ounaies, Z.; Park, C.; Wise, K. E.; Siochi, E. J.; Harrison, J. S. *Composites Science and Technology* **2003**, 63, (11), 1637-1646.
231. Keblinski, P.; Phillpot, S. R.; Choi, S. U. S.; Eastman, J. A. *International Journal of Heat and Mass Transfer* **2002**, 45, (4), 855-863.
232. Talbot, P.; Konn, A. M.; Brosseau, C. *Journal of magnetism and magnetic materials* **2002**, 249, (3), 481-485.
233. Ditsch, A.; Laibinis, P. E.; Wang, D. I. C.; Hatton, T. A. *Langmuir* **2005**, 21, (13), 6006-6018.
234. Ahmed, S. R.; Ogale, S. B.; Kofinas, P. *Ieee Transactions on Magnetics* **2003**, 39, (5), 2198-2200.
235. Picu, R. C.; Ozmusul, M. S. *Journal Of Chemical Physics* **2003**, 118, (24), 11239-11248.
236. Starr, F. W.; Schroder, T. B.; Glotzer, S. C. *Macromolecules* **2002**, 35, (11), 4481-4492.
237. Vacatello, M. *Macromolecules* **2001**, 34, (6), 1946-1952.
238. Vacatello, M. *Macromolecules* **2002**, 35, (21), 8191-8193.
239. Vacatello, M. *Macromolecules* **2003**, 36, (9), 3411-3416.
240. Vacatello, M. *Macromolecular Theory And Simulations* **2003**, 12, (1), 86-91.
241. Yuan, Q. W.; Kloczkowski, A.; Mark, J. E.; Sharaf, M. A. *Journal Of Polymer Science Part B-Polymer Physics* **1996**, 34, (9), 1647-1657.
242. Nowicki, W. *Macromolecules* **2002**, 35, (4), 1424-1436.
243. Cosgrove, T.; Griffiths, P. C.; Lloyd, P. M. *Langmuir* **1995**, 11, (5), 1457-1463.

- 244. Zhang, Q. H.; Lippits, D. R.; Rastogi, S. *Macromolecules* **2006**, 39, (2), 658-666.
- 245. Kopesky, E. T.; Haddad, T. S.; McKinley, G. H.; Cohen, R. E. *Polymer* **2005**, 46, (13), 4743-4752.
- 246. Lin, H.; Erguney, F.; Mattice, W. L. *Polymer* **2005**, 46, (16), 6154-6162.
- 247. Chen, P.; Zhang, J.; He, J. S. *Polymer Engineering And Science* **2005**, 45, (8), 1119-1131.
- 248. Yu, T. S.; Lin, J. P.; Xu, J. F.; Ding, W. W. *Journal Of Polymer Science Part B-Polymer Physics* **2005**, 43, (21), 3127-3134.

MICHIGAN STATE UNIVERSITY LIBRARIES



3 1293 02845 5230